This is to certify that the

dissertation entitled

TRANSPORT, BREAKDOWN AND NON-GAUSSIAN
STATISTICS IN DISORDERED SYSTEMS

presented by

Yongsheng Li

has been accepted towards fulfillment
of the requirements for

Ph.D. degree in Physics

Major professor

Date December 1, 1989

TRANSPORT, BREAKDOWN AND NON-GAUSSIAN STATISTICS IN DISORDERED SYSTEMS

By

Yongsheng Li

A DISSERTATION

Submitted to

Michigan State University

in partial fulfillment of the requirements

for the degree of

DOCTOR OF PHILOSOPHY

Department of Physics and Astronomy

1989

ABSTRACT

TRANSPORT, BREAKDOWN AND NON-GAUSSIAN STATISTICS IN DISORDERED SYSTEMS

By

Yongsheng Li

After reviewing previous work on transport and breakdown in disordered systems, I discuss the ability of random walk algorithms to calculate the effective conductivity of a continuum percolation problem. I quantify the convergence properties by simulating the effective conductivity of regular arrays of inclusions and find that the following two conditions are necessary for convergence: 1) The distance the random walker travelled >> the correlation length; 2) The random walk step ≤ size of the narrowest neck.

An extreme scaling analysis is used to estimate the size of hotspots in random networks and the consequences these hotspots have for network strengths. The most surprising result is that brittle networks exhibit a "dilute limit catastrophe", in which any finite fraction of disorder drastically reduces the network strengths. This is in contrast to transport or elastic moduli which are linear in

dilution with slope O(1) near the pure limit. A logarithmic size effect also occurs in this limit. The origin of this difference is explained by the fact that strength depends on extreme fluctuations, while moduli depend on an average over all fluctuations.

In the language of local load distributions, I argue that transport properties are related to the low moments, while breakdown strengths are related to the very high moments. Thus, the moment spectrum links and quantifies the crossover between these two very different classes of properties. I study this crossover behavior by analyzing the moment spectrum and find the critical moment m_c at which the crossover occurs.

Another implication of the dependence of breakdown properties on extreme fluctuations is that breakdown strengths conform to extreme statistics distributions and exhibit large sample to sample fluctuations [$O(1/\ln V)$]. In contrast, the conductivity or elastic moduli follow the central limit theorem and have Gaussian distributions with small sample to sample variations [$O(1/V^{1/2})$]. The thesis closes with a broad discussion of the role of non-Gaussian processes in disordered systems.

ACKNOWLEDGMENTS

I would like to express my sincere thanks to the following people:

My thesis advisor Professor P. M. Duxbury for his careful and patient guidance during the last three years and for his support, understanding, and encouragement to me. His knowledge of statistical mechanics and solid state physics and his approach to research have been a real inspiration to me.

Professor M. F. Thorpe, S. D. Mahanti and D. Tomanek for their valuable lectures, advice and many helpful conversations. Their influence on my graduate study is greatly appreciated and acknowledged.

Professor P. A. Schroeder, W. Repko and D. Stump for their valuable suggestions, encouragement and service on my Ph.D guidance committee.

My family for their support and encouragement, Mrs. Janet King for her help, Professor J. S. Kovacs for his assistance and the members of the physics department at M.S.U. for many interesting discussions in various branches of physics.

Dr. W. Xia, Dr. W. Jin, Dr. J. Gales, B. Pi, F. Zhu, W. Gong, H. Yan, Y. Cai, W. Zhong, X. Yu, and W. Liu for their many relaxed discussions throughout my graduate study and valuable help in preparation of this thesis.

Financial support from the Center for Fundamental Materials Research and the Composite Materials and Structures Center at Michigan State University is gratefully acknowledged.

PUBLICATIONS

1. Size and location of the largest current in a random resistor network.

   Y.S. Li and P. M. Duxbury, Phys. Rev. B36, 5411 (1987).

2. Current-dependent resistance of dilute switching networks.

   Y. S. Li, P. M. Duxbury and A. C. Orrick, Phys. Rev. B37, 5629 (1988).

3. Crack arrest by residual bonding in resistor and spring networks.

   Y. S. Li and P. M. Duxbury, Phys. Rev. B38, 9257 (1988).

4. From moduli scaling to breakdown scaling: a moment-spectrum analysis.

   Y. S. Li and P. M. Duxbury, Phys. Rev. B40, 4889 (1989).

5. Moment scaling, fractals and multifractals in breakdown phenomena.

   Y. S. Li and P. M. Duxbury, preprint.

6. Scaling theory and fluctuations of the strength of composites.

   P. M. Duxbury and Y. S. Li, Proceeding of the SIAM workshop on Random Media and Composites, Leesburg, Virginia, Dec. 1988.

7. Moment scaling, fractals and multifractals.

   Y. S. Li and P. M. Duxbury, Proceeding of NATO Advanced Study Institute in Disorder and Fracture, Corsica, France, 1989.

8. Scaling theory and fluctuations of the strength of percolation networks.

   P. M. Duxbury and Y. S. Li, Proceeding of NATO Advanced Study Institute in Disorder and Fracture, Corsica, France, 1989.

TABLE OF CONTENTS

List of Tables

List of Figures

Chapter I. Introduction 1

I.1 Transport properties in a lattice percolation system 3

I.2 Introduction to breakdown in a random medium 12

Chapter II. Transport Properties of Continuum Percolation Systems 27

II.1 Diffusion in random systems 28

II.2 Computational algorithms 30

II.3 Convergence properties of random walk algorithm 38

II.4 Conclusion and possible application to elastic moduli 45

Chapter III. Size and Location of the Largest Current in a Random Resistor Network -- Anomalous Size Effect in Breakdown 48

III.1 Introduction 49

III.2 Analytic study 51

III.3 Numerical Simulations 60

III.4 Conclusion 71

Chapter IV. Comparison of Moduli and Breakdown Scaling
-- A Moment Spectrum Analysis 72
IV.1 Introduction 73
IV.2 Moment scaling due to an isolated crack-like flaw 75
IV.3 Systems with flaw distributions 86
IV.4 Multifractal spectrum induced by crack pattern 92
IV.5 Conclusion 105

Chapter V. Statistics of Transport Properties and
Breakdown Strengths 106
V.1 Review of various statistics 109
V.2 Conductivity distribution and fluctuation in
percolation networks 124
V.3 The resistance distribution in disordered
quantum systems 127
V.4 Strength distribution and fluctuation in
percolation models of breakdown 135
V.5 Conclusion and discussion 143

Chapter VI. Overview and Future Perspective 147
VI.1 Relaxation processes in disordered systems 149
VI.2 Transport in quantum systems 151

Appendix A. Computer Code to Calculate the Breakdown Current
and Voltage in A Random Resistor Network 154
Appendix B. Analytic Solutions for Defect Problems 160
References 183

LIST OF TABLES

Table 2.1 Values of effective conductivity σ_{eff} for square array of insulating cylinders with various volume fractions f and the minimum values of N required to obtain the corresponding accuracy. 41

LIST OF FIGURES

Fig. 1.1	Examples of percolation lattices.	5
Fig. 1.2	A piece of two dimensional "Swiss-Cheese".	9
Fig. 1.3	Narrow portion of a neck, passing between three overlapping spherical holes, in the 3-dimensional "Swiss-Cheese" model.	10
Fig. 1.4	Examples of breakdown phenomena.	13
Fig. 1.5	I-V characteristic for a single ideal fuse.	16
Fig. 1.6	Example of random fuse networks and topology of their final breakdown path.	17
Fig. 1.7	Plot of an external breakdown voltage V_i as a function of the number of broken fuse N_i.	19
Fig. 1.8	(a) Pure network for an LxL square lattice; (b) Single-defect problem on an LxL square lattice.	22
Fig. 1.9	"Lifshitz defect" of size n for the square lattice fuse problem.	24
Fig. 2.1	A diffusion trajectory in a piece of "Swiss-Cheese".	32
Fig. 2.2	The distance travelled by a ant as a function of time.	35
Fig. 2.3	A comparison between the simulated conductivity and the experimental results.	37
Fig. 2.4	A portion of the square array of insulating	

cylinders of radius a. 39

Fig. 2.5 The conductivity of a square array of circular inclusions as a function of the volume fraction. 43

Fig. 2.6 The conductivity as a function of the random walk step length for two fixed inclusion radii a=0.40 and a=0.45 respectively. 44

Fig. 3.1 (a) A failure-inducing single defect in the square lattice random resistor network; (b) An elliptical defect that acts as a continuum-limit representation of the defect in (a). 52

Fig. 3.2 (a) A strong current-enhancing defect configuration in the square-lattice random resistor network; (b) A continuum representation of the defect in (a); (c) The defect configuration under a conformal transformation. 57

Fig. 3.3 The size of the largest current as a function of the lattice size L. 61

Fig. 3.4 A comparison of the size of the bond currents, $\langle I_{max} \rangle$ and $\langle I_{com} \rangle$, as a function of lattice size L. 62

Fig. 3.5 (a) The probability distribution of bond currents for square lattice random resistor network; (b) The data of (a) plotted on a log-linear scale to emphasize the exponential tail. 64

Fig. 3.6 The probability D that a bond distance x from one free surface carries the largest current in the

network. 66

Fig. 3.7 A plot of the ratio of the maximum of Fig. 3.6 to the bulk average as a function of system size L. 67

Fig. 3.8 The effect on I_{max} of moving the defect of Figs. 3.1(a) and 3.2(a) towards the free surface of the random resistor network. 69

Fig. 4.1 The geometry of the 2-dimensional ellipse problem. 79

Fig. 4.2 (a) Electric field as a function of distance from the tip of an ellipse;
(b) Stress field as a function of distance from the tip of an oblate ellipsoid in an elastic background. 82

Fig. 4.3 Moment scaling as a function of dilution for square lattice random resistor networks. 89

Fig. 4.4 $\langle I_0 \rangle / \langle I^m \rangle^{1/m}$ as a function of system size L. 90

Fig. 4.5 The voltage distribution for random resistor networks at p=0.90. 95

Fig. 4.6 M(m) as a function of system size L at p=0.90. 97

Fig. 4.7 M(m) as a function of system size L at p=0.70. 98

Fig. 4.8 M(m) as a function of system size L for the nearly pure networks. 99

Fig. 4.9 P(m)/ν as a function of m. 101

Fig. 4.10 A fractal-like dielectric breakdown pattern. 103

Fig. 4.11 M(m) as a function of system size L for fractal-like dielectric breakdown models. 104

Fig. 5.1 Conductivity distribution. 126

Fig. 5.2 Resistance distribution for one-dimensional chains of 500 scatters. 133

Fig. 5.3 The distribution of the largest current. 136

Fig. 5.4 A breakdown current distribution. 140

Fig. B.1 (a) The single slit representation of the elliptic defect;
(b) The geometry after conformal transformation. 169

CHAPTER I

Introduction

A basic aim of theoretical solid state physics is to understand and predict various properties of solids, such as their structures, mechanical, electrical and magnetic properties. This basically has been accomplished for crystalline solids[1], in which the periodicity of the lattice structure and electronic band structures play a fundamental role. In reality, due to impurities, lattice distortion and some other reasons[2,3], most solid materials have non-crystalline structures and the periodicity is violated. To understand the properties of solids of this sort has been a great challenge. These properties have been studied intensively for last twenty years with the achievement of a reasonable understanding. Various models have been developed in this field (a typical example is the percolation theory[4]). Today, it is a well established field, but there are still many open questions. Two such questions, which will be studied in this thesis, are the transport properties of a continuum percolation system and the breakdown properties of a random medium. It is interesting to note the fact that the second one is a new class of problem. It has attracted a lot of attention recently, and is providing new insights to breakdown phenomena as well as to the statistical mechanics of extreme phenomena[5].

In this chapter, I will first give a overview about the understanding of the transport properties in lattice percolation systems, which will naturally lead to the diffusion calculation of the effective conductivity for continuum percolation systems in chapter II. Then, I will give a general introduction to the recently developed statistical mechanics approach to breakdown in random media. Some of these results are based on original work done in this thesis (chapters

III and IV). In chapter V, the theory of extreme fluctuations is placed in the broad context of non-Gaussian statistics in disordered systems. Finally, in chapter VI, this thesis concludes with an overview and future perspective.

I.1 Transport Properties in a Lattice Percolation System.

There exist many inhomogeneous composite materials. Examples of these materials include mineral rocks, sandstones, metal-insulator alloy and fiberglass. These composites are characterized by the so called effective transport properties such as the electrical conductivity and elastic modulus, which reflect the average behaviors of the bulk materials. The study of these effective transport properties of composites has been a subject of great interest for more than a century. There existed many different approaches to this problem. A good general review on this subject has been given by Landauer[6]. Here I will concentrate on one of these approaches, i.e., the percolation theory.

Percolation theory provides a well-defined, transparent, and intuitively satisfying pedagogical model for spatially random processes. It can be applied to a broad range of physical phenomena. The transport properties of a percolation systems have been the subject of many recent theoretical and experimental studies. These studies, apart from their theoretical interest, may serve as guidance for understanding the transport properties of many types of inhomogeneous materials, such as polymer gels near sol-gel transition[7,8] and low-porosity sedimentary rocks[9].

Let us first review the "standard" discrete lattice percolation model and its transport properies[10].

As a typical example of percolation process, consider the square network shown in Fig. 1.1, where each bond is a conductor and a fixed external voltage is applied to the network. Starting from the pure network, which is a conductor, we remove fraction (1-p) of the conducting bonds randomly from this network. As more bonds are removed, the conductivity of the network decreases and less current flows through it. Finally, it becomes an insulator and the percolation transition occurs. The value of p at which the percolation transition occurs is called the percolation threshold p_c. The network is connected when $p>p_c$, and it is disconnected when $p<p_c$. As we can see from Fig. 1.1, there is no connected path which links the top and bottom of the square network when p is less than 0.5. Therefore, the percolation threshold p_c is equal to 0.5 for two dimensional square networks. This model can be generalized to various other properties, such as elastic moduli (in this thesis, I will mostly concentrate on the electrical problem). Generally, given a network, we can define the percolation model as follows:

1) For the electrical problem, each bond is a conductor and is assigned a conductivity σ according to the following distribution:

$$P(\sigma) = p\delta(\sigma-\sigma_0) + (1-p)\delta(\sigma) \qquad (1.1)$$

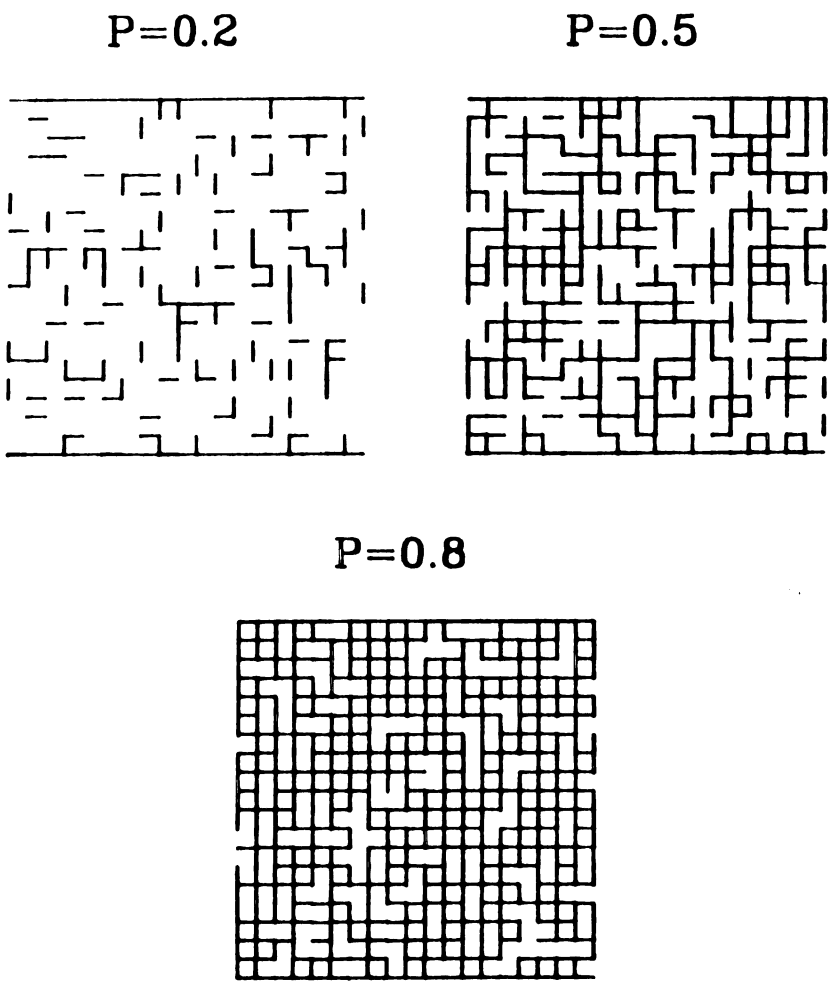

Fig.1.1 Examples of percolation lattice with L=20: p=0.20 ($p<p_c$); p=0.50 ($p=p_c$); p=0.80 ($p>p_c$).

2) For the central force elastic problem, each bond is a spring and is assigned a spring constant k according to the following distribution:

$$P(k) = p\delta(k-k_0) + (1-p)\delta(k) \qquad (1.2)$$

For simplicity, we usually choose the constants σ_0 and k_0 to be unity. For any percolation system, there is a percolation threshold p_c, But it varies from system to system. The percolation transition has been extensively studied and the geometric properties show universal scaling behaviors similar to critical phenomena near thermodynamic phase transitions[10].

Transport properties of these percolation lattices have been studied by many researchers. Their results can be summarized as follows.

1) Near to the percolation threshold p_c, the effective conductivity has a universal scaling behavior[10]:

$$\Sigma(p) \sim (p - p_c)^t \qquad (1.3)$$

where t is called the conductivity exponent, which is independent of the detail of the lattice geometry and only depends on the dimensionality of lattice [for elastic problem, Young's modulus Y has a similar behavior:

$$Y(p) \sim (p - p_c)^f \tag{1.4}$$

where f is called the elasticity exponent]. For example,

$$t \approx \begin{cases} 1.3 & \text{for two dimensional lattice} \\ 2.0 & \text{for three dimensional lattice} \\ 3.0 & \text{for Bethe lattice} \end{cases} \tag{1.5}$$

2) Outside the critical region, one can obtain an accurate analytic calculation of the effective conductivity by using the effective medium theory[11-15]. Typically, in the weak disorder limit, there is a linear correction to the effective conductivity:

$$\Sigma \sim \Sigma_0 - O(1-p) \tag{1.6}$$

where Σ_0 is the conductivity of pure lattice.

3) Numerical simulation[10] is capable of accurately simulating the effective conductivity of percolation lattice over the whole range of p.

In order to compare these results with real composites, we have to generalize these lattice percolation models to include the complicated micro-geometry of composites. Therefore, the continuum percolation model was proposed. The simplest example is the so-called "Swiss-Cheese" model[16-19], where uniformly-sized circular (spherical) holes are placed at random in a 2-dimensional (3-dimensional) uniform transport medium. The holes are allowed to overlap with one another. It is quite obvious that there exists a critical hole-volume fraction

q_c such that when $q>q_c$ the system ceases to support any transport. For $q\leq q_c$, one can again define all the transport percolation exponents through: $\Sigma \sim (q_c-q)^{t'}$ and $Y \sim (q_c-q)^{f'}$. In Fig. 1.2, a piece of two dimensional Swiss-Cheese is shown. It was found that the transport exponents of continuum percolation models are dependent on the detailed geometry of the models. This is because near the percolation threshold q_c, the transport properties of this class of models are limited by narrow "necks", which are bounded by interpenetrating holes (see Fig. 1.3). A good review article is given by Feng, Halperin and Sen[19], where the continuum percolation critical exponents are estimated.

When the concentration of one of the components (for simplicity, we will consider only two-component composite systems) is extremely low, the behavior of transport quantities like the electrical conductivity can be adequately described by the Clausius-Mossotti equation[20-25]. In between these two extremes, i.e., close to the percolation threshold and the weak disorder limit, an exact microscopic theory or detailed computer modeling of the transport properties is very difficult and till recently neither was available. One of the difficulties is the lack of good numerical simulations, which has been a major research tool to understand the lattice percolation systems. The obvious reason is that even the largest available machines can not store enough information to meaningfully discretize continuum systems.

Recently, a novel approach to this problem has been introduced[26], in which the true continuum structure is maintained, and the effective conductivity of a composite structure is calculated using random walk

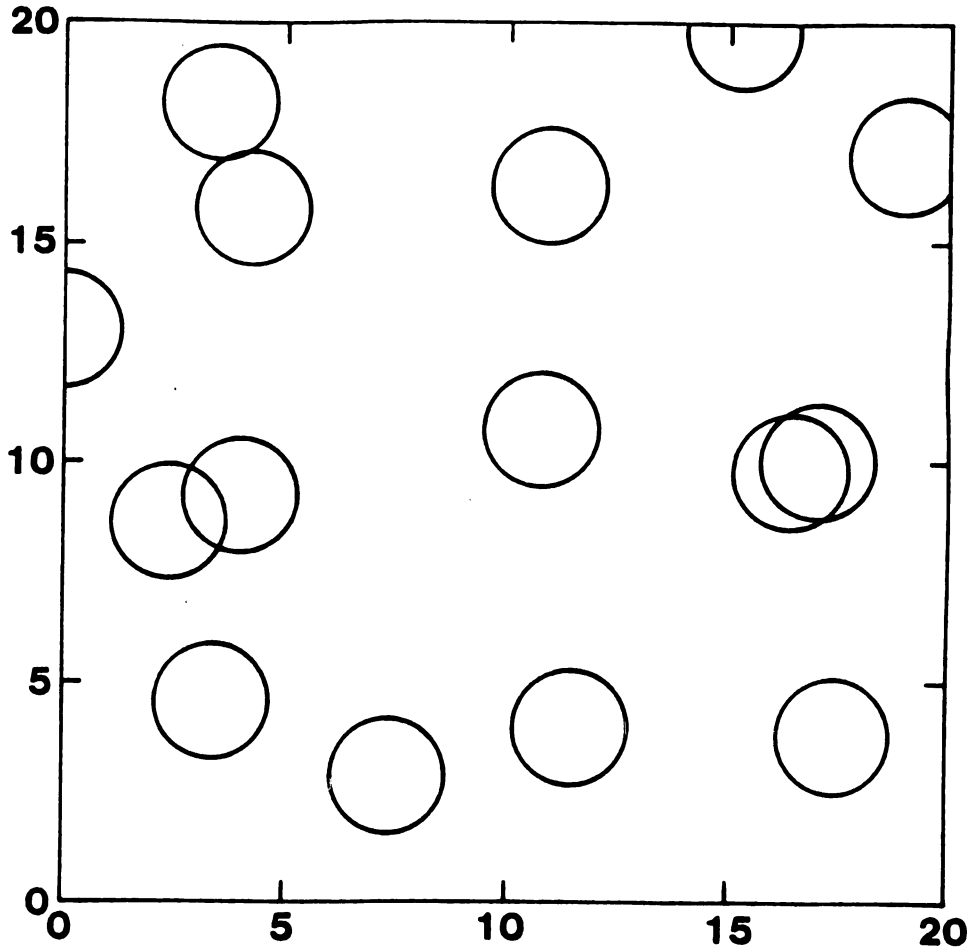

Fig.1.2 A piece of two dimensional Swiss-Cheese, where the circular fraction is 0.20.

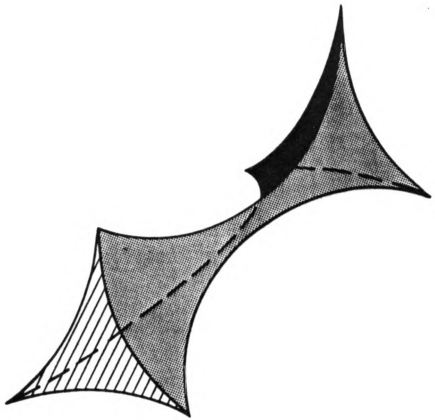

Fig.1.3 Narrow portion of a neck, passing between three overlapping spherical holes, in the three-dimensional Swiss-cheese model.

techniques. We applied this new method (see chapter II) to composite structures and tested the accuracy of the method by comparing numerical results on Swiss-Cheese percolation structures with analog experiments[27,28].

I.2 Introduction to Breakdown in a Random Medium

If one applies tensile stress to a solid, it elongates and becomes strained. The stress (σ)-strain (ε) relation is usually linear for small stresses (Hooke's law) after which nonlinearity appears. Finally at a critical stress σ_c, depending on the material, the specimen, geometry and loading condition, the solid breaks into macroscopic pieces -- fracture occurs [see Fig. 1.4(a)]. In the case of brittle solids, the fracture occurs immediately after the Hooke's linear region, and consequently the linear elasticity theory can be applied to study the (essentially nonlinear and irreversible) static fracture properties of brittle solids[29-37].

Similarly, if one applies voltage V across a conducting electrical circuit, a current I flows through it. For small voltages, the I-V relation is linear (Ohm's law). Finally, at a critical applied voltage V_c, depending the circuit, the circuit fuses as the current through some part of the circuit exceeds its threshold value [see Fig. 1.4(b)]. In dielectric materials, when the voltage gradient exceeds its threshold value, a similar (dielectric) breakdown occurs [Fig. 1.4(c)]. A similar behavior occurs in a superconducting material, where a superconductor becomes a normal conductor when the current reaches a critical value [Fig. 1.4(d)].

What happens to such responses when the solid contains random quenched impurities, dilution for example? Obviously with more and more random voids, the linear responses like the modulus of the elasticity Y of the solid decreases, or with more and more

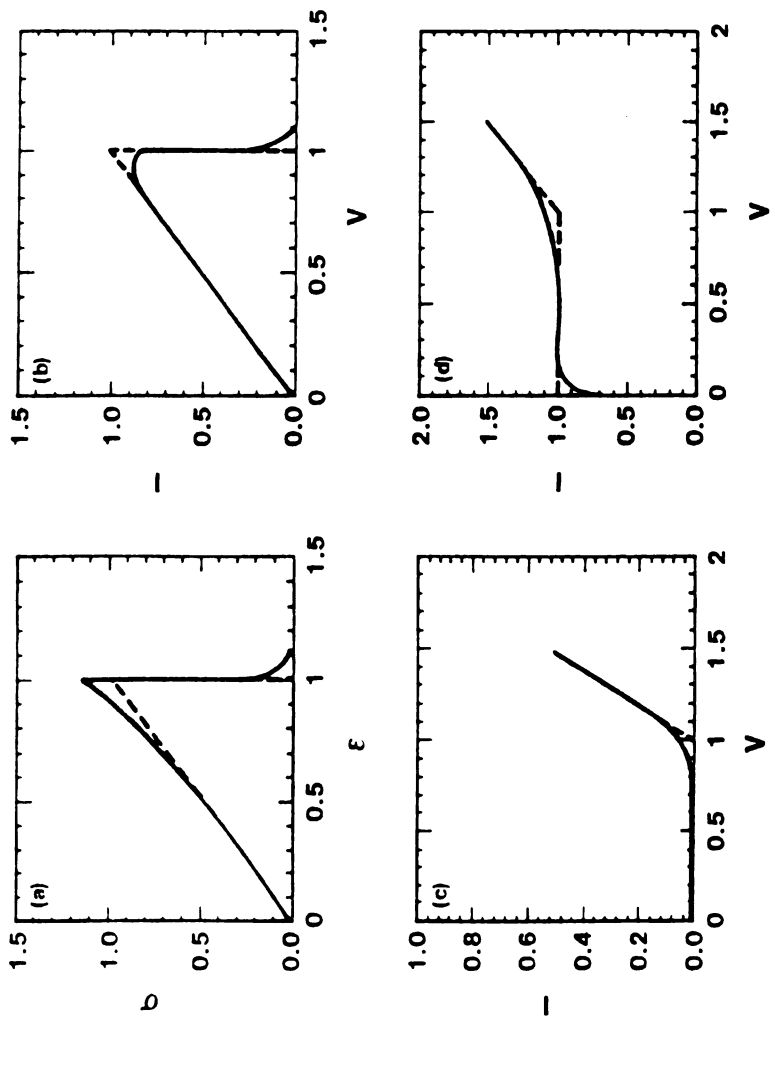

Fig.1.4 Examples of breakdown phenomena a) The failure of a spring; b) The failure of a fuse; c) The failure of a dielectric and d) A superconductor characteristic. In all of these figures, the dotted line is a discontinuous idealization of the more realistic (solid line) characteristic.

nonconducting elements in a network the conductivity Σ of the network decreases. So does the breaking strength of the material: the fracture strength σ_c of the specimen, or the fuse voltage V_b of the network, or the breakdown voltage V_b of the dielectric, or the critical current I_c of the superconducting network, all decrease (occasionally V_b increases due to the decreasing of conductivity) on the average with the increasing concentration of random impurities (random voids, insulators, conductors, or normal conductors respectively). These breakdown strengths are properties of prime importance in most applications of composites. Prediction of the effect of composite microstructure on breakdown strength is however, at a far more primitive stage than corresponding predictions of effective conductivity or elastic moduli. Recent generalizations of the percolation model to study breakdown phenomena[5,38-47] provide a new starting point in this class of problem, and an important pedagogical system in which to test the relative importance of various microstructural features and randomness on breakdown phenomena. In this section, I give an introduction and overview of the ideas and results that have been recently derived using this class of model.

There exist many percolation models for various breakdown problems. Examples include the random resistor network model for dielectric breakdown[44], random fuse network model for electrical breakdown[39,41-43], Hookean spring network model for mechanical fracture[45,46] and the superconducting network model for dirty superconductors[47]. In this thesis, I will concentrate on the random fuse network model and study the electrical breakdown problem. Most

results for this system can be easily extended to other categories of problems.

The random fuse model is described as follows. For simplicity, consider a d-dimensional hypercubic percolation lattice with percolation probability p, i.e., p fraction of bonds are conductors and the remaining fraction (1-p) of vacant bonds act as insulators. Assume each conductor is a fuse and has a resistance of 1Ω and a breakdown point of 1A (1V). Its current-voltage characteristic is shown in Fig. 1.5. Above 1V, the fuse becomes an insulator. There is a fuse network only when the concentration is above the percolation threshold ($p_c \leq p \leq 1$). Now, two busbars are separately installed horizontally across the top and bottom of the system and an electric field or voltage drop is applied vertically between two bars. If a sufficiently small voltage is applied then the system conducts just as a random resistor network in the ordinary percolation problem. Now if this externally applied voltage V is sufficiently large some of the fuses will break. And if enough fuses break there will no longer be a connecting path between the busbars so we will say that there has been a breakdown of the entire network. By studying the breakdown behavior of this model, we can get a general insight to breakdown in random media in general. In Fig. 1.6, the geometry of a typical random fuse network and its breakdown path for 50x50 networks are shown.

Next we describe the numerical technique to calculate the breakdown voltages or currents within the random fuse network model. The breakdown procedure for each lattice realization is as follows:

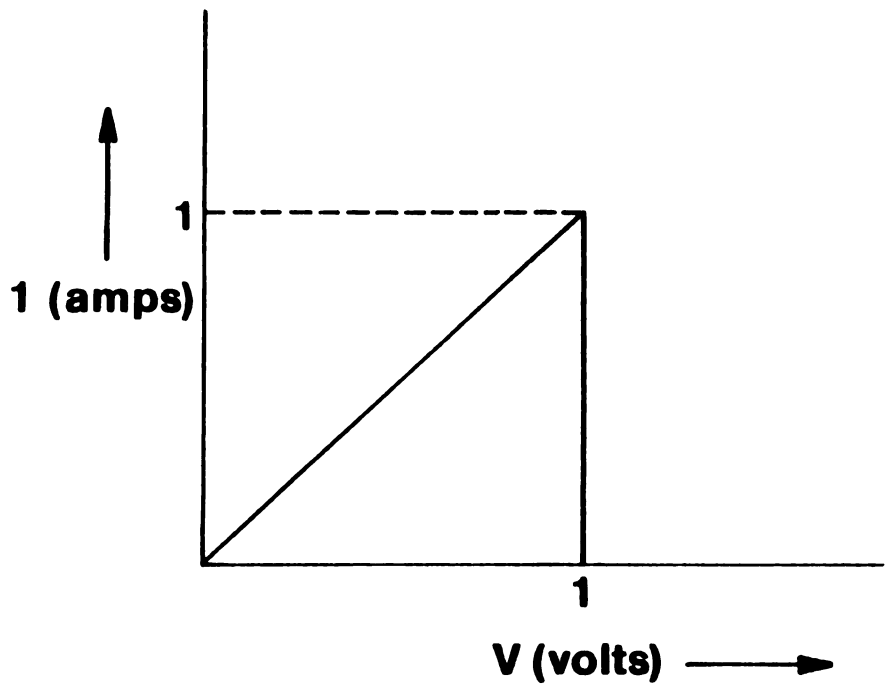

Fig.1.5 I-V characteristic for a single ideal fuse.
Above a voltage of 1V, no current flows.

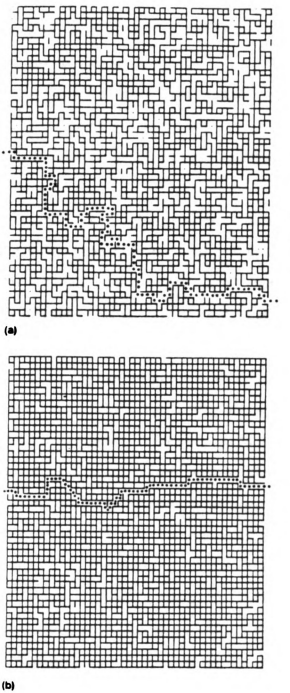

Fig.1.6 Example of random fuse networks and topology of their final breakdown path on 50x50 square network: (a) p=0.70; (b) p=0.90 (from Ref. 42).

(1) By using the Conjugate-Gradient method, we numerically solve the Kirchhoff's equation on a given lattice network and find all the voltages (currents) carried on each bond;

(2) Find the fuse which carries the largest voltage (current), i.e., hottest bond, and remove it;

(3) Repeat this procedure until the network becomes disconnected.

In all the calculations, a unit voltage drop is imposed across the opposite edges of the system and free boundary conditions are used in the transverse direction. The currents are determined to within an accuracy of 10^{-9} (a computer code for this calculation is given in Appendix A). Since the set of equations to be solved is linear, it is easy for each step in the iterative process to find the external voltage required to break the hottest bond. Following this procedure, we can get a sequence of breakdown voltages or currents. A typical sequence of external voltages that induce failure in the hottest fuse in a 100x100 network with p=0.70 is displayed in Fig. 1.7. We define V_1 (the corresponding current is I_1) as the external voltage at which the first fuse blows, and V_b is the maximum of the external voltages which is the external voltage to induce the global failure to the network (the maximum external current required to break this network is I_b). We also define the numbers, N_1 and N_f , of fuses that are broken at V_b and just before the network disconnects, respectively. In most study, we are interested in the scaling behavior of the breakdown strength as a function of disorder and system size.

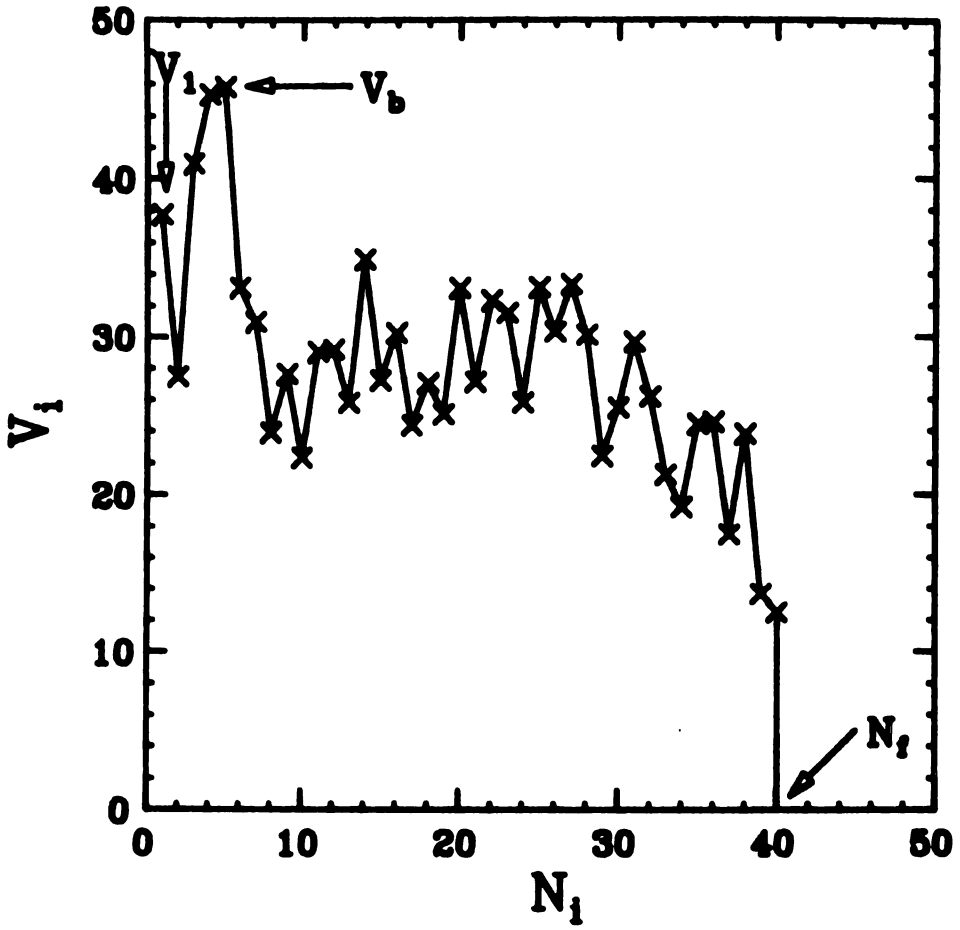

Fig.1.7 Plot of a external voltage V_i, which is the external voltage need to be applied to break the hottest bond in the network, as a function of the number of broken bonds N_i for a 100x100 square network with p=0.70.

Since V_1 and V_b scale in qualitatively same way, we can understand the breakdown strength (V_b) by studying V_1.

Compared to transport properties, the most surprising result in breakdown problems is that random networks exhibit a dilute limit singularity, in which any finite amount of disorder drastically reduces the network strength. A logarithmic size effect also occurs in this limit. The origin of this difference can be explained by the fact that strength depends on extreme fluctuations, while transport properties depend on an average over all fluctuations[49-51]. We will give detailed explanation and discussion of these difference in chapters III - V of this thesis.

For network models, the dilute limit singularity mentioned above can be easily explained by a Lifshitz type argument first given by Duxbury, Leath and Beale[42]. Consider the pure limit (p=1) when there are no defects in the network, as illustrated in Fig. 1.8 (a) for an LxL square lattice. It is obvious that the same current flows in each vertical fuse and no current is carried in the horizontal fuses. Therefore, all fuses break at once so that $V_1 = V_b$. We can easily calculate the breakdown voltage and current and find:

$$V_b = V_1 = L, \quad \text{i.e.,} \quad v_1 = V_b/L = V_1/L = 1 \tag{1.7}$$

and

$$I_b = I_1 = L^{d-1}, \text{ i.e., } i_1 = I_b/L^{d-1} = I_1/L^{d-1} = 1 \tag{1.8}$$

and all the vertical fuses break so that

$$N_f = L^d/d \tag{1.9}$$

A single defect placed in the horizontal hyperplane of the network has no effect on the properties of the network. However, when placed on a vertical bond [as shown for 2D square lattice in Fig. 1.8 (b)] a single defect has a rather dramatic effect. Due to the presence of a single defect of this sort, the currents carried on those vertical fuses next to this defect will be enhanced. The enhancement can be calculated in terms of the equilibrium Green's functions of the pure system. From which, the enhanced current is found to be,

$$I = i + 4(1/\pi - \tfrac{1}{4})i = 4i/\pi \tag{1.10}$$

where i is the externally applied current per column ($I = iL^{d-1}$). Now, the bond labeled 1 in Fig. 1.8 (b) breaks when $I_{fuse} = 1$, so by setting Eq. (1.10) equal to 1, we find $i_1 = I_1/L^{d-1} = \pi/4$. After the first fuse breaks the fuses adjacent to them [labeled 2 in Fig. 8 (b)] feel even greater enhancement of current and hence immediately also break. Indeed, the network will break into two parts. Thus, for a single vertical defect, we find

$$i_b = i_1 = I_b/L^{d-1} = I_1/L^{d-1} = \pi/4 \tag{1.11}$$

and

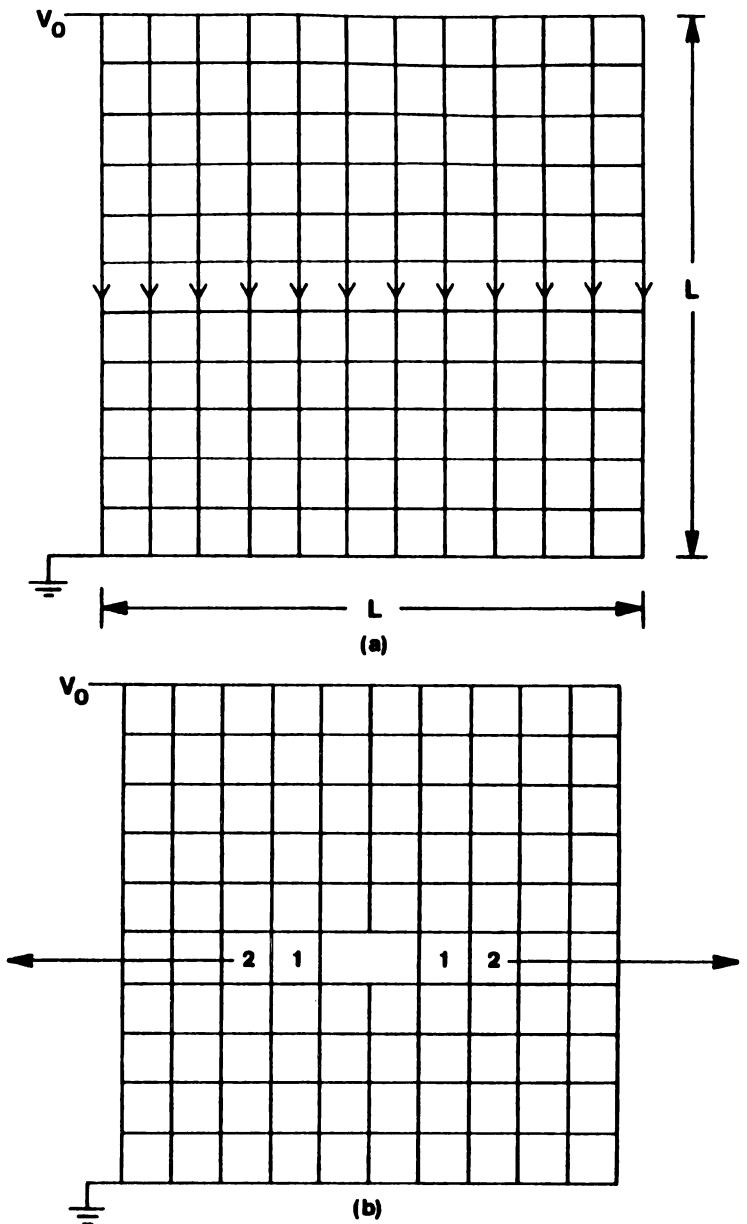

Fig.1.8 (a) Pure network for an LxL square lattice, the vertical bonds all carry the same current. The horizontal bonds carry no current. (b) Single-defect problem on a LxL square lattice. The bonds labeled 1 break first. The bonds labeled 2 then feel an enhanced current, and hence break. A crack propagates outward in the direction of the arrows in the figure.

$$v_b = v_1 = V_b/L = V_1/L = \pi/4(1 + O(1/L)) \qquad (1.12)$$

The order 1/L correction in Eq. (1.12) accounts for the change in conductivity due to removing the one bond. Eq. (1.11) and (1.12) clearly demonstrate the dilute limit singularity. Therefore, any finite concentration of defects will have an even more dramatic effect. And clearly the defects dominate this problem.

Another fact to demonstrate the importance of defects in breakdown problem is the logarithmic size effect in dilute limit where $0 < 1-p << 1$. From the discussion above, it was seen that a single vertical defect has a profound effect on the breakdown strength, clearly a cluster of such defects although less probable to occur, will have an even larger effect. Therefore, we can understand the breakdown strength by studying the most critical defect. One critical defect in two dimensions is a horizontal line of removed vertical bonds (see Fig. 1.9) simply because in this case the dipole fields for the removed bonds add constructively to produce the maximum current enhancement at the defect edge. In order to quantify the identification of the most critical defect, it is necessary to answer two questions: (1) What is the current enhancement at the edge of the critical defect cluster; and (2) Given a defect fraction 1 - p, what is the probability that the critical defect occurs somewhere within this network?

The answer to the first question is that the enhanced current I_{tip} at the defect tip depends on the size of defect as

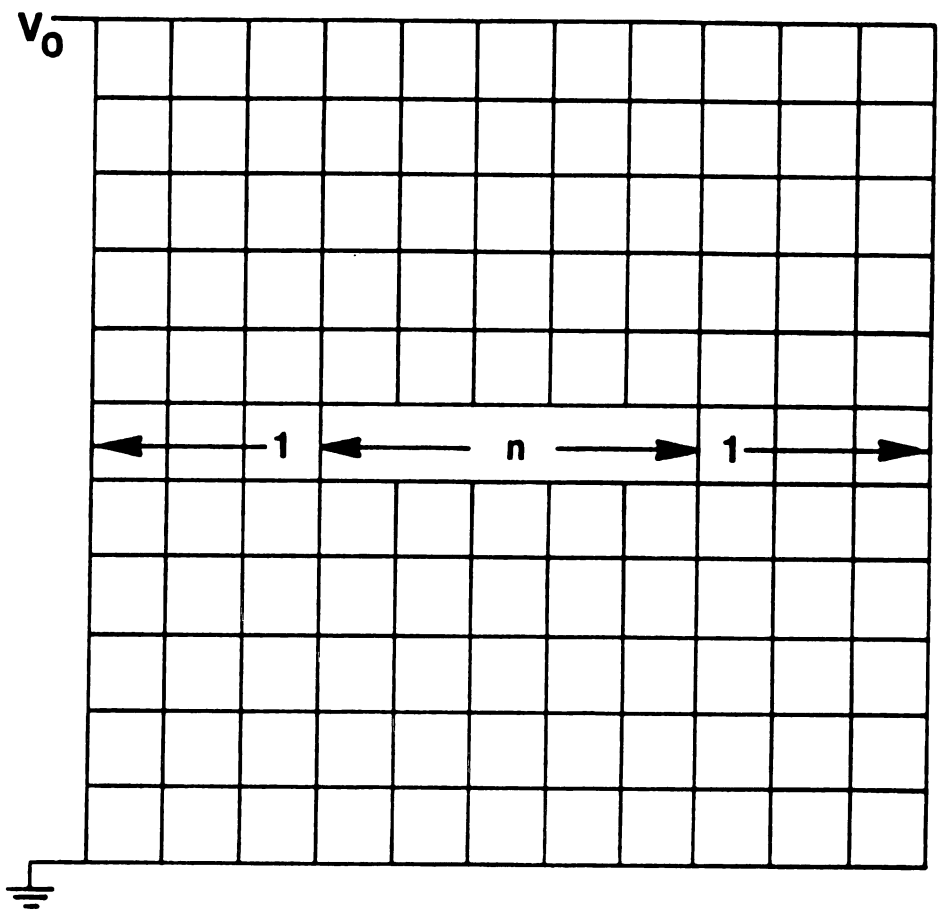

Fig.1.9 "Lifshitz defect" of size n for the square lattice fuse problem. The bonds labeled 1 break first, and a crack propagation outward in the direction of the arrows.

$$I_{tip} \sim c_1 + c_2 n^{\alpha} \tag{1.13}$$

where c_1, c_2 and α are constants, n is the size of the critical defect. More detail study will be given in chapter III.

The second question is what is the probability P(n) that n adjacent vertical defects in the hypercube will be missing somewhere in the L^d network. Since $(1-p)^n$ is the probability of n bonds missing and L^d measures approximately the number of places that the critical defect cluster can be placed on the lattice, P(n) is approximately

$$P(n) \sim (1 - p)^n L^d \tag{1.14}$$

For characteristic critical defect certainly occurring somewhere in the lattice, P(n) should be of order 1. Therefore, we can find the size of the characteristic largest defect n_c by

$$P(n_c) \sim (1 - p)^{n_c} L^d \sim 1,$$

which implies,

$$n_c \sim [-d/\ln(1-p)]\ln L \tag{1.15}$$

Combining Eq. (1.13) and (1.15), we then can predict the breakdown current by using the Lifshitz-type argument, which is

$$i_1 = I_1/L \sim 1/\{c_1 + c_2([-d/\ln(1-p)]\ln L)^{\alpha}\} \tag{1.16}$$

A similar result can be found for the breakdown voltage. Therefore, the external current or voltage that needs to be applied to breakdown the bonds at the tips of the largest defect is reduced by a factor of order lnL. This is the so-called logarithmic size effect.

Before closing this chapter, I would like to point out the fact that the study of breakdown problem is a broad field, which has been linked to many other interesting topics in statistical mechanics and solid state physics, such as pattern growth, instability analysis and the statistics of extremes[5]. Some of these connections will become more evident in chapters V and VI of this thesis, where we will discuss other physical properties which obey unconventional non-Gaussian statistics.

CHAPTER II

Transport Properties of Continuum Percolation Systems

There exist many methods and techniques to calculate the effective transport properties of random media. Effective medium theory, scaling arguments and random walk algorithms are some examples. These methods have been proven effective for lattice or discrete-like percolation problems. In reality, most composites have continuum structures, which are not well characterized by those lattice models. Recently a number of researchers[26,52,53] have been exploring the use of random walk algorithms to calculate the diffusion constant, and thus through an Einstein's relation, the conductivity of continuum systems. An advantage of this method is that the true continuum structure is maintained. In this chapter, the detailed computation algorithm is presented. Then the effective conductivity of the "Swiss-Cheese" model is calculated using this algorithm. Finally, I study the convergence properties of this random walk algorithm by simulating the effective conductivity of regular arrays of inclusions, and comparing with accurate results found using multipole expansion methods. The ability of this algorithm to calculate elastic moduli is also discussed.

II.1 Diffusion on Random Systems.

The problem of diffusion and transport in random materials has been the subject of considerable experimental and theoretical interest[54-60]. One prototype system that has been the object of recent investigation is the random resistor network (RRN). Here one studies the random walk motion of particles on percolation lattices.

A general review on this subject is given by Pandey et al[61], where they presented a detailed Monte Carlo study for random walks on various percolating lattices. The algorithm can be described as follows. For a given percolation lattice, one selects a site randomly as local origin; from here the ant starts its random motion. One of the nearest-neighbor sites is selected randomly, and the ant is moved to this site if the bond linking these two sites is connected; otherwise the ant stays at its previous place. In both cases the time is increased by a unit step, whether the attempt to move was successful or not. This process is repeated again and again for a preset time, the maximum time. From the calculated rms distance R as function of time t at various concentration p we can calculate the radii, diffusivities, and the anomalous diffusion exponent.

The motion of the particle depends on the percolation probability of the network. If the particle starts for $p<p_c$ from an arbitrary origin, due to the absence of infinite cluster, the mean square displacement $R^2 = \langle r^2(t) \rangle$ after a long time t approaches

$$R^2 = R_\infty^2 - A\exp[-(t/T)^W] + \ldots \qquad (2.1)$$

where A is some p-dependent constant, R_∞ is the saturation value for R and is some average cluster radius diverging at the percolation threshold. Also the characteristic time T diverges at p_c. For $p>p_c$, R grows with time asymptotically according to a diffusion law:

$$dR^2/dt = \text{constant} + B\exp[-(t/T')^{W'}] + \ldots \qquad (2.2)$$

Right at $p=p_c$, the asymptotic behavior of R(t) is presumed to follow an anomalous diffusion law[62]

$$R \propto t^k + \ldots \tag{2.3}$$

de Gennes proposed that one can equally think of the random resistor network as a diffusion problem[54], since the Einstein relation connecting diffusion to conductivity applies regardless of whether or not the system is random[63]. His term "ant in a labyrinth" to describe the random walker on a random substrate has led to many new results for the RRN[54-58], such as the scaling relations among the exponents describing conductivity and percolative quantities[56,64,65]. This is an important conceptual advance and has been generalized to various different problems, for example, random superconducting networks[66-68] and two-component networks where bonds have two finite conductivities (called termite diffusion)[69,70]. In the later case, the ant has different weights to correctly model the different conductivities when it crosses the two-component boundaries. In this chapter, we use an "ant" algorithm to calculate the effective conductivity of continuum percolation systems.

II.2 Computational Algorithm.

In order to generate the a Swiss-Cheese system (see Chapter I) with a given percolation probability p, we first calculate the number of insulator circles we need to put into the system. This can be calculated by using the formulae given by Xia and Thorpe[25],

$$p = \exp(-n\pi a^2) \tag{2.4}$$

where a is the radius of circles, n is the area density of holes. Then, for a two-dimensional system with size LxL and percolation probability p, the number of holes is

$$N = -L^2/(\pi a^2) \ln p \tag{2.5}$$

Having this number, we can randomly put these holes into the system. A typical example of this is plotted in Fig.1.2, where periodic boundary conditions are used.

The random walk algorithm to find the electrical conductivity consists of allowing an ant to land in a random location on the system. If it lands on a void, the ant dies and is removed, if it lands on a remaining part of the background, it begins to diffuse. The step length of the ant is a variable in the algorithm, and must be chosen to be sufficiently small to properly sample the inclusion geometry (it must be much less than the void diameter). Detail discussion about this will be given in the later section about the convergence problem. The ant randomly picks a direction and moves one step in that direction. If the ant hits any inclusions, the ant stays at its original place, but the clock advances one step forward. In Fig.2.1, one diffusion trajectory is plotted. The electrical conductivity is related to the diffusion constant via the Einstein relation

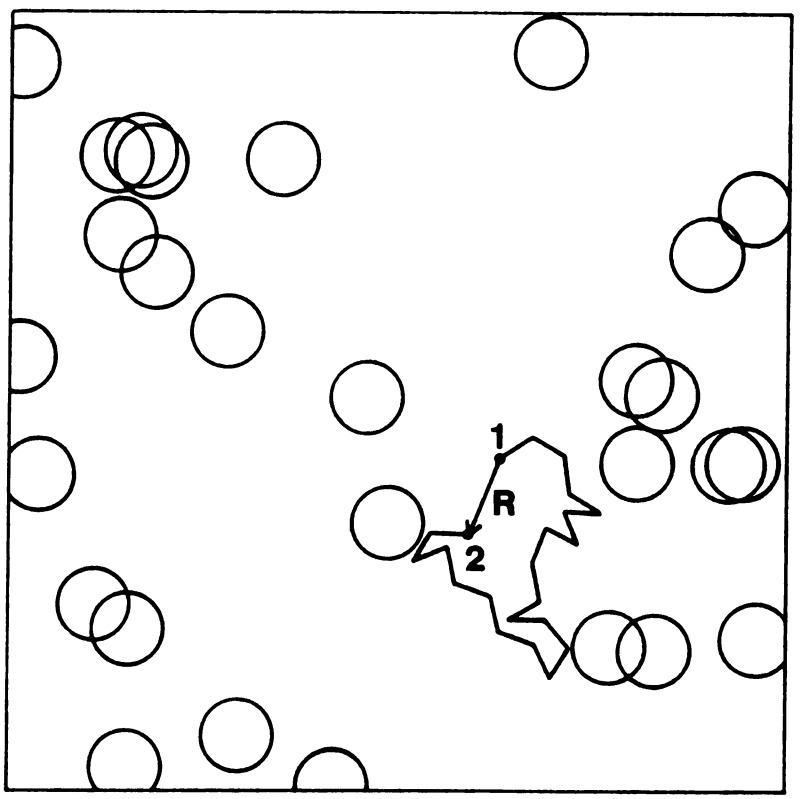

Fig.2.1 A diffusion trajectory is shown, where the ant starts from position 1 and arrives at position 2 at time t. And the distance the ant travelled is R.

$$\sigma = e^2 n D / k_b T \tag{2.6}$$

where σ is the conductivity, e is the electric charge on the ant, D is the diffusion constant, k_b is Boltzmann's constant, T is temperature and n is the carrier density. The diffusion constant is related to the distance that the ant travels in a time t via:

$$R^2 \propto Dt \tag{2.7}$$

where R is the radial distance travelled in time t. The simulation method consists of measuring R^2 for long times, averaging over many initial configurations and walkers, and extracting D from the data. Actually, the effective conductivity is calculated by the following formula:

$$\sigma(p)/\sigma_0 = D(p)/D_0 \; p \tag{2.8}$$

where $\sigma(p)$ and σ_0 are the the effective conductivity and background conductivity respectively, D(p) and D_0 are the diffusion constants for systems with percolation probability p and background (same diffusion step length r is very important). The factor p occurs because we only take into account those ants which start from the remaining background. For simplicity, we chose the value σ_0 to be unity. The diffusion constant D_0 for background is related to the diffusion step length r via:

$$D_0 \sim r^2 \tag{2.9}$$

An example of this procedure is given in Fig. 2.2 for the Swiss-Cheese case with void fraction q=1-p=0.20. The value of $\sigma/\sigma_0 = Dp/D_0$ extracted from these calculations is 0.67 ± 0.01, and is comparable with the best available estimates from perturbation expansions and (rather tedious) analog experiments[29].

We have calculated the conductivity of Swiss-Cheese systems in two dimensions for various percolation probability p (see Fig. 2.3). In all of these calculations, the system size is L=50, the radius of the inclusions is a=1.0 and the diffusion step length is fixed at r=0.1. The typical maximum time is of the order 10^6. The calculations are averaged over 50 system configurations and 20 walkers per configuration. In Fig. 2.3, we have plotted the available experimental results[27] which were found from measurements of the conductivity of a metal sheet with randomly punched holes in it. In this experiment, about 3300 circular holes were drilled on each of two steel and two molybdenum sheets (these materials are used instead of copper or aluminum to avoid deformation during the drill). The size of the sheets are 16cm x 16cm and the radius of the holes is 0.32cm. The thickness of the sheets are 0.13mm, 0.25mm and 0.38mm respectively. Effects due to the thickness of samples are negligible after observing no change among the samples with different thickness. The finite size effect only occurs for p very close to p_c [typically when $(p-p_c)/p_c \leq 2\%$]. Thus, we believe that this experiment provided a reliable data to test our numerical calculations.

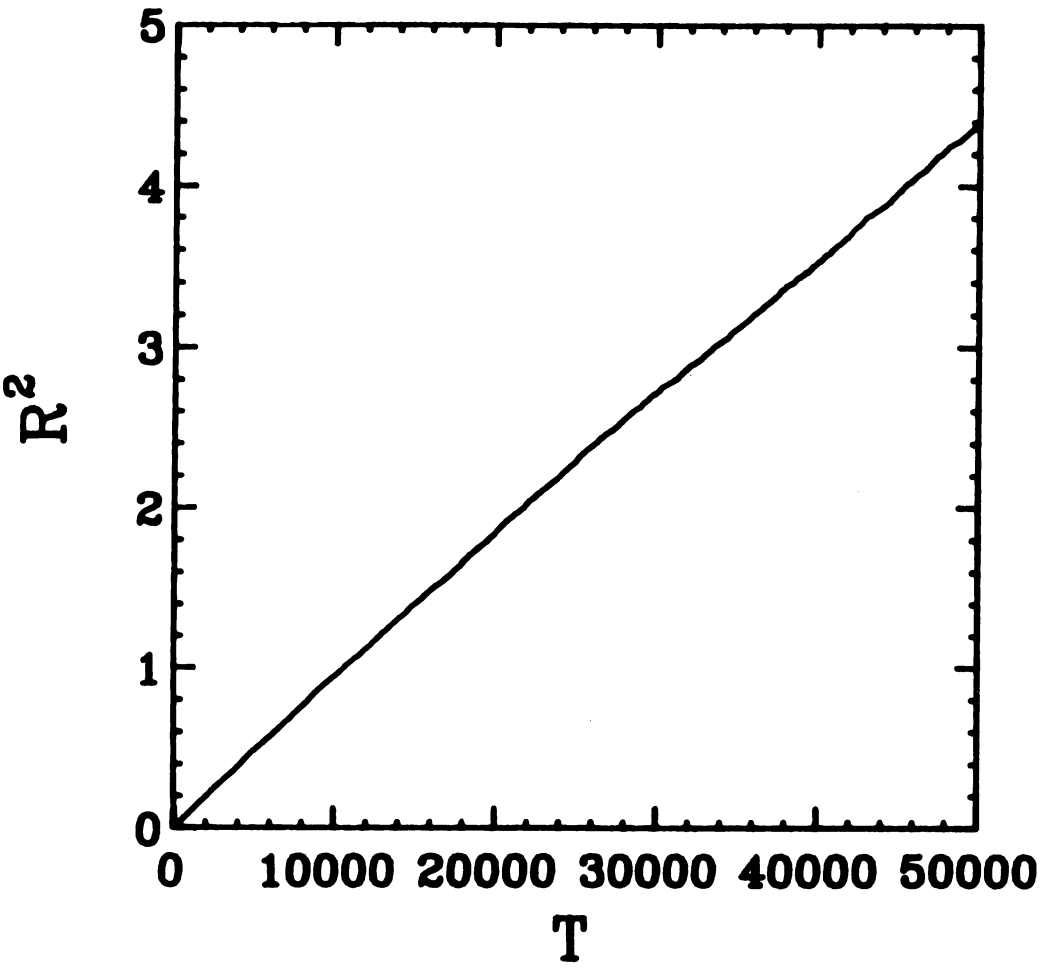

Fig.2.2 The distance travelled by the ant as a function of time. The diffusion constant is given by the slope at long time. Here p=0.90, system size is L=50, the radius of circles is a=1.0 and the random walk step is r=0.01. This calculation is done by averaging over 50 system realizations and 100 different ant trajectories per realization.

As shown in Fig. 2.3, the calculated conductivities agree well with the experimental data except in the region close to the percolation threshold p_c. We believe that the large discrepancy in this regime is due to the following three reasons: 1) There exists a large finite size effect as in lattice percolation problems; 2) The maximum diffusion time is not large enough to find the correct limiting diffusion constant near p_c. This is because the diffusion behavior only sets in when the distance travelled by the ant is much larger than the percolation correlation length ξ, which diverges close to p_c ($\xi \sim |p-p_c|^{-\nu}$); 3) The random walk step length is not small enough to simulate the narrow necks that occur near to p_c. In fact the size of the smallest neck δ is related to the percolation probability p[18,19] by

$$\delta \sim 1/L_1 \sim (p - p_c) \tag{2.10}$$

where L_1 is the number of singly connected bonds and is proportional to $(q_c-q)^{-1}$.

Since there exist many discussions[10,19,61] about solving the first two problems listed above, we concentrate on the third problem and try to characterize the effect of random walk step size on the convergence of the random walk algorithm.

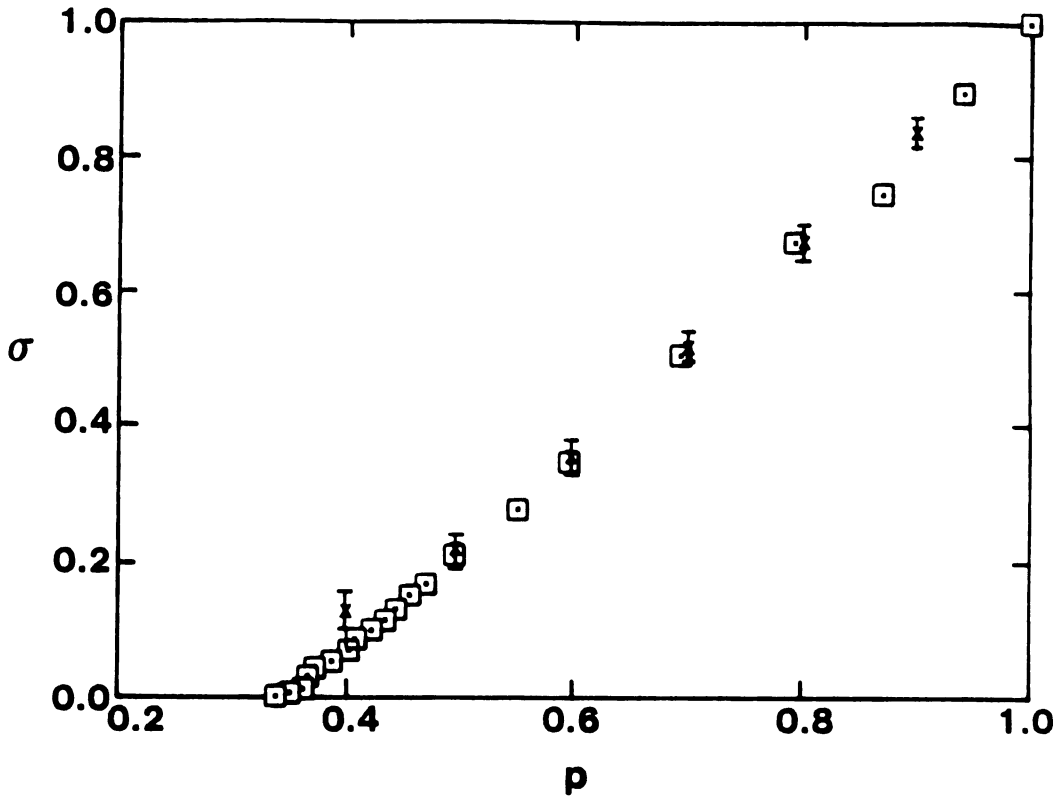

Fig.2.3 A comparison between the simulated conductivities (x) and the experimental results (□).

II.3 Convergence Properties of Random Walk Algorithm.

In this section, we study the convergence properties of random walk algorithms and test the ability of random walk simulation methods to handle narrow necks by simulating the effective conductivity of regular arrays of inclusions. The reason to use this system is: 1) For this system, there exist more accurate results found using multipole expansion methods[71-75]; 2) It is easy to clarify this issue since disorder does not play any role in this system. 3) Due to the periodic structure of this system, the diffusion regime sets in much earlier than in the disordered systems. Therefore, more accurate diffusion constants can be found.

We first briefly review the multipole expansion method for calculating the effective conductivity[75-78]. Consider a square array of cylinders each having radius a and unit separation between their centers (see Fig.2.4). The cylinders have zero conductivities and the matrix separating the cylinders has a unit conductivity. The effective conductivity of this composite is σ_{eff}, which needs to be determined. Set up polar coordinates (r,θ) with r being measured from a cylinder center P and θ from a line joining neighboring centers. Following Rayleigh[76] we can expand the potential $V(r,\theta)$ about P as

$$V(r,\theta) = A_0 + \sum_{l=1}^{\infty} (A_l r^l + B_l/r^l) \cos l\theta \qquad (2.11)$$

for r>a and with the zero radial derivative at the cylinder surfaces. The application of boundary conditions at the cylinder surface enables

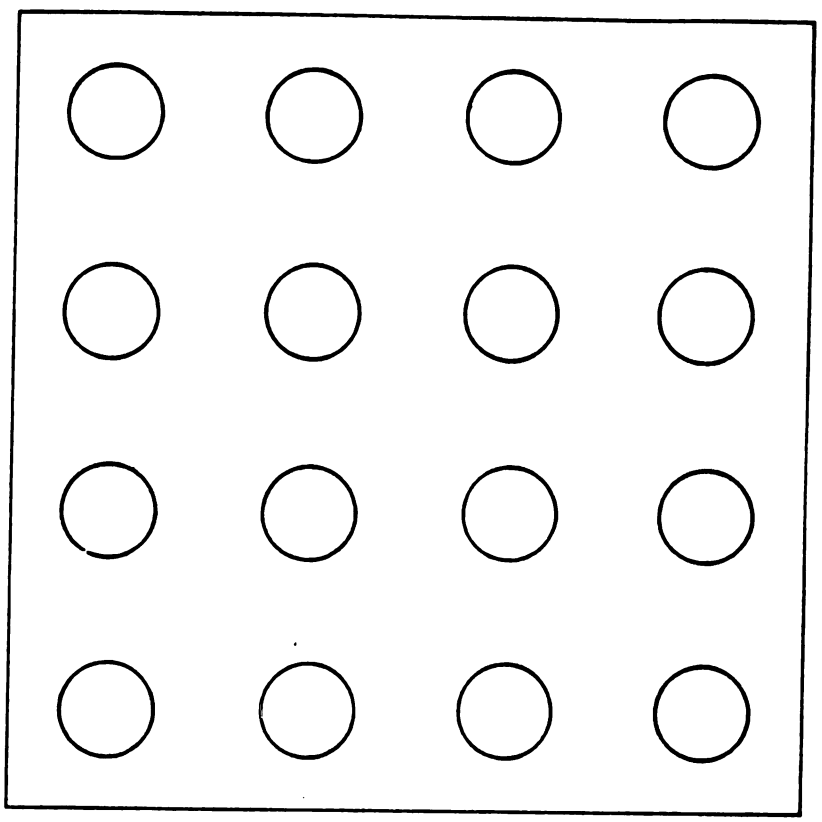

Fig. 2.4 A portion of the square array of insulating cylinders of radius a is shown.

each A_l to be expressed in terms of B_l. Symmetry conditions constrain l to run over odd values. The set of unknown B_l up to any desired order can be obtained by truncation and solution of the following set equations:

$$\delta_{n,1} - n!\, B_n/a^{2n} = \sum_{l=1,3,\ldots} S_{n+l}\, B_l\, (n+l-1)!/(l-1)! \qquad (2.12)$$

for $n=1,3,\ldots$. Here the S_l are given by the sum over integers m and n:

$$S_l = \sum_{m=-\infty}^{\infty} \sum_{n=-\infty}^{\infty} 1/(m+in)^l \qquad (2.13)$$

where (0,0) is excluded from the summation. By using the Green theorem[73] it can be shown that the effective composite conductivity σ_{eff} depends only on B_1:

$$\sigma_{eff} = 1 - 2\pi B_1 \qquad (2.14)$$

Thus in order to calculate σ_{eff} for a given order of solution (i.e., for a given number of unknown B_l) the appropriate number of lattice sums S_l must be calculated from Eq.(2.13); this enables the inversion of the truncated system Eq.(2.12) to give the value of B_1, which is then inserted in Eq.(2.14).

In table 2.1, we list the calculated values σ_{eff} for various volume fractions, $f=\pi a^2$, and the minimum order, N, of solution required to achieve the accuracy shown there. An analytic expression for σ_{eff} of this array based on square truncation to order N=3 is[79]:

Table 2.1 Values of conductivity σ_{eff} for the square array of insulating cylinders with various volume fractions f and the minimum values of N required to obtain the corresponding accuracy.

f	σ_{eff}	N
0.1	0.8182	1
0.2	0.6665	2
0.3	0.5376	2
0.4	0.4254	4
0.5	0.3247	6
0.6	0.2303	8
0.7	0.1345	16
0.75	0.0784	36
0.77	0.0489	40
0.78	0.0278	100

$$\sigma_{eff} = 1 - 2f/[1 + f - 0.305827f^4/(1 - 1.402958f^8) - 0.013362f^8] \quad (2.15)$$

It is an interesting fact that σ_{eff} is a monotonically increasing function of the order of solution N. Thus, the numerical values converges from below to the true solution, as N increases.

Another important piece of information is the conductivity exponent for this system. This can be calculated by the multipole expansion method given above. But an easier and more physical calculation has been done by Keller[80], where he noted that it can be found by calculating the conductivity contribution from the narrow necks. By calculating the effective conductivity, he found that the exponent t=0.5.

We applied the random walk algorithm to this system and calculated the conductivity for various volume fractions f (see Fig.2.5). In these calculations, a fixed random walk step length r=0.01 was used. From this figure, we can see that, comparing to the multipole expansion method, the random walk algorithm gives very good results until $f_c - f \sim 0.1$. Near f_c, there is a large discrepancy [see Fig. 2.5(b)]. Therefore, the conductivity exponent t calculated from these conductivities is quite far away from the right value. This suggests that close to the critical volume fraction f_c the random walk step length is not small enough to get a reliable result. In order to confirm this, we calculate the conductivity for two fixed volume fractions (radius of inclusions a=0.40 and a=0.45 respectively) as a function of the random walk step length r. And the result is plotted

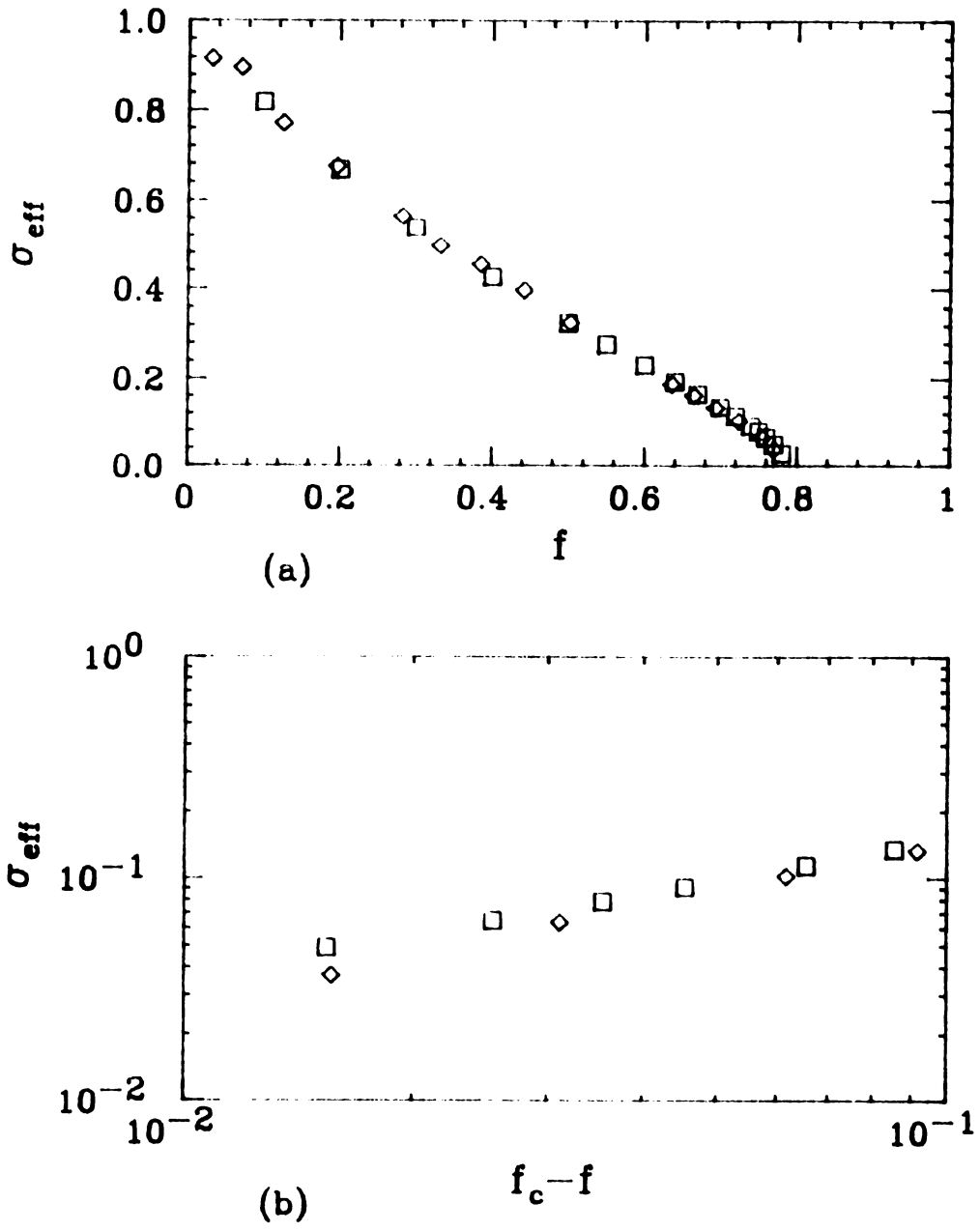

Fig.2.5 (a) The conductivity of a square array of circular inclusions as a function of the volume fraction f (◇). For comparison, the results from the multipole expansion method is also plotted (□). (b) The data of (a) plotted on a log-log scale to emphasize the large discrepancy near f_c.

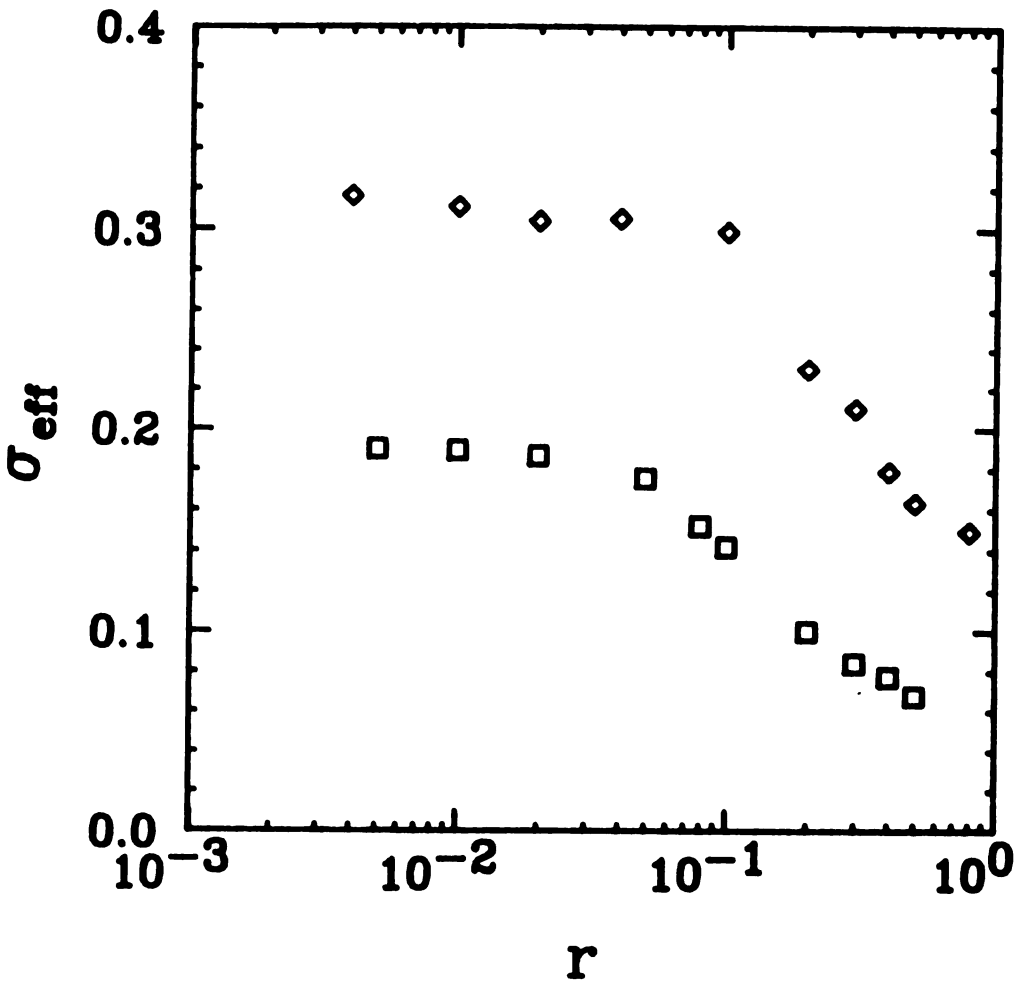

Fig.2.6 The conductivity as a function of the random walk step length for two fixed inclusion radius a=0.40 (◇) and a=0.45 (□) respectively. This implies that the conductivity saturates when the walk step length is below a critical walk step.

in Fig.2.6. As shown in the figure, the calculated conductivity increases as the random walk step length decreases. It finally saturates when the walk step length is below a critical length. This is physically reasonable, as if the random walk step is much larger than the size of the conducting narrow neck, the ant can not diffuse through the narrow necks. Thus, we calculate a lower diffusion constant which leads to a lower estimate of the effective conductivity. As the random walk step length decreases, the diffusion constant becomes more accurate. When the walk step length is of the order of the neck size, the diffusion constant saturates. This diffusion constant leads to a good estimate of the conductivity.

II.4 Conclusion and Possible Application to Elastic Moduli Calculation.

In summary, we have addressed the question of transport property in a continuum composite. We have found that a simple random walk algorithm is able to calculate the effective conductivity in systems of this sort. We have made extensive simulations of two different specific models (Swiss-Cheese model and a square array of circular insulating inclusions embedded in a conducting background), and obtained results in agreement with those obtained from experiments and multipole expansion method. We also studied the convergence properties of these random walk simulations. Our main results is: in order to have good estimate of the effective conductivity the following two conditions are necessary:

(1) The distance the ant travelled $R >> \xi$ the correlation length over which the disorder is correlated, which insures the diffusion region sets in.

(2) Random walk step length $\leq$ size of the narrowest neck. This guarantees that the algorithm correctly samples the narrow necks which have a significant contribution to effective conductivity for high inclusion fraction.

One disadvantage of this algorithm is that it is an inefficient use of computer time. This is because the walker spends too much time in the background without getting very close to any inclusions. Tobochnik[52] proposed an algorithm to improve this, where the first passage times are used. The basic idea is as fellows. For a given composite structure and a particular random walker position, we first find the largest circle (or D dimensional sphere in D dimensions) which does not overlap any inclusion and is centered at the present position of the walker. Then we move the walker immediately to a random position on this circle (or sphere) and update the time by picking it from a distribution of first passage time to the circle. The first passage time distribution can be determined by solving the diffusion equation with the right boundary and initial conditions (for details, see Ref. 52).

Finally, we briefly discuss the possible application of this random walk algorithm to the calculation of the elastic moduli of composites. The random walk algorithm appropriate to elastic systems is vector in nature[81], and has not yet been properly formulated and tested, even on the much simpler lattice problems. The random walker is no longer a scalar quantity but rather a vector quantity. This is

because isotropic elasticity involves two degrees of freedom, leading to two diffusion rates (related to the longitudinal and transverse sound velocities) and two elastic moduli -- the shear modulus and the bulk modulus. Therefore, the diffusion algorithm in this case involves the walker both hopping, as in the scalar case, but also rotating according to well defined rules. At long times the probability distribution is the sum of two Gaussian-like distributions; one depending on the longitudinal sound velocity and the other on the transverse sound velocity. But, we have not developed a good way of extracting these two sound velocities from the long time behavior. This is the major technical problem in implementing the random walk algorithm for the elastic moduli, and is under investigation now. If this problem is solved for a lattice, it could be easily extended to elastic continuum systems.

CHAPTER III

Size and Location of the Largest Current in a Random Resistor Network — Anomalous Size Effect in Breakdown

III.1 Introduction.

As discussed in chapter I, the random resistor network is a paradigm for the study of transport in random media[4] and can be extended to the study of breakdown in random media[39,41-44]. It has been briefly illustrated in chapter I that it provides a nontrivial starting point in the study of crack initiation due to defects, and a simple starting point for the study of breakdown in quenched random media. In this chapter, I will use these networks to study the anomalous size effect in breakdown problems.

An analytic study of breakdown networks centers on the bonds carrying the largest loads, and in the case of the fuse network, the bond carrying the largest current. In this chapter, we will study the properties of the largest currents, in particular, we will show that the largest bond current in a random resistor network (RRN) with p ($p>p_c$) present bonds of resistance 1Ω, and 1-p vacant bonds, scales with L, the linear dimension of the network, as

$$I_{max} \sim (\ln L)^{\alpha} \tag{3.1}$$

$$I_{com} \sim (\ln L)^{\beta} \tag{3.2}$$

in the dilute limit, i.e., for L (the linear dimension of the network)$>>\xi_p$ (the percolation correlation length). This is the so-called anomalous size dependence in breakdown problem. I_{max} is the largest current in the random resistor network, and I_{com} is the largest current in a failure initiating bond. α and β are enhancement

exponents. In this chapter, we will analytically calculate the largest current in some special cases, give general arguments to support Eqs. (3.1) and (3.2), and suggest that α and β obey the approximate inequality

$$1/[2(D-1)] \leq \alpha \leq \beta \leq 1 \tag{3.3}$$

where D is the spatial dimension. Numerical simulations which support the analytic predictions for two-dimensional random resistor networks are also given. In addition, we study the location of the largest current in the network and find that in a system with free boundary conditions, there is a strongly enhanced probability near the free surfaces of the network. Translated into breakdown language, this implies that cracks are often initiated near the surfaces of a sample.

III.2 Analytic Study.

In the dilute limit, where $L>>\xi_p$, defect clusters are well separated, and may, in a first approximation, be treated independently. We consider L^D random resistor (1Ω per present bond) networks that have a current of 1A through each vertical bond in the pure limit. Upon adding a small fraction 1-p of defects (which have zero conductivity), we then wish to find the size of the current in the hottest bond (the bond carrying the largest current). As discussed in Chapter I, in two dimensions, long thin defects are especially efficient at causing current enhancements near their ends [see Fig.3.1(a)], and our analysis begins by calculating the current enhancements due to defects of this sort. The largest defects of this sort have the largest current enhancements, and as we have shown in Chapter I, the largest defects of this form are of size lnL. To find the current at the end of a defect like that shown in Fig.3.1(a) on the lattice, we use the continuum approximation shown in Fig.3.1(b). The solution to this problem in two dimensions may be found using elliptical coordinate solutions to Laplace's equations, and is given in Appendix B, from which we take the result

$$j_{tip}(x) = j_\infty\left[1 + \frac{\cosh\xi_a \exp(\xi_a-\xi)}{\sinh\xi}\right], \qquad (3.4)$$

where $j_{tip}(x)$ is the current density at distance x from the tip (at x=a) of the defect along the y=0 axis, $\xi=\cosh^{-1}(x/a)$, and j_∞ is the current density at a large distance away from the defect. To find the

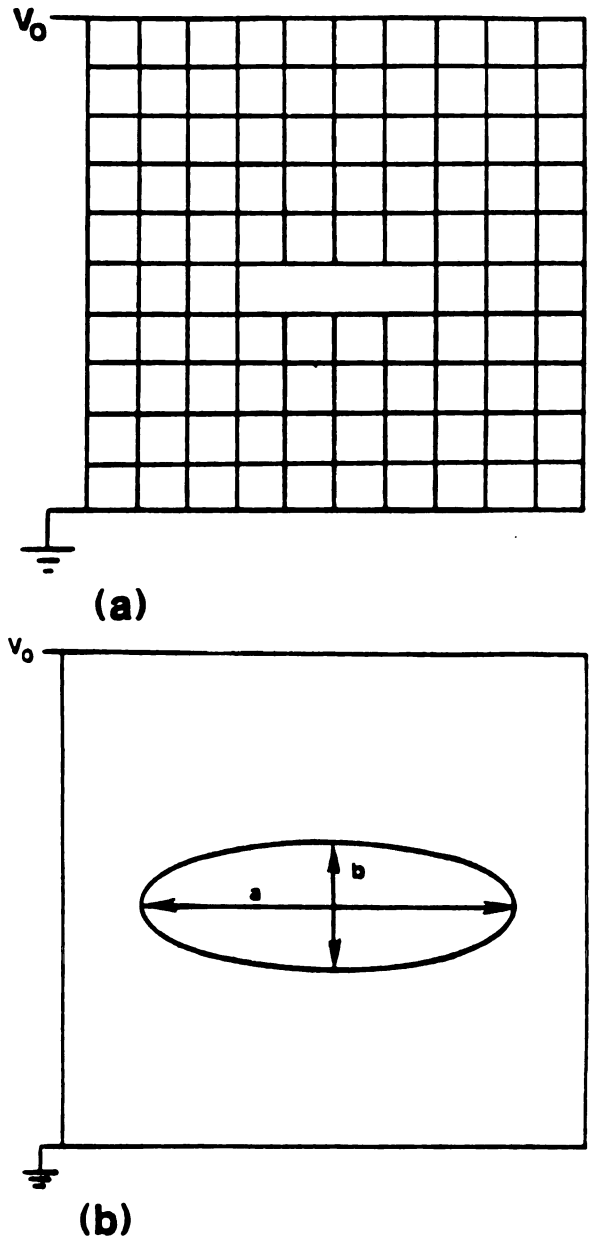

Fig.3.1 (a) A failure-inducing single defect in the square lattice random resistor network. (b) An elliptical defect that acts as a continuum-limit representation of the defect in (a).

prediction that this result makes in the lattice problem, we must integrate over the lattice spacing d, to find

$$I_{tip} = \int_a^{a+d} j_{tip}(x)dx$$

$$= \int_{\xi(a)}^{\xi(a+d)} j_\infty [1 + \frac{\cosh\xi_a \exp(\xi_a - \xi)}{\sinh\xi}] \, c\sinh\xi d\xi$$

$$= I_\infty \{1 + \frac{a}{d}[1 - \exp(\xi_a - \xi_{a+d})]\} \qquad (3.5)$$

where $\xi_a = \cosh^{-1}(a/c)$, $\xi_{a+d} = \cosh^{-1}[(a+d)/c]$, and $I_\infty = j_\infty d$ if the current flowing in a vertical bond is a long way from the defect. For simplicity, we take $I_\infty = 1$. In terms of d, a, and b, there are two limiting behaviors in I_{tip},

$$\text{(i) } da \ll b^2, \qquad \text{where } I_{tip} \sim I_\infty (1 + a/b) \qquad (3.6)$$

$$\text{(ii) } da \gg b^2, \qquad \text{where } I_{tip} \sim I_\infty [1 + \sqrt{(2a/d)}] \qquad (3.7)$$

For L^D (D is the spatial dimension) RRN, the lattice spacing d=1. In addition, b corresponds to the thickness of the long defect of Fig.3.1(a) in the y direction, and so b=1. Since a ~ lnL, the limit $da \gg b^2$ is the correct limit to take in comparing the ellipse result with the lattice problem. Using the single-ellipse result, one then finds that somewhere in the RRN there is a bond whose current scales as

$$I_{2D\ ellipse} \sim (\ln L)^{1/2} \tag{3.8}$$

Now consider the random resistor network to be a breakdown network by changing all of the resistors to 1-Ω, 1-A fuses. The failure of the bond at the end of an "ellipse-like" defect will lead to the eventual failure of the whole network, as the crack grows from the outer tips of the long thin defect in Fig.3.1(a). The ellipse thus gives an estimate of the current in a "failure-initiating" bond, and from it we obtain the estimate $I_{com} \geq I_{ellipse}$. There are, however, defect configurations that lead to large current enhancements and do not lead to the failure of the whole network. One such configuration is shown in Fig.3.2(a). The bond in the middle of the two cracks in this figure carries the most current. However, when it fails it does not necessarily lead to the eventual failure of the whole network[82]. This sort of crack configuration is considered further below. Before doing this, we find I_{com} in three dimensions based on calculations using a oblate spheroidal defect found by forming a solid of revolution about the y axis of Fig.3.1(b). Solving Laplace's equations in oblate spheroidal coordinates[83] (the detailed solution is given in Appendix B), one finds, for the current density as a function of distance from the edge of the y=0, r=a circle,

$$j_y = j_\infty\{1-[\cot^{-1}(\sinh u)-(\sinh u)^{-1}]/[\cot^{-1}(\sinh u_0) - \sinh u_0/(1+\sinh^2 u_0)]\}, \tag{3.9}$$

where $a=c\cosh u_0$, $r=(x^2+z^2)^{1/2}=c\cosh u$, $b=c\sinh u_0$, $a^2=b^2+c^2$. This is integrated over the lattice spacing d in the x and z directions, and again taking the limit $da>>b^2$, with $b \sim d$ to obtain the lattice limit, we find

$$I_{tip} = \int j_y \, dxdz$$

$$= 2\pi c^2 \int_{u(a)}^{u(a+d)} \cosh u \sinh u \, j_y du$$

$$= \pi c^2 j_\infty \{\cosh^2 u - [\sinh^2 u \cot^{-1}(\sinh u) -$$

$$\sinh u - \tan^{-1}(\sinh u)]/[\cot^{-1}(\sinh u_0) -$$

$$\sinh u_0/(1 + \sinh^2 u_0)]\}_{u(a)}^{u(a+d)}$$

$$\sim I_\infty 2^{3/2}/\pi \, (a/d)^{1/2}, \qquad (3.10)$$

with the result $a \sim n_{max}^{1/2} \sim (\ln L)^{1/2}$ in three dimensions (3D)[41-43], and we find, further,

$$I_{com} \geq (\ln L)^{1/4} \quad \text{(in 3D)}. \qquad (3.11)$$

Again, this defect leads to the eventual failure of the whole network as the crack grows from the outer edges of the "penny-shaped" crack. Combining the equations above for I_{com} in two and three dimensions, we find

$$I_{com} \sim (\ln L)^{\beta} \quad \text{with } \beta \geq 1/[2(D-1)]. \tag{3.12}$$

Here we have written $\beta \geq 1/[2(D-1)]$ because although the isolated ellipse and spheroidal defects that we have studied will certainly lead to the failure of the network, there may be other configurations that we have not studied that lead to failure more readily. The ellipse result thus provides an approximate lower bound on β. It is only an approximate lower bound, as we cannot rigorously exclude the possibility that the network may be stronger than the prediction found from the ellipse result; although on physical grounds we consider it unlikely, and the numerical evidence[41-43] (also see next section) supports Eq. (3.12).

It is straightforward to find a defect configuration that leads to a greater current enhancement than that induced by the ellipse. In two dimensions, one such defect is shown in Fig.3.2(a). The bond between the two cracks carries the most current, and we can make an analytic estimate of its current by solving a continuum two-crack problem. It is not possible to solve the two-ellipse problem, but it is possible to solve the problem of two infinitesimally thin slits in two dimensions by using conformal transformation techniques. We thus replace the lattice problem of Fig. 3.2(a) by the continuum problem of Fig. 3.2(b). By conformal transformation[84-86] (see Appendix B), the two-slit problem is transformed as depicted in Fig. 3.2(c), a problem that is trivially solvable for infinitesimally thin slits. The form of the conformal transform is quite complex, however, so we defer detailed calculations to Appendix B. The current density between the two slits of Fig. 3.2(b) is then integrated over the lattice spacing

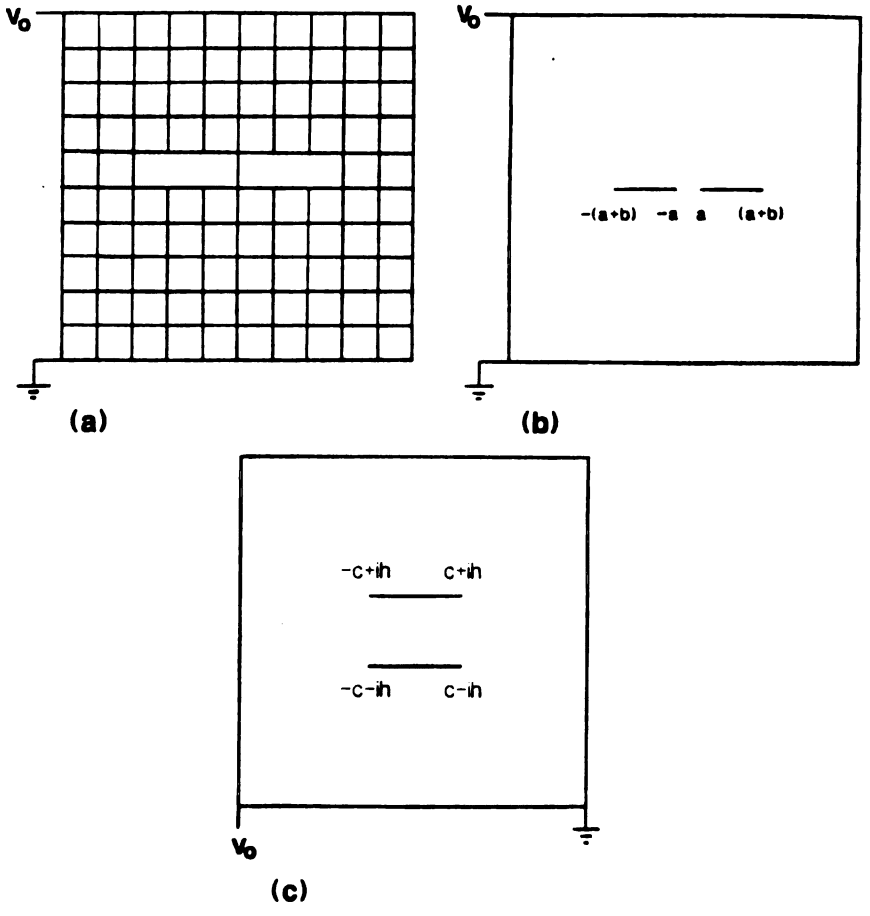

Fig.3.2 (a) A strong current-enhancing defect configuration in the square-lattice RRN. The bond between the two defects carries a large current. (b) A continuum representation of the defect in (a). The defects are infinitesimal slits lying along the x axis. (c) Under a conformal transformation, the defect configuration of (b) is transformed to that shown in this figure. The calculation of the electric field in this geometry is trivial.

d, to find, for the current between the two slits in the lattice limit,

$$I_{slits}=2j_{\infty}(a+b)[E(k)-K(k)+E(k')K(k)/K(k')], \qquad (3.13)$$

where 2a is the distance between the two cracks [see Fig. 3.2(b)], b is the length of each crack, $k=a/(a+b)$, $k' = \sqrt{(1-k^2)}$, and K(k) and E(k) are,respectively, elliptic integrals of the first and second kind. When the cracks are close so that $a/b \to 0$ and $k \to 0$, we find

$$I_{total} \sim (a+b)/\ln[a/(a+b)], \qquad (3.14)$$

which implies

$$I_{max} \sim \ln(L)/\ln[\ln(L)], \qquad (3.15)$$

or $\alpha=1$, ignoring the $\ln[\ln(L)]$ correction. As a technical aside, it is interesting to note that although the single-slit result does not produce the same current density at the slit tip as is found at the ellipse tip, after integrating over the lattice spacing the ellipse and the slit give the same expression for the current (this is demonstrated in Appendix B).

In general, we believe that it is always possible to find a defect configuration that channels a current proportional to the defect size through one critical conducting bond, and hence that $\alpha=1$ for any dimension. In any case, $\alpha=1$ is an upper bound on the amount of current that can be channelled by an isolated defect cluster, just due to current conservation. Based on the isolated defect cluster

calculations described above and Eq. (3.12), we thus find the approximate inequality given in the Introduction [Eq. (3.3)],

$$1/[2(D-1)] \leq \beta \leq \alpha \leq 1 \tag{3.16}$$

The only way that this result can be invalidated is for the cumulative effects of many defect clusters to lead to qualitatively new behavior. We may estimate the maximum enhancement this effect may have by replacing each defect cluster by a dipole current source, and considering a random distribution of such dipoles on the lattice. The maximum cumulative effect of such a distribution of dipoles is

$$I_{max} \sim \int_1^L dr\, r^{D-1}(1-p) I_{dipole}/r^D, \tag{3.17}$$

where I_{dipole} is the average strength of one dipole [O(1) for $L \gg \xi_p$]. The integrand is the maximum contribution to a bond current at the origin due to all dipoles on the hypersphere at distance r. Upon doing the integral, one finds

$$I_{max} \sim \ln L \qquad \text{in all dimensions.} \tag{3.18}$$

The failure of such a bond does not necessarily lead to the failure of the network, and the long range cumulative effects of dipole current sources thus leads to the prediction $\alpha \leq 1$ as found above using defect-cluster arguments. We thus believe that Eq. (3.16) provides reliable bounds on α and β, and that the evidence is quite strong that $\alpha = 1$ in two dimensions. In the next section we test the analytic predictions

that we have made above by doing numerical simulations on the two-dimensional random fuse network.

III.3 Numerical Simulations.

In order to test our predictions, we have performed numerical simulations on LxL square-lattice random resistor networks. As described in Chapter I, we use the Conjugate-Gradient method to solve Kirchhoff's equations on this network. In the calculations described here, we apply an external current of 1A per vertical bond and free boundary conditions in the transverse direction. The solution is considered to have converged adequately when the residual vector[42] is less than 1.0×10^{-7}.

In Fig.3.3 we plot the maximum current I_{max} (averaged over 50 realizations) as a function of lattice size L, with L ranging from 10 to 200 for several values of p. At all values of p presented in the figure, the data suggest that I_{max} is linearly dependent on lnL, and hence that $\alpha=1$ in two dimensions. These numerical data thus support the prediction found from the analytic arguments of the preceding section, and we thus believe $\alpha=1$ in two dimensions for $L>>\xi_p$.

As discussed previously[41-43], $I_{com} = I_{max}$ when there are no defects in the system, and also that $I_{com} \sim I_{max}$ at the percolation point. We thus have chosen to do a detailed comparison of I_{com} with I_{max} at p=0.75, as any differences between two quantities should be noticeable at this defect fraction. It is much more time consuming computationally to calculate I_{com} as it involves carrying the crack-propagation process to completion. The data presented in Fig.3.4 on

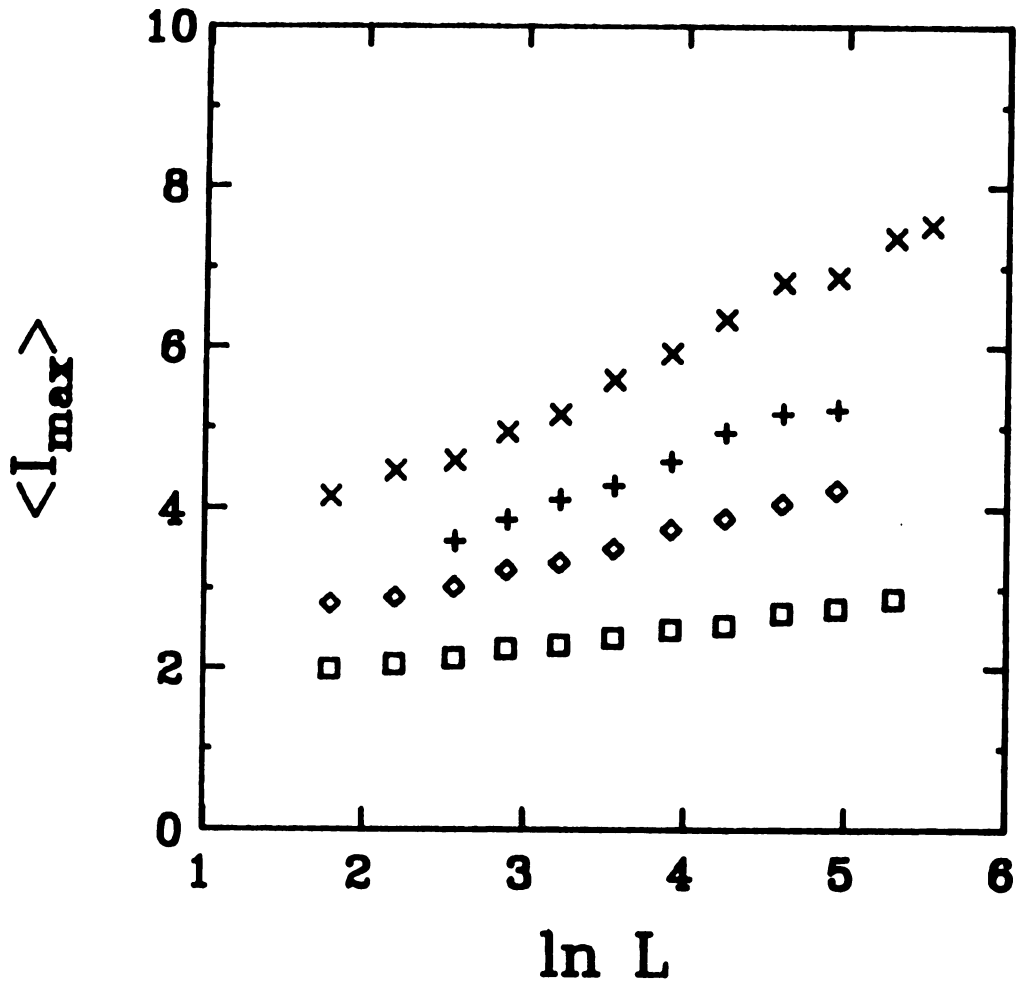

Fig.3.3 The size of the largest bond current, $\langle I_{max} \rangle$, on LxL square lattice random resistor networks as a function of the lattice size L, for p=0.90 (□), p=0.80 (◇), p=0.75 (+), and p=0.70 (x). Each point is an average over 50 realizations.

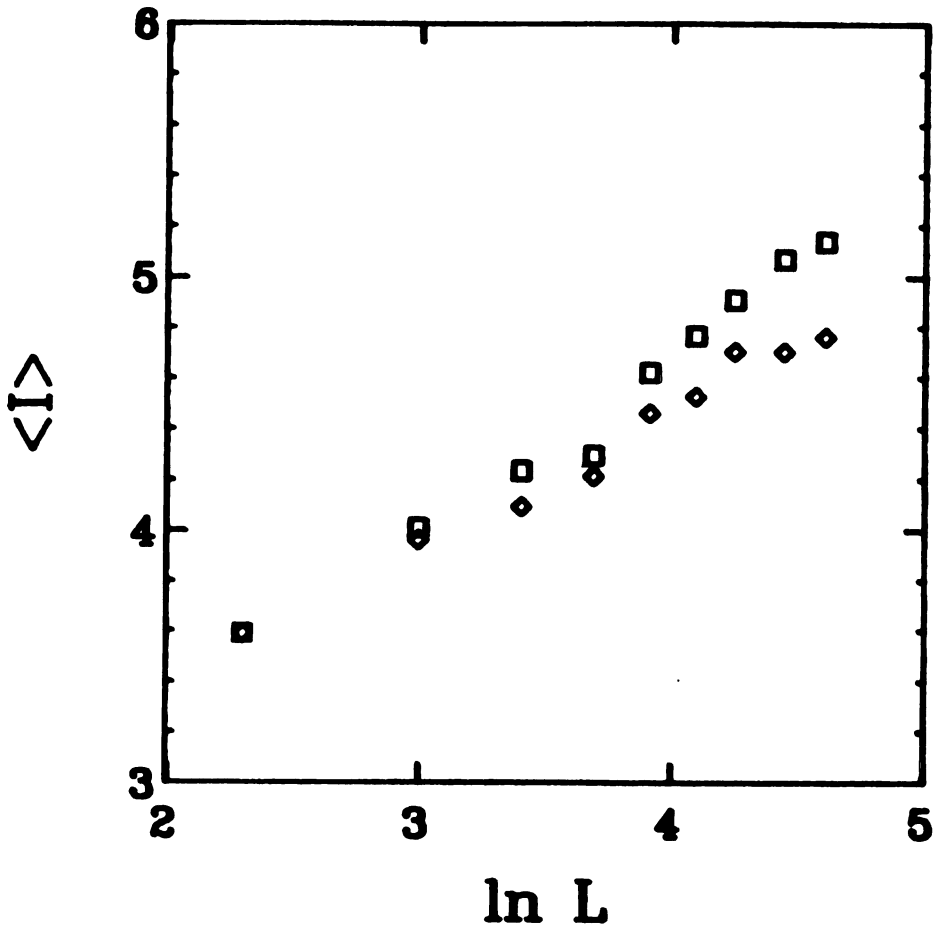

Fig.3.4 A comparison of the size of the bond currents, $\langle I_{max} \rangle$ (□) and $\langle I_{com} \rangle$ (◇), as a function L for p=0.75. Each point is an average over 50 realizations.

square lattices of sizes from L=10 to 100 with 50 realizations per lattice size took 5 h of Cyber 205 CPU time. The data are consistent with the equality $\alpha=\beta=1$ in two dimensions, although the I_{com} data have some downward curvature. The data are certainly consistent with the theoretical prediction given in Eq. (3.16) of the preceding section.

The prediction that $\alpha=1$ in two dimensions has implications for the nature of the tail of the bond-current distribution occurring in the RRN. The fact that the largest current increases logarithmically implies that the tail of the bond-current distribution is exponential, as can be seen from the following equation,

$$L^{D}\exp(-BI_{max}) \sim 1, \tag{3.19}$$

where B is independent of L, and so

$$I_{max} \sim \ln L. \tag{3.20}$$

The relationship between the extreme values of a distribution and the nature of the distribution tail is well studied in statistics, and may be found, for example, in the book by Gumbel[87]. Another numerical test of the exponent α is thus to study the form of the tail of the distribution of bond currents. The bond-current distribution for L=80 square networks with p=0.80 and 0.90 is shown in Fig.3.5(a). The two-peak structure of the distribution in Fig.3.5(a) is a reflection of the fact that when there are no defects in the network, the vertical bonds all carry the same current, while the horizontal ones carry none. In the pure limit the distribution function is thus two delta

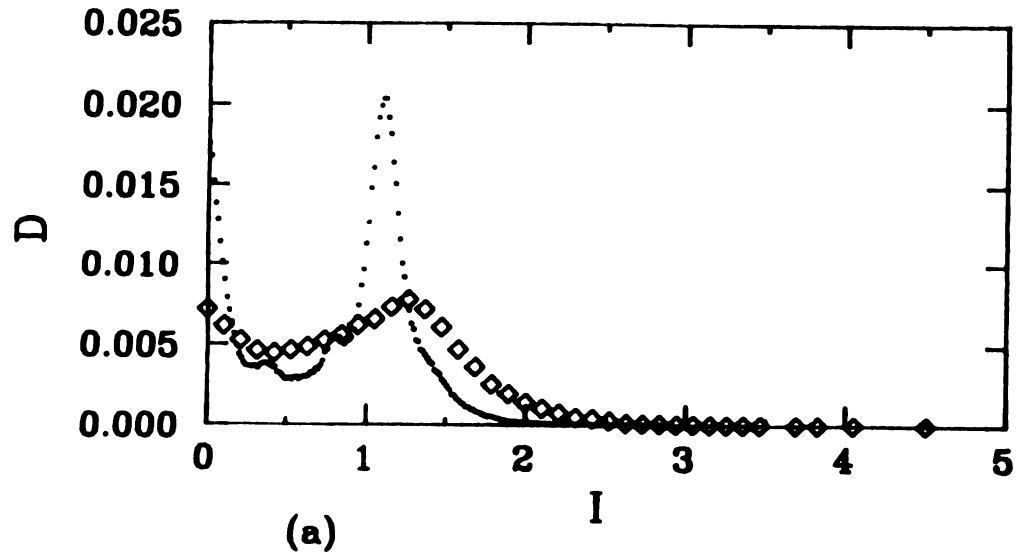

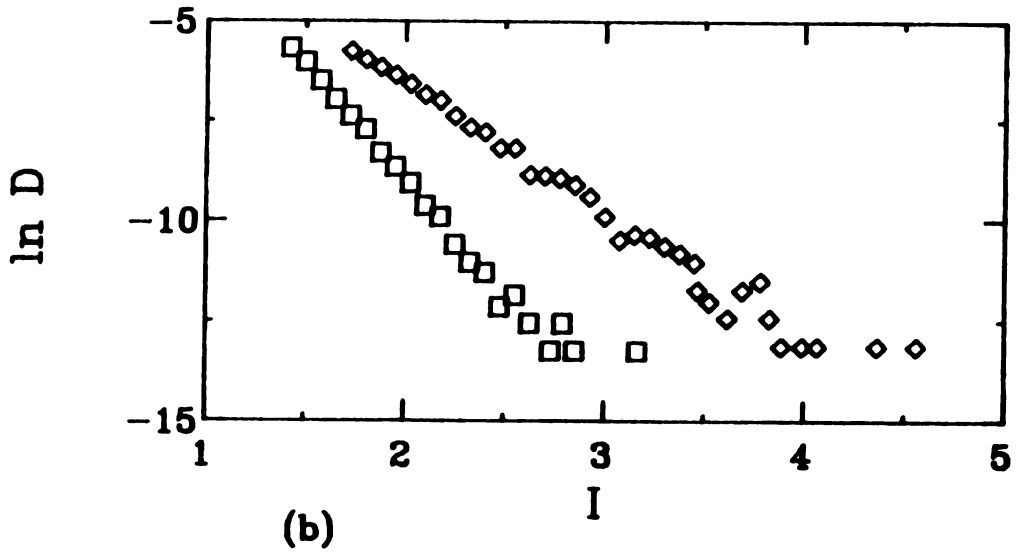

Fig.3.5 (a) The probability distribution of bond currents for the square-lattice random resistor network for p=0.90 (•) and p=0.80 (<>). The figure was constructed from 50 realizations of a 80x80 square lattice. (b) The data of (a) plotted on a log-linear scale to emphasize the exponential tail of the distribution function. If the tail of (a) is exponential, we expect the tail in this figure to be linear.

functions, one at the origin and one at a current 1A. This two-peak structure persists for defect fractions quite close to the percolation point. In this chapter we most interested in the tail of the distribution function, and, in particular, we expect the tail to be exponential in I, if the value $\alpha=1$ is correct in two dimensions. The bond-current distribution data in the tail of the distribution of Fig.3.5(a) is plotted to fall on a straight line if the tail is exponential, and , to the accuracy of the numerical data, it does.

The location of the largest current in the RRN also shows an interesting behavior as a function of the distance from the free edges of the network. This is shown in Fig.3.6(a) and 3.6(b) for L=50 and 90 RRN at p=0.90. These figures show that there is a greatly enhanced probability of finding the bond with the largest current near the surfaces of the network. This may be quantified by measuring the ratio

$$R(L) = P_{max}/P_{bulk}, \tag{3.21}$$

where, for L=50, P_{max} is the maximum of the curve in Fig.3.6(a) and P_{bulk} is an average over the central region of the same graph. R(L) appears to increase algebraically with system size, as shown in Fig. 3.7, which implies that with increasing system size the probability that the bond carrying the largest current, lies near the surface, increases.

The results depicted in Fig. 3.6 and 3.7 may be qualitatively explained on the basis of isolated defect-cluster arguments. The

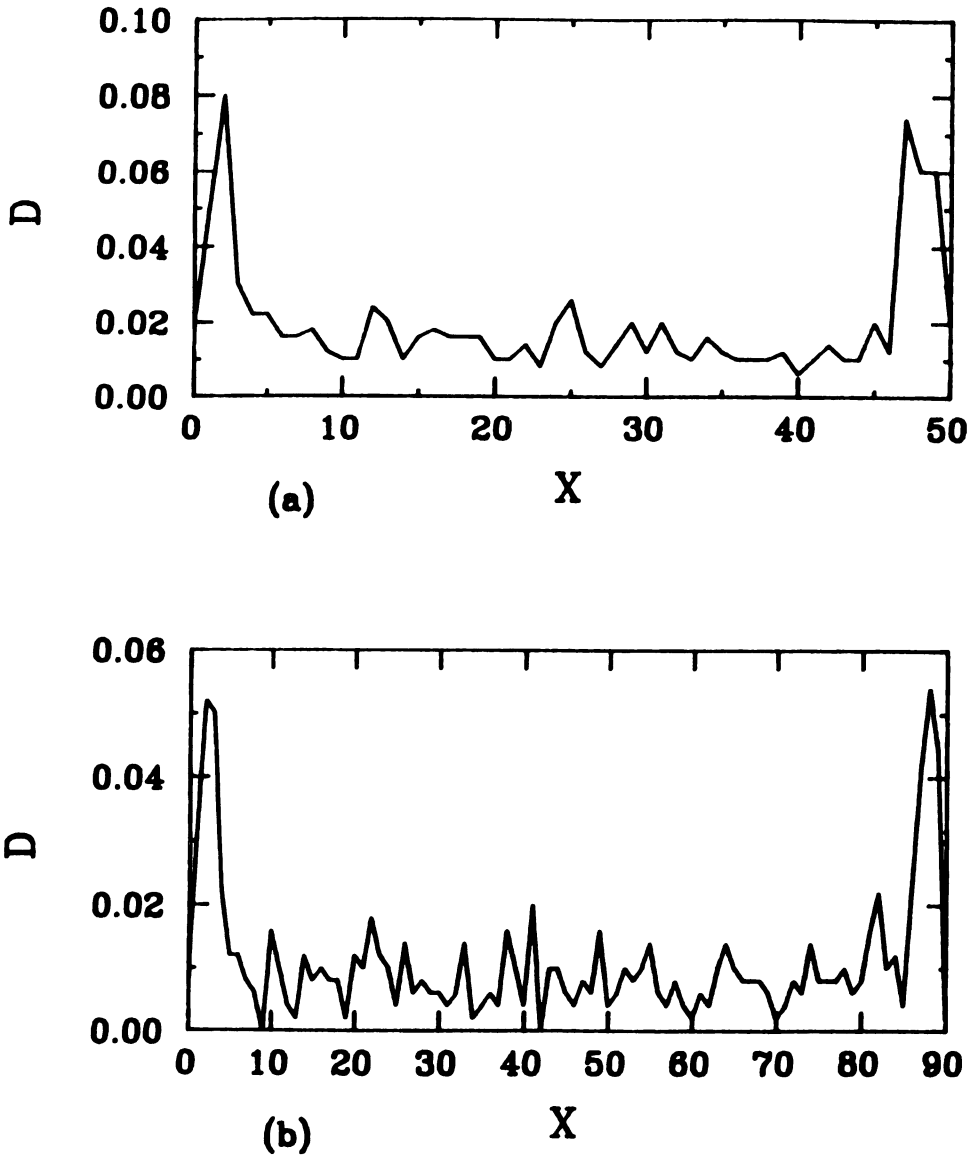

Fig.3.6 The probability D that a bond distance x from one free surface of a square-lattice RRN carries the largest current in the network. The distribution function was constructed from 500 realizations of RRN's at p=0.90 for (a) L=50 and (b) L=90.

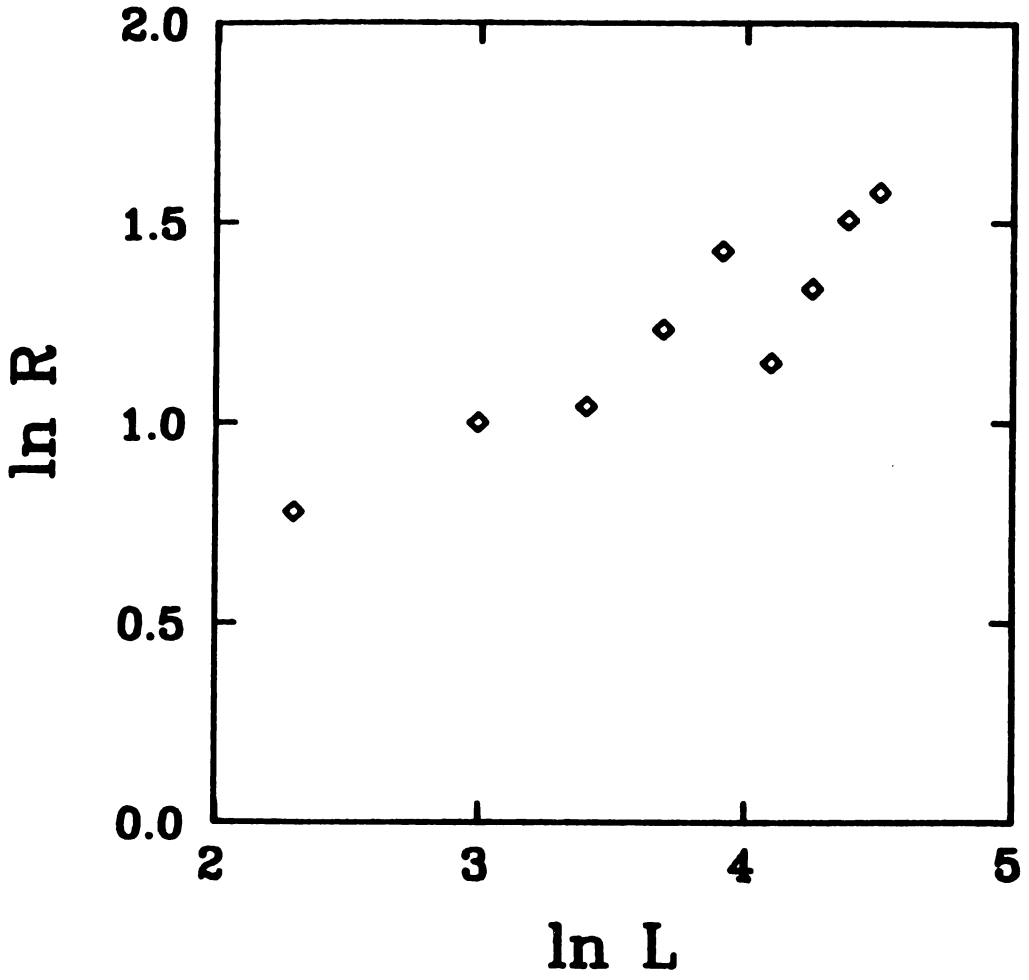

Fig.3.7 A plot of the ratio of the maximum of Fig.3.6 to the bulk average as a function of system size L, for L from 10 to 90 at p=0.90.

effect is reflected in a isolated-defect problem, in the statement that as the isolated defect is moved closer to a free boundary the current at its tip increases markedly. A graphical representation of this effect is also given in Fig.3.8 (rectangles), where the current at the tip of the defect of Fig.3.1(a) is monitored, as the defect is moved towards the edge of the system. A similar effect occurs for the defect of Fig.3.2(a), and is shown in Fig.3.8 (triangles), where the current in the bond at the center of the two cracks in Fig.3.2(a) is shown as a function of distance from the free edges of the network. From Fig.3.8 it is seen that defects close to the free edges of the networks lead to greater current enhancements than the same defects in the bulk. An approximation to the enhanced surface probability is to frame the question in a slightly different way. Namely, what size surface defect do we need to have to produce the same current as a reference defect in the bulk? In the case of the defect of Fig. 3.2(a) the defect at the surface needs to be about 3/4 (for an 80x80 lattice) the size of its bulk counterpart. One then finds for this type of defect cluster the following enhancement in finding the defect at the surface,

$$R = P_{surface}/P_{bulk}$$

$$\sim (1-p)^{-3\ln L/4[\ln(1-p)]}/(1-p)^{-\ln L/\ln(1-p)}, \qquad (3.22)$$

where we have used Eq.(1.19) and (1.20) in Chapter I to derive Eq. (3.22). We then find

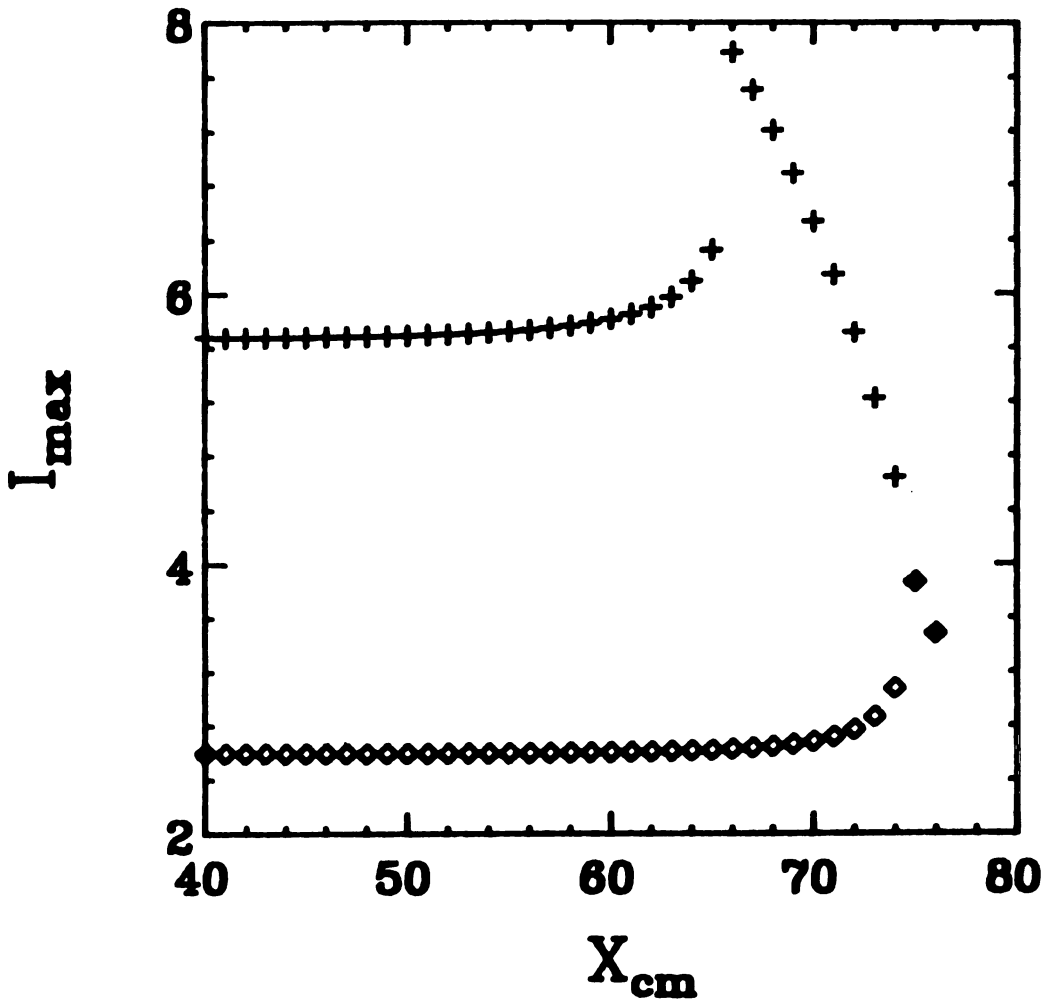

Fig.3.8 The effect on I_{max} of moving the defect of Figs. 3.1(a) (<>) and 3.2(a) (+) towards the free surface of the RBN. The calculation was performed on a 80x80 lattice, with nine bond defects. X_{cm} measures the center of the isolated defect, and the figure gives the size of I_{max} as a function of X_{cm}.

$$P_{surface}/P_{bulk} \sim L^{1/4}. \tag{3.23}$$

We expect that the qualitative behavior is correctly given by these arguments for general lattice dimensions and when the random distribution of defects is included into the network, but with a different exponent. From the results of simulations of the full network presented in Fig.3.7, we find this surface probability exponent, x, to be (at p=0.90)

$$R= P_{max}/P_{bulk} \sim L^{x}, \tag{3.24}$$

with

$$x=0.3\pm0.05. \tag{3.25}$$

Translated into breakdown language, the results of Eq.(3.24) and (3.25) suggest that cracks are often initiated near the surfaces of the sample. This is an effect that is often observed in both electrical and mechanical breakdown situations, but is usually attributed to extra surface defects or surface inhomogeneities. Although these probabilities do often occur in real situations, the results discussed above show that the presence of a free surface is of itself enough to induce a greatly enhanced probability of crack initiation in its vicinity.

III.4 Conclusions.

In this chapter we have studied the size and location of the largest current in a RRN. Our conclusions are follows.

(1) The largest current in a RRN, with fraction 1-p of zero-conductivity bonds, on length scales $L >> \xi_p$, has the scaling behavior $I_{max} \sim (\ln L)^{\alpha}$, while the size of the current in the failure-initiating bond has the scaling behavior $I_{com} \sim (\ln L)^{\beta}$. Analytic arguments place approximate bounds on α and β, as given in Eq.(3.3). Numerical simulations in two dimensions indicate that $\alpha \approx \beta \approx 1$.

(2) The probability of finding the bond with the largest current near the free surfaces of the network is much larger than that of finding the largest current in the bulk. This is quantified by ratio

$$R = P_{surface}/P_{bulk}$$

$$\sim L^{x}.$$

Numerical simulations suggest $x=0.30\pm0.05$ at $p=0.90$ in two dimensions.

The methods and results of this chapter can be used to study many other network models of breakdown, particularly, the brittle fracture and dielectric networks described in Chapter I.

CHAPTER IV

Comparison of Moduli and Breakdown Scaling — A Moment Spectrum Analysis

IV.1 Introduction.

In this chapter, we will study the origin of the very different scaling behaviors for transport and breakdown properties by analyzing the moment spectrum of the local load distribution. If a constant external electric field or stress is applied to an inhomogeneous material, the local stress or electric field shows strong spatial fluctuations[43,82,88-94]. The size of these local load fluctuations is quantified by a distribution function we call the local load distribution L(x). This distribution function has been intensively studied recently in the context of the voltage distribution at the percolation point, where it has been labeled multifractal[88,89,95]. In this chapter, we show that the moment spectrum induced by a random environment provides a useful concept in which to understand the differences between the scaling behavior characteristic of transport[10] and elastic[96-98] moduli and the very different scaling behavior characteristic of breakdown properties[5,41-46,49,99-101].

It is known that the effective conductivity of an inhomogeneous material is related to the second moment of L(x)[10], while the resistive noise is related to the fourth moment of this distribution[102-105]. In a similar way, properties such as elastic constant and thermal conductivity are related to the second moment of the appropriate local load distributions. By contrast, fracture strength, dielectric strength and other breakdown properties are initiated in regions where the local load is largest[5,41-46,49,99-101]. It is intuitively plausible, and in this chapter we give quantitative

evidence that, these load hotspots are related to the very high moments of the local load distribution. A study of the full moment spectrum thus allows us to understand in detail the crossover from low-moment scaling (transport properties, etc.) to high-moment scaling (hotspots and breakdown properties).

To study this crossover, we first focus attention on isolated cracklike flaws that most enhance local fields. The low-moment-to-high-moment crossover of systems containing such isolated cracks is discussed in section 2. To carry out the analysis, we need simple scaling forms for the local stress or electric field distributions near isolated cracks. These forms are derived in the Appendix B, and are summarized in Eq. (4.15) and (4.22).

When a distribution of flaws is present in a material, it is not possible to find the detailed form of the stress or electric field distribution. Despite this, we argue in section 3 that it is possible to estimate the point at which the crossover from low moment to extreme scaling occurs, by studying the form of the tail of the local load distribution. This analysis is carried out for systems with exponential, algebraic, and multifractal tails in L(x). A numerical illustration of these arguments is provided by calculating the moment spectrum as a function of dilution for two-dimensional random resistor networks. The results are displayed in Fig.4.3.

In section 4, we study numerically the origin of multifractal behavior in electrical breakdown problem by using random resistor networks. We find the local load (voltage) distribution change radically during the breakdown process, and that the narrow neck occurring just before failure generates a broad voltage distribution. This

broad voltage distribution leads to a multifractal scaling, and it even occurs in systems very near the pure limit. The precise form of the spectrum is sensitive to the initial randomness of the networks. Finally, we conclude this chapter in section 5.

IV.2 Moment Scaling due to an Isolated Cracklike Flaw.

As in the most traditional theories of mechanical fracture[48], consider an isolated crack of length, a, and with a curvature at the crack tip, κ, in an otherwise, homogeneous system with large volume $V = L^d$ ($a \ll L$). It is known that such an isolated crack (which is modeled as a cracklike void) makes negligible contribution to the overall conductivity[11-15] [see Eq. (1.6)], Σ_{eff}, i.e., that,

$$\Sigma_{eff}/\Sigma_0 \sim 1 - O(V_{inc}/V), \tag{4.1}$$

where Σ_0 is the background conductivity and V_{inc} is the volume of the inclusion. In contrast, such an isolated crack drastically reduces the electrical and mechanical strength of the system, as near the crack tip, strong load enhancements occur, and for the electrical case one finds[5,43,45,46,49],

$$E_{tip}/E_0 \sim (a/2\kappa)^{1/2} \quad (\text{for } a \gg 1),$$

which leads to an electrical strength of order

$$E_b(a)/E_b(0) \sim E_0/E_{tip} \sim (2\kappa/a)^{1/2} \quad (\text{for } a \gg 1) \tag{4.2}$$

where $E_b(a)$ and $E_b(0)$ are the electrical strength of the sample with a flaw in it and with no flaws respectively, and the electric field is applied perpendicular to the crack. Similar expression to Eq. (4.2) hold for the tensile strength of brittle materials with E_b and E_0 replaced by stresses, and with a different constant prefactor. The important scaling behavior that we want to emphasize is that in many materials electrical and mechanical strength decrease as the square root of crack length, while conductivity and elastic moduli have corrections of order (1/V) for $a \ll L$. The result in Eq. (4.2) is based on field intensity calculations. Fracture strength reduction due to cracks is most often discussed using energy balance arguments, in which the elastic energy reduction due to increasing crack length is balanced against the energy to form new fracture surfaces. For the linear elastic case this is a classical calculation, and leads to the (plane strain) Griffith's formula[50],

$$2\Upsilon = \pi \sigma_b^2 a/e \quad \text{which implies} \quad \sigma_b = (2\Upsilon e/\pi a)^{1/2} \tag{4.3}$$

where Υ is the energy needed to create new crack surfaces, while e is the elastic modulus of the background. An analogous result[51] is also available for the dielectric strength of a two dimensional insulator containing a long thin piece of metal (this is a dielectric "crack") oriented parallel to the direction of applied electric field. However, this analogy does not carry over to 3 dimensions where a penny shaped crack is most important for mechanical and electrical failure, while a finger-like defect is most important for dielectric failure.

In this chapter, we use stress and electric field intensity formalism, as they provide a framework in which to better understand the crossover from moduli scaling to breakdown scaling.

To demonstrate that the moment spectrum of the local load distribution contains Eqs. (4.1) and (4.2) as limiting cases, note that the maximum electric field occurring in a system may be written,

$$E_{max} \sim \langle E^m \rangle^{1/m}_{m\to\infty}, \tag{4.4a}$$

so that

$$E_b(\text{flawed system})/E_b(0) \sim \langle E_0 \rangle / \langle E^m \rangle^{1/m} \quad \text{as } m\to\infty. \tag{4.4b}$$

For the case of insulating inclusions, it can be seen that the effective conductivity is related to the second moment of the electric field distribution by noting that the power P

$$P = VE_0^2\, \Sigma_{eff} = \int E^2 \Sigma(r) dV = \Sigma_0 \langle E^2 \rangle V, \tag{4.5}$$

so that

$$\Sigma_{eff}/\Sigma_0 = \langle E^2 \rangle / \langle E_0^2 \rangle. \tag{4.6}$$

Comparing Eqs. (4.4b) and (4.6), it is seen that study of the function

$$R_m = \langle E_0 \rangle / \langle E^m \rangle^{1/m} \tag{4.7}$$

provides a simple quantity that typifies the crossover from low-moment to extreme moment scaling as a function of m. For a system containing an isolated crack, this quantity shows a crossover from O(1/V) corrections when m is small to the typical breakdown scaling of Eq.(4.3) when m becomes large. We now study this crossover analytically for electrical, mechanical, and dielectric systems containing an isolated crack.

Consider an isolated cracklike elliptical void in the geometry shown in Fig.4.1. In elliptic coordinates, ξ, η,

$$x=c\cosh\xi\cos\eta, \quad z=c\sinh\xi\sin\eta \tag{4.8}$$

with the ellipse equation being

$$x^2/a^2 + z^2/b^2 = 1 \tag{4.9}$$

and

$$c^2 = a^2 - b^2$$

and the electric field applied in the z direction has amplitude E_0 far from the ellipse. Solving Laplace's equation in elliptical coordinates yields the electric potentials,

$$\phi_{in} = -Ac\sinh\xi\sin\eta \tag{4.10a}$$

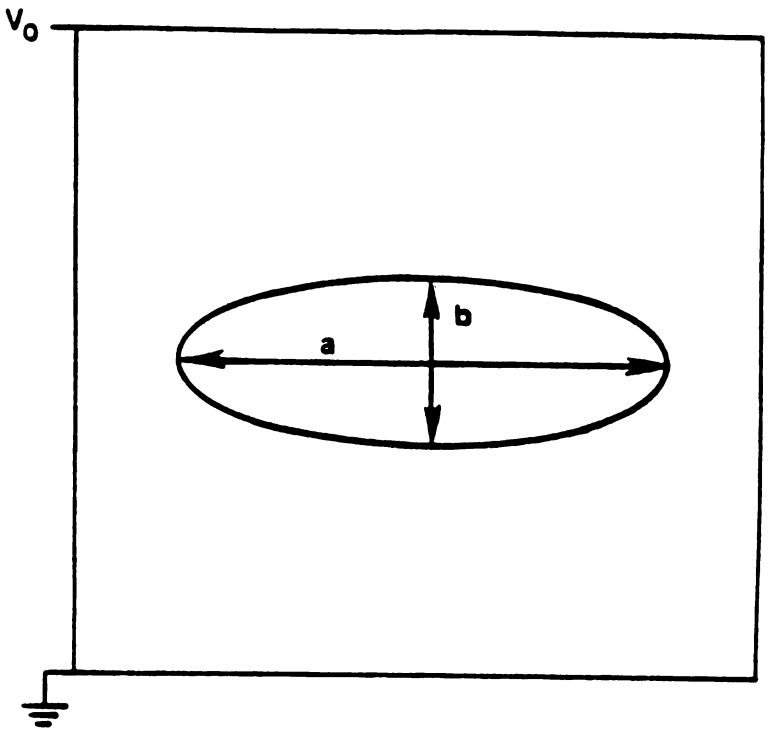

Fig.4.1 The geometry of the two-dimensional ellipse problem.

$$\phi_{out} = -E_0 c \sinh\xi \sin\eta + Be^{-\xi}\sin\eta \qquad (4.10b)$$

with

$$A=E_0(a+b)/B, \quad B=-E_0 a(a+b)/c \qquad (4.10c)$$

The electric fields are then given by

$$E_\xi = -(1/\tau)\partial\phi/\partial\xi, \quad E_\eta = -(1/\tau)\partial\phi/\partial\eta \qquad (4.11)$$

where

$$\tau = c(\sinh^2\xi + \sin^2\eta)^{1/2} \qquad (4.12)$$

The full expression for the electric field moments is given by

$$\langle E^m\rangle = (1/V)\int_V (E_\xi^2 + E_\eta^2)^{m/2} dV \qquad (4.13)$$

It is known that the second moment (m=2) and inclusion energy scale as

$$\langle E^2\rangle/\langle E_0^2\rangle \sim 1 + O(1/V) \qquad (4.14)$$

the corrections to the conductivity due to the isolated crack are related to the second moment [see Eq. (4.6)], and this implies Eq. (4.1) for a single crack. We have not been able to analytically evaluate Eq. (4.13) for any m>2, but the important scaling behavior may be

found by noting that the electric field as a function of radial distance parallel to the major axis of the ellipse behaves as shown in Fig. 4.2 (a). The important scaling behavior that occurs in this figure is summarized mathematically by (see Appendix B)

$$E_z(r)/E_0 \sim \begin{cases} 1 + \alpha_{2e}/r^d & \text{for } r>>a \quad (4.15a) \\ c_{1e} + c_{2e}(a/2r)^{1/2} & \text{for } \kappa<r<a \quad (4.15b) \\ k_{1e} + k_{2e}(a/2\kappa)^{1/2} & \text{for } r<\kappa \quad (4.15c) \end{cases}$$

where α_{2e} is a dipole moment for the two-dimensional problem of a crack in a resistive background, κ is the crack tip curvature ($=b^2/a$) for an ellipse, and c_{1e}, c_{2e}, k_{1e} and k_{2e} are constants for the two-dimensional (2D) electrical problem. In fact, the scaling behavior of Eq. (4.15) is highly universal, and applies (with different α, c, and k) to ellipse, ellipsoidal, and slitlike cracks in 2D and 3D linear elastic (plane stress) and electric problems (see Appendix B). This is illustrated for the 3D elastic problem in Fig.4.2(b) where the z-direction stress is plotted as a function of radial distance from the tip of an oblate ellipsoidal void (in the x-y plane). Again, the near-field square-root behavior crosses over to a far-field dipole form, in agreement with Eq. (4.15). As seen from Eq. (4.15b), an important singular behavior occurs near the crack tip, and the angular dependence (to x axis) of this singular behavior is

$$\begin{aligned} E_r(r,\theta) &\sim E_0(a/2r)^{1/2}\sin(\theta/2), \\ E_\theta(r,\theta) &\sim E_0(a/2r)^{1/2}\cos(\theta/2) \end{aligned} \qquad (4.16)$$

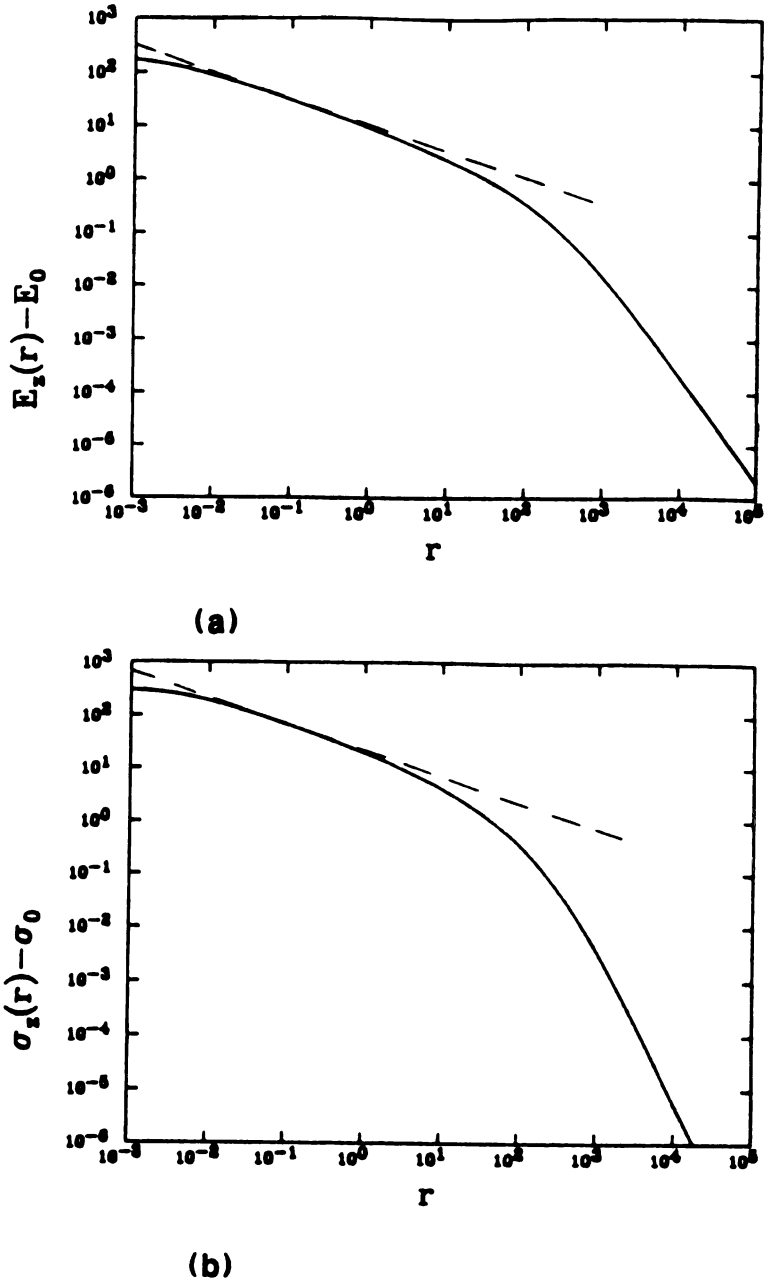

Fig.4.2 (a) The (z=0) electric field, $E_z(r)$, as a function of distance from the tip of an ellipse (a=200, b=1). The mathematical form of the scaling behavior in $E_z(r)$ is given in Eq. (4.15) of the text. (b) The z=0 stress field, $\sigma_z(r)$, as a function of r for an oblate ellipsoid (a=200, b=1) in an elastic background. The dashed line has slope $-\frac{1}{2}$.

for θ small. This more general form does not, however, change the moment scaling behavior derived below, and henceforth we use Eq. (4.15) in our scaling analysis. The most important physical observation is that as the moment value is increased, the regions (4.15b) (4.15c) increase their contribution to the integral (4.13). This is explicitly seen by subdividing and approximating the integral (4.13) as shown below

$$V \langle [E(r)/E_0]^m \rangle \sim \int_{r>a} r dr \, (1+a_{2e}/r^2)^m$$

$$+ \int_{\kappa<r<a} r dr \, [c_{1e}+c_{2e}(a/2r)^{1/2}]^m$$

$$+ \int_{r<\kappa} r dr \, [k_{1e}+k_{2e}(a/2\kappa)^{1/2}]^m \qquad (4.17)$$

keeping the most singular terms in each integral, we find,

$$\langle [E(r)/E_0]^m \rangle \sim 1 + mO(V_{inc}/V) + (a/2\kappa)^{m/2}\kappa^2/V \qquad (4.18)$$

where V_{inc} is the volume of the inclusion. The $O(V_{inc}/V)$ term is estimated by considering the leading term in the first integral, and including the correct angular terms. This is necessary, as this term is a dipole integral, in which care must be taken to ensure that all terms are included, and that boundary terms do not produce unphysical results. The result is a term of order the inclusion energy, which leads directly to the result quoted.

From Eq. (4.18), we can see that R_m [see Eq. (4.7)] has the following scaling forms:

$$R_m \sim \begin{cases} 1 - O(V_{inc}/V), & m \ll m_c, \\ (2\kappa/a)^{1/2}, & m \gg m_c, \end{cases} \tag{4.19}$$

where m_c is found from

$$(a/2\kappa)^{m/2}\ \kappa^2/V \sim 1 \tag{4.20}$$

or

$$m_c \sim 2\ln(V/\kappa^2)/\ln(a/2\kappa). \tag{4.21}$$

Due to the universality of Eq. (4.15), this result straightforwardly generalizes to three-dimensional electric problems and to elastic problems in two and three dimensions.

There is also a great deal of similarity between the problem of an insulating crack in a conducting background and the problem of a conducting crack in an insulating background. The former problem has been discussed as the simplest example of an electrical breakdown problem[5,41-46,49,99-101], while the latter is the simplest starting point for understanding defect-induced dielectric breakdown[5,41-46,49,99-101]. It is well known that in two dimensions, the electric field enhancement at the tip of a metal ellipse oriented parallel to the applied electric field in an insulating background, is the same as that at the tip of a void inclusion oriented perpendicular to the applied field and in a conducting background (see the Appendix B). The asymptotic form (4.15) then applies equally well to the

dielectric problem in two dimensions, and hence that Eqs. (4.17)-(4.21) express the moment scaling appropriate to that problem. The dielectric problem is different in three dimensions, however, as there the most important cracklike defect is a fingerlike inclusion[5,41-46,49,99-101], which induces the following electric field behavior near its tip (for detail calculation, see Appendix B):

$$E_z(r)/E_0 \sim \begin{cases} 1 + \alpha_{3d}/r^3 & \text{for } r>a \\ \ln(r/2a) + a/2r & \text{for } \kappa<r<a \\ 1 + (a/b)^2/\ln(2a/b) & \text{for } r<\kappa \end{cases} \tag{4.22}$$

in this case the integration over the region near the crack tip leads to

$$V\langle[E(r)/E_0]^m\rangle \sim \int_a^L r^2 dr\ (1+\alpha_{3d}/r^3)^m + \int_\kappa^a r^2 dr[\ln(r/2a) + a/2r]^m + \kappa^3[1 + (a/b)^2/\ln(a/b)]^m, \tag{4.23}$$

so that

$$\langle[E(r)/E_0]^m\rangle \sim 1 + mO(V_{inc}/V) + (a/2\kappa)^m\kappa^3/V \tag{4.24}$$

The moment value at which crossover between low-moment scaling and extreme scaling occurs is then given by

$$m_c \sim \ln(V/\kappa^3)/\ln(a/2\kappa). \tag{4.25}$$

For extremely sharp cracks ($\kappa \to 0$), it is seen from Eqs. (4.18) and (4.24) that if κ becomes sufficiently small, a singular behavior can occur for low-moment values. For the problems described by Eq. (4.18) this moment value is

$$m_{c1} = 4 \tag{4.26}$$

while for the 3D dielectric problem [see Eq. (4.24)],

$$m_{c1} = 3 \tag{4.27}$$

For $m > m_{c1}$, moments are affected by extremely sharp cracks, and in fact these moments are singular as $\kappa \to 0$.

IV.3 Systems with Flaw Distributions.

In this section, we consider systems with a distribution of voids. These voids are randomly distributed and may have any shape. When such a distribution of flaws is present in a material, a distribution of local loads is induced. The point at which extreme scaling sets in, is determined by the form of the tail of the local load distribution L(x). In this section we consider exponential, algebraic, and multifractal load distribution tails. A specific illustration of our results is provided by numerical studies on random resistor networks.

A. Exponential tails in L(x) -- $p > p_c$ random resistor networks

When the dilution, f=1-p, is small, the distribution of bond currents (and hence voltages) in the 2D LxL random resistor network is known to be exponential[43]. In this case, the largest current in a system of size L^d is of order $I_{max} \sim \ln L$, and for a fixed applied current of L amps, the high moments of L(I) are then approximated by

$$\langle I^m \rangle \sim A \int^{I_{max}} I^m \exp(-AI)\, dI \qquad (4.28)$$

This is true as long as $m/A \gg 1$, and $A \sim -\ln(1-p)$ for p small. As p approaches p_c, A becomes small, and a multifractal bond current distribution must be considered[88,89]. This integrand in Eq. (4.28) has a maximum at $I_{peak} \sim m/A$, after which it decays exponentially. If this peak lies far above the upper limit of the integral in Eq. (4.28), the algebraic term dominates, and the integral is approximated by

$$\langle I^m \rangle \sim (\ln L)^{m+1}/(m+1) \quad \text{for } m > m_c \sim \ln L \qquad (4.29)$$

so that

$$\langle I^m \rangle^{1/m} \sim \ln L \sim I_{max} \qquad (4.30)$$

Thus, for $m > m_c \sim \ln L$, moments drawn from an exponential local load distribution exhibit extreme scaling,. For $m < m_c$ the full integral in Eq. (4.28) must be calculated, and that in this regime the systems exhibit low-moment scaling. To illustrate the crossover from low-moment

to high-moment scaling numerically, we present in Fig.4.3 these moments calculated for 100x100 random resistor networks for a range of values of p. In these calculations we find $\langle I_0 \rangle / \langle I^m \rangle^{1/m}$ for fixed external supplied current as a function of p. As in the single crack case, $m \to \infty$ yields a crossover to breakdown scaling, while low moments are nonsingular near the pure limit, as is the conductivity. A plot of these moments as a function of system size is shown in Fig.4.4, where it is seen that low moments saturate at a finite value for large system sizes, while extreme moments continue to decrease logarithmically as a function of system size (this is the characteristic "size effect" of breakdown in random media). Since $m_c \sim \ln L$, we find that each moment has a critical length associated with it, and that this critical length is given by $L_c \sim \exp(m)$. For $L > L_c(m)$, the moments show the $1/\ln L$ size effect characteristic of breakdown. In this sense, the breakdown limit is a critical point in moment space at which $L_c \to \infty$ exponentially.

B. Algebraic tails in L(x).

Consider a bond current distribution which is algebraically decaying in I and depends on a single exponent s. The current moments are then given by

$$\langle I^m \rangle \sim \int^{I_{max}} I^{m-s} \, dI \qquad (4.31)$$

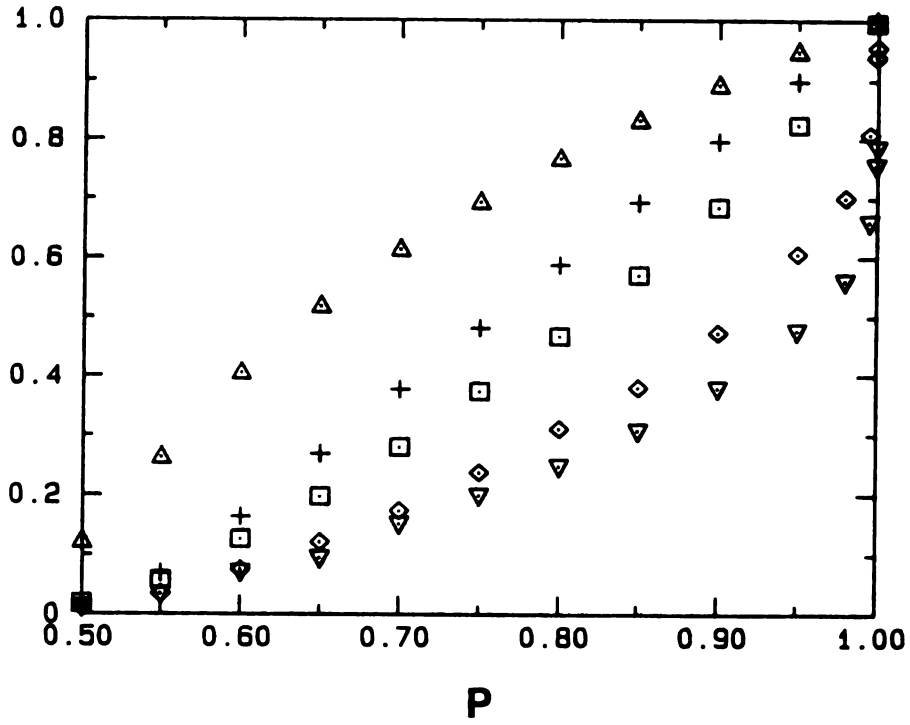

Fig.4.3 Moment scaling as a function of dilution for 100x100 square lattice random resistor networks. $\langle I_0 \rangle / \langle I^m \rangle^{1/m}$ is plotted on the vertical axis for m=2 (Δ); m=12 (□); m=30 (◇); I_b (▽). For comparison the conductance is also plotted (+).

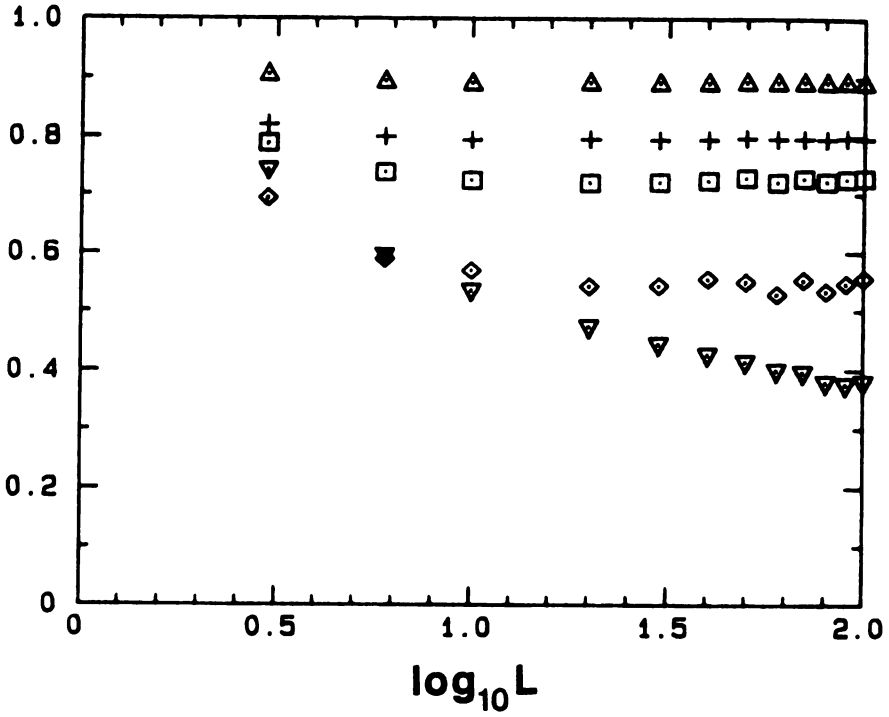

Fig.4.4 $\langle I_0 \rangle / \langle I^m \rangle^{1/m}$ as a function of system size for p=0.90 random resistor networks, for m=2 (Δ); m=10 (□); m=20 (<>); I_b (∇). For comparison the conductance is also plotted (+).

I_{max} is found from

$$I_{max}^{-s} L \sim 1,$$

which implies

$$I_{max} \sim L^{1/s} \tag{4.32}$$

Evaluating the integral gives,

$$\langle I^m \rangle \sim (L^{(m-s+1)/s} - 1)/(m-s+1) \tag{4.33}$$

For m>s-1, the first term in the parentheses dominates, and

$$\langle I^m \rangle \sim L^{x(m)/\nu} \qquad \text{for } m>s-1, \tag{4.34}$$

where

$$x(m) = (m-s+1)\nu/s, \tag{4.35}$$

Here ν is the percolation correlation exponent and is included in the definition of x(m) for comparison with systems having a multifractal local load distribution (e.g., the percolation problem at p_c). From Eq. (4.34), we see that

$$\langle I^m \rangle^{1/m} \sim I_{max} \sim L^{1/s} \tag{4.36}$$

provided m>>s-1. That is, the bigger s is, the more slowly the cross-over to extreme scaling occurs. As $s \to \infty$ the distribution becomes exponential, and $m_c \sim \ln L$ applies.

C. Multifractal L(x).

In this case, it is known that a moment scaling like that of Eq. (4.34) occurs, but that x(m) is nonlinear in m [we note in passing that a plot of Eq. (4.33) also looks nonlinear in m]. However, for large enough m, the multifractal spectrum does become linear in m, and once this has occurred, the moment scaling is strongly affected by large currents. However, breakdown scaling does not become dominant until the condition m>>s prevails. In the multifractal case, s is the exponent one would get if the asymptotic linear behavior in the multifractal spectrum were extrapolated back to the origin. For the percolation problem it is seen from the data of Ref. 89 (Fig. 6) that $s \sim 4$, so that extreme scaling and low-moment scaling become identical for moments in the part of the multifractal spectrum that is both linear and satisfies m>>4.

IV.4 Multifractal Spectrum induced by Crack Pattern.

An interesting fact is that the propagating crack induces multifractal behavior in the moment spectrum just prior to eventual failure[106,107]. In this section, we study numerically this multifractal behavior in electrical breakdown problem by using the deterministic crack propagation model in random resistor networks. We

clarify the origin of this multifractal behavior by showing that a propagating crack even in a nearly pure system always exhibits this effect, but that the form of the multifractal spectrum is sensitive to the amount of initial disorder.

To study this effect, we generate a two-dimensional random resistor network of size L with fraction of (1-p) bonds removed. We grow a crack pattern in this network using the hottest bond algorithm (see the breakdown procedure described in chapter I). A typical sequence of the external voltage that induce failure in the hottest bond in the network with L=100 and p=0.70 is displayed in Fig. 1.7.

Next, the voltage distribution is calculated. Here, we are interested in the voltage distributions at three different breakdown stages. They are the voltage distribution of initial networks, at voltage V_b and just before breaking the last bond. From these voltage distributions, we calculated the average moments M_m, which are defined as,

$$M_m = \Sigma\, n(V)\, V^m \qquad (4.37)$$

where n(V) is the number of bonds carrying voltage drop V. By the scaling relation $M_m \sim L^{-P(m)/\nu}$, we calculated the moment exponents $P(m)/\nu$ for a range of m values.

In order to check our program, we first did these calculations for the networks with p=0.50 (percolation threshold p). They show a multifractal scaling, as in other calculations[88-90]. The various moment exponents $P(m)/\nu$ are consistent with previous calculations[88,89] at $p=p_c$, as shown in Fig.4.9.

It is obvious that at p_c the network structures at the three different breakdown stages -- initial, at V, and before breaking the last bond -- are almost the same. This leads to three similar multifractal voltage distributions in this case. But for $p>p_c$, there are many parallel paths to channel current in the initial network. As more bonds break, we cut more current channels. Finally, there is one single link remaining in the network structure and this induces a radical change in the voltage distribution. This is illustrated in Fig. 4.5, where we have plotted the current distributions for 40x40 networks with p=0.90. Since N_1 (the number of broken bonds at voltage V_b) is very small for all p, there is no significant lattice structure change at V_b. We therefore expect a similar voltage distribution at this stage, as shown in Fig. 4.5(a) and 4.5(b). In both of these figures, the distribution has a sharp peak and a exponential tail[43]. Therefore, for various moments,

$$M_m = \int V^m P(V) dV \tag{4.38}$$

the large V tail in P(V) gives small contributions, and there is a strong dominance in this integral due to the sharp peak. This implies that there is one characteristic voltage which is responsible for the scaling behavior for all moments. Thus, there should be a constant-gap scaling behavior for the voltage distributions at these two stages. But, just before breaking the last bond, there is a very broad peak and a long tail in the voltage distribution as shown in Fig. 4.5(c). There exists a competition between V^m and P(V) in Eq. (4.38) and this long tail gives a larger contributions for higher

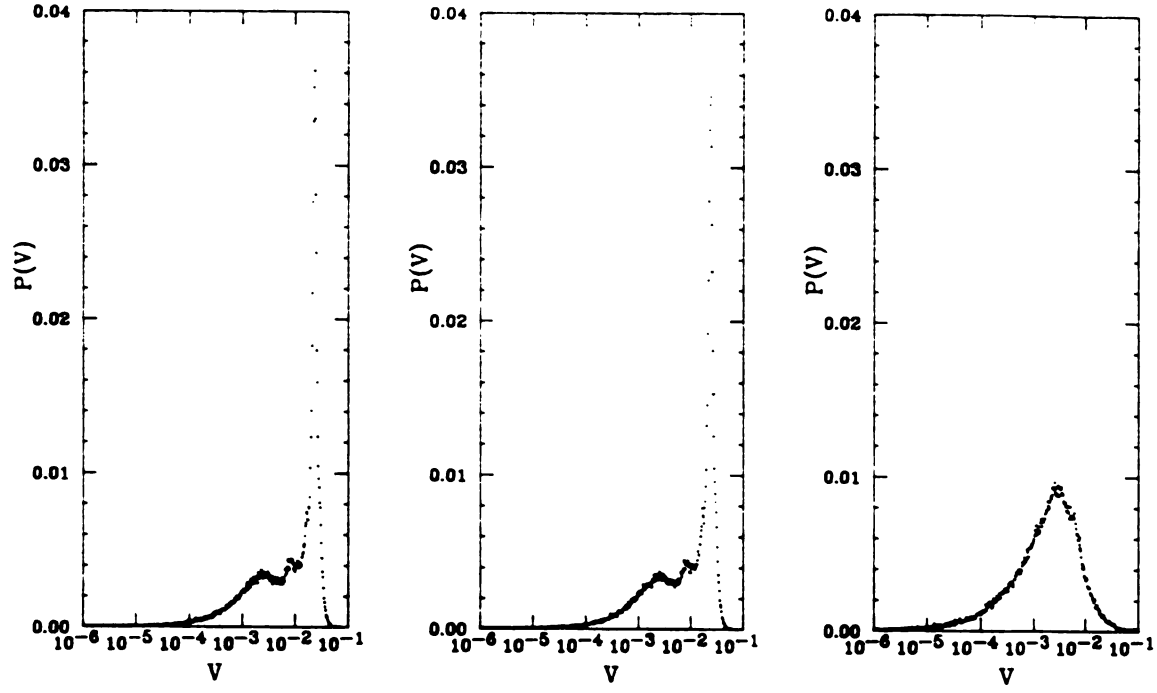

Fig.4.5 The voltage distribution for square random resistor networks at p=0.90. These figures were constructed from 100 realizations of an 40x40 square lattice. (a) is the distribution for the initial networks, (b) is at the maximum voltage V_b and (c) is just before breaking the last bond.

moments. This leads to a set of different characteristic voltages for various voltage moments, i.e., multifractal scaling behavior occurs.

In order to quantify this, we calculated the average moments, M_m, as a function of the system size L, for a range of m values. Typically, the calculations are averaged over 2000 samples for L=5; 500 samples for L=10, 20, 30 and 50; and 50 samples for L=80 and 100. To demonstrate that each moment scales independently as a function of L, we consider the normalized moment $M(m) = [M_m / M_0]^{1/m}$. If there exists a constant-gap exponent in the scaling behavior of the successive moments, then all the M(m) should scale identically. In Fig. 4.6 and Fig. 4.7, we plot the behavior of M(m) for three breakdown stages at p=0.90, and p=0.70. Constant gap scaling is clearly seen in the data for the initial configuration and at V_b [in figure (a) and (b)], while multifractal behavior occurs just before breaking the last bond [in figure (c)].

The presence of one or more single link bonds in all of the networks showing multifractal behavior suggests that this is the origin of the multifractal behavior. In order to confirm this, we generate 1000 LxL (for a set of L values in the range from 5 to 100) p u r e resistor networks with a single link bond in a random position inside each network. We calculate the voltage distribution of these systems. A broad peak and a long tail are found in these voltage distributions. As shown before, this suggests that there exists a multifractal behavior in these systems. In Fig. 4.8, the normalized moment M(m) for these systems is displayed and it does show a multifractal scaling. In contrast to the random resistor networks, these systems are weakly disordered. This implies that multifractal

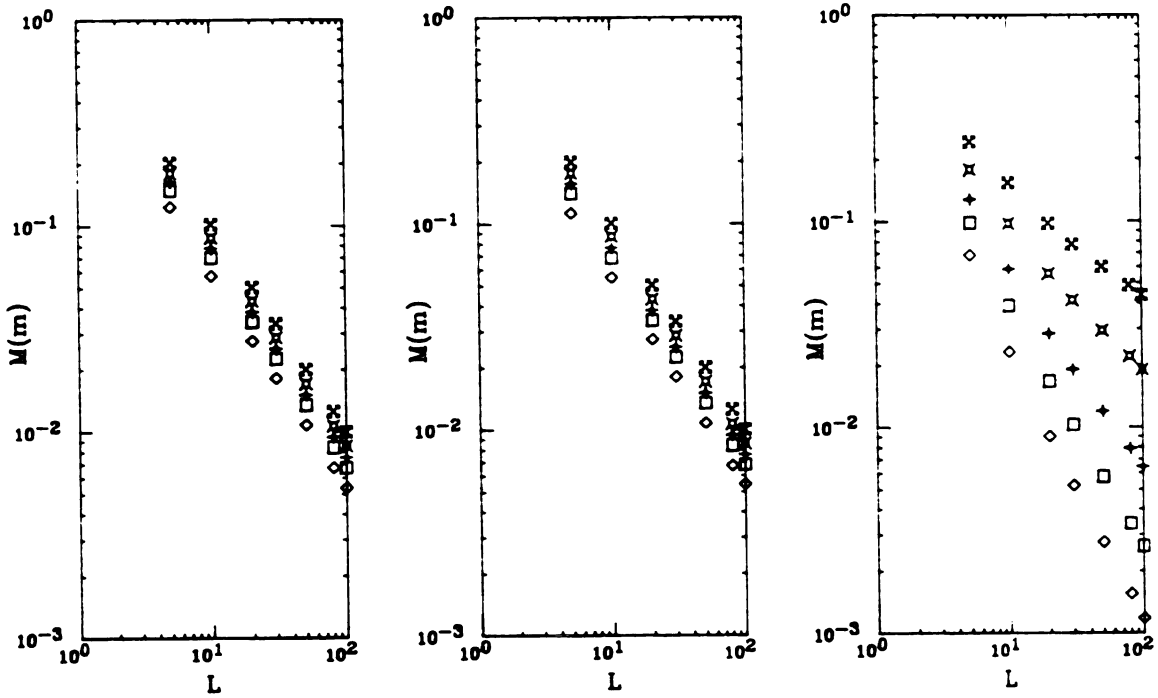

Fig.4.6 Double logarithmic plot of $M(m) = [\Sigma\, n(V)V^m/\Sigma\, n(V)]^{1/m}$ as a function of system size L at p=0.90 and for m=1 (<>), m=2 (□), m=3 (+), m=5 (o) and m=9 (x). (a) and (b) are for initial networks and networks at V_b, the data fall on parallel lines showing constant-gap scaling. (c) is for the networks just prior to failure. The different slopes show a non-constant-gap scaling.

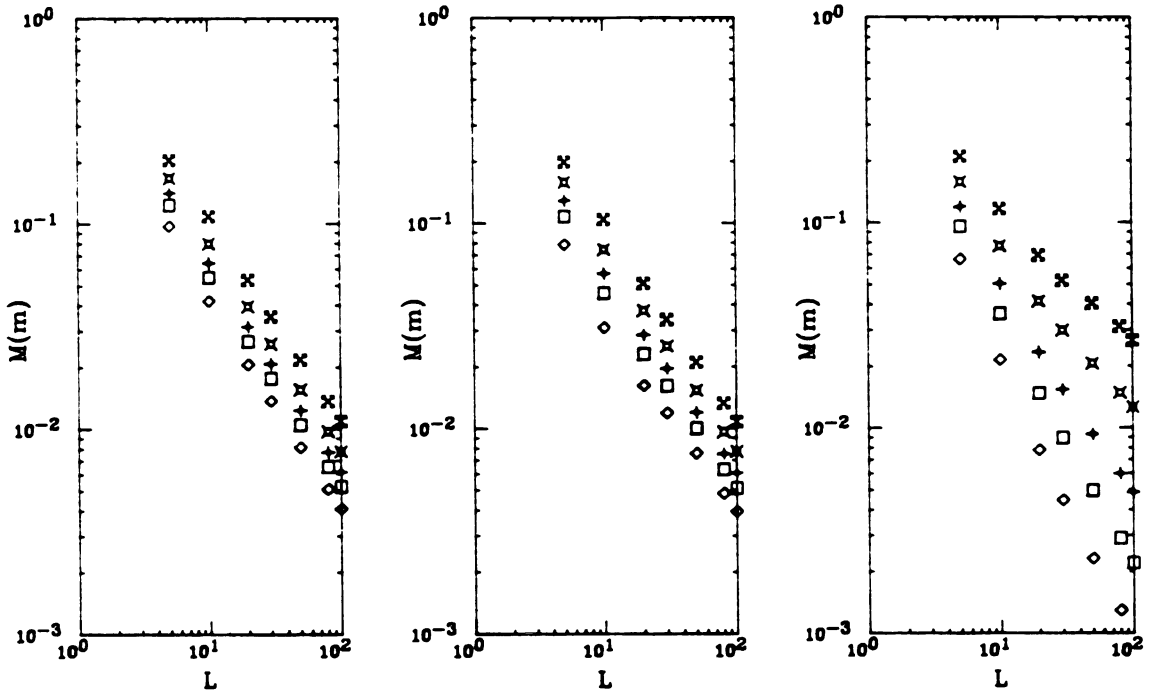

Fig.4.7 The same plot as in Fig.4.6 at p=0.70 and m=1 (<>), m=2 (□), m=3 (+), m=5 (o) and m=9 (x).

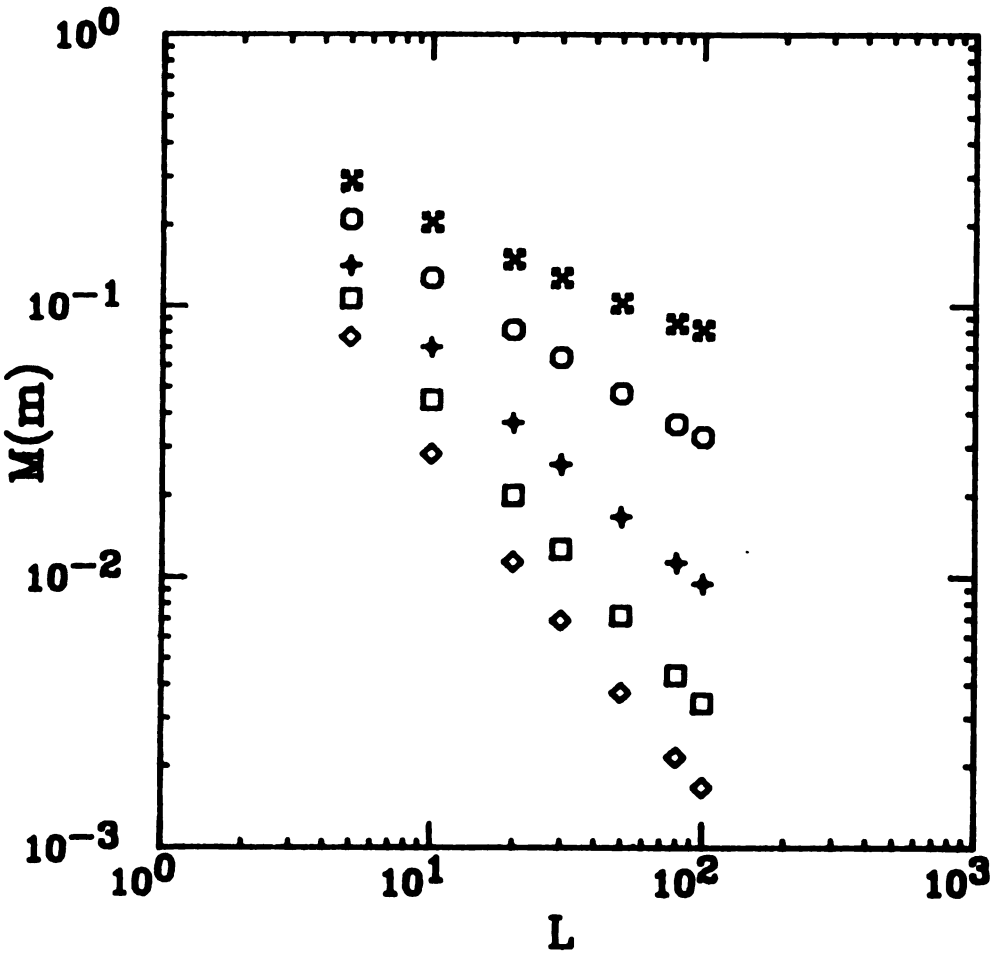

Fig. 4.8 Double logarithmic plot of M(m) as a function of size L for the nearly pure networks and m=1 (<>), m=2 (□), m=3 (+), m=5 (o) and m=9 (x). The data suggest a non-constant-gap scaling.

scaling behavior can even occur in systems very near the pure limit.

In Fig. 4.9, we plot the exponents $P(m)/\nu$ as a function of m for various systems. The curvature in small m region suggests a nonlinear relation between $P(m)/\nu$ and m. It becomes linear as $m \to \infty$. As shown in the figure, the slopes decrease as the systems become less disordered. It is consistent with the fact that the strongly disordered system has a small conductivity. This is because the large m slope is expected to give the conductivity exponent[88,89]. The value of the intercept of this line (as $m \to \infty$) with the vertical axis gives the fractal dimension of the single link bonds. From this figure, we can see that this fractal dimension decreases from the value $1/\nu = 0.75$ at $p=0.50$ to 0 for the nearly pure systems. The very different values of $P(m)/\nu$ for various systems in this figure is due to the different geometric structures of the networks in this problem.

In general, we believe that the origin of the multifractality of the voltage distribution just before the systems breaks is due to current channelling through narrow necks. To illustrate the generality of this idea, we did similar calculations for the fractal-like dielectric breakdown problems by using the stochastic dielectric breakdown model[108-110]. This model has been used to study the fractal dimension of dielectric breakdown pattern[108-110] and submarine cable damage[111-113]. The structure of the breakdown pattern is often fractal[108-126] and is very different from that occurs in the random resistor models. Here, the calculation was carried on an LxL square lattice with potential V=0 along the discharge pattern and V=1 at the top of the lattice. The probability p_i to add the segment i connected to the pattern is related to the local potential drop V_i,

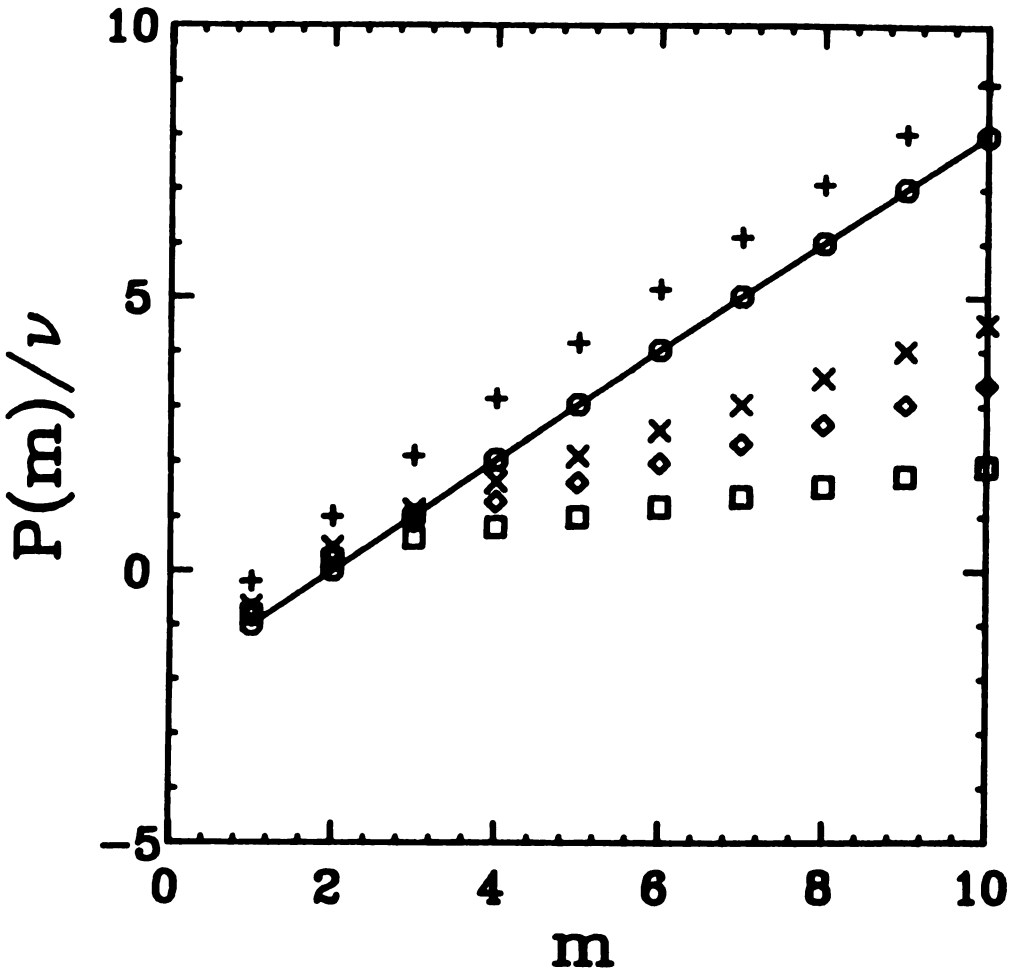

Fig.4.9 Plot of the various exponent P(m)/ν as a function of m, p=0.50 (+), p=0.70 (x), p=0.90 (◇) and nearly pure systems (□). For comparison, the exponent P(m)/ν for constant-gap scaling (p=0.90 initial network) is also shown (o). The straight line is added as a guide ti the eye.

$$p_i \propto V_i \tag{4.39}$$

In Fig. 4.10, we show a final breakdown pattern for a 40x40 lattice and it has a fractal structure. The moment spectrum calculated just before breaking the last bond is shown in Fig. 4.11. As seen from this figure, the moment spectrum is again multifractal as expected from our previous discussion.

In conclusion, we have studied the origin of multifractal behavior in the breakdown of random resistor networks and flawed dielectrics. We found that during the breakdown process the voltage distribution changes its behavior and that just prior to failure the distribution has a multifractal structure. Multifractality originates from the broad voltage distribution produced by even a single narrow neck, but the precise form of the multifractal spectrum depends on the initial disorder, as is seen from Fig. 4.9.

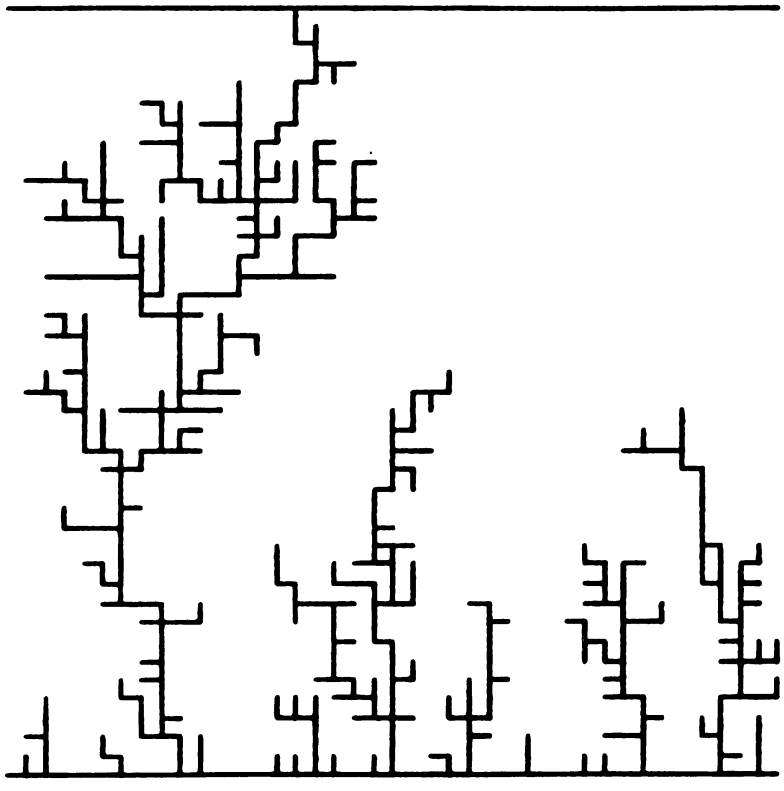

Fig. 4.10 A final breakdown pattern for a 40x40 square lattice. It is a fractal structure with fractal dimension D = 1.75.

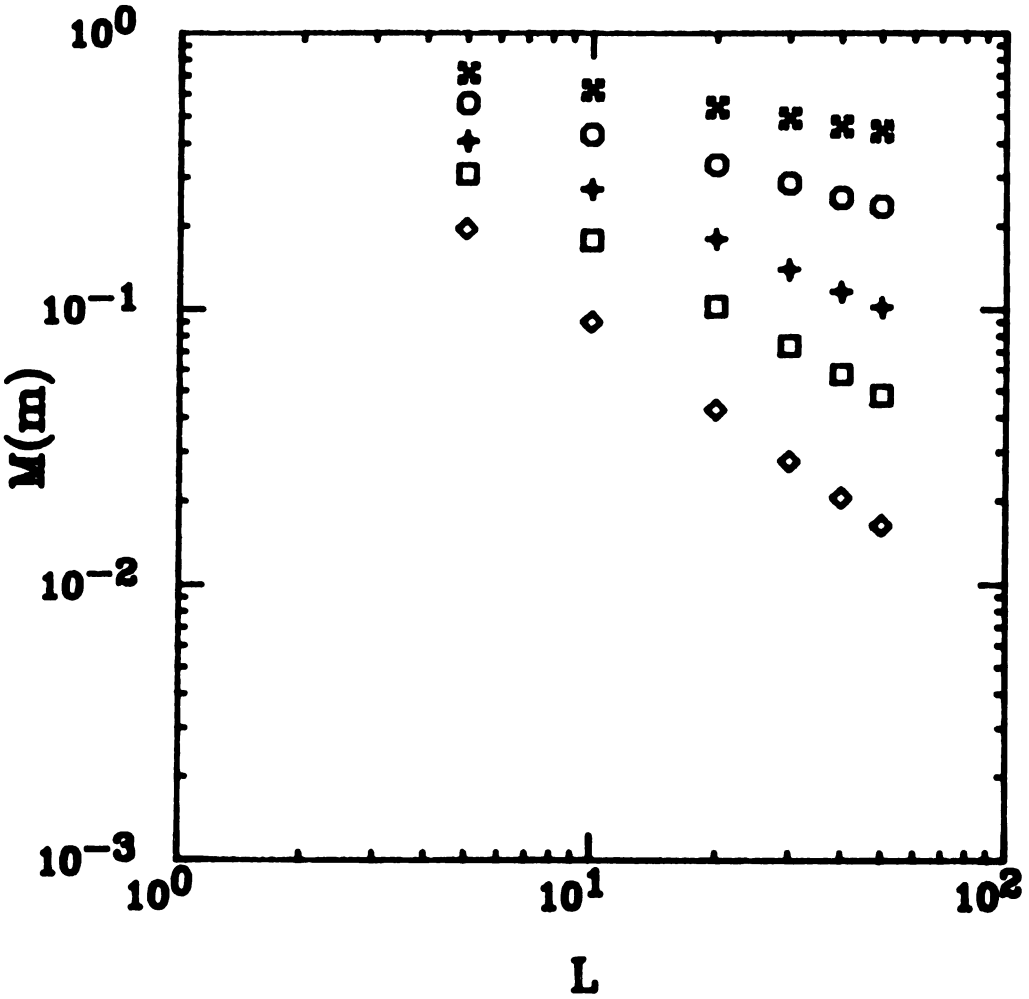

Fig. 4.11 Double logarithmic plot of M(m) as a function of size L for stochastic dielectric breakdown models. m=1 (<>), m=2 (□), m=3 (+), m=5 (o) and m=9 (x).

IV.5 Conclusion.

1) We show that the strength of brittle systems is related to the very high moments of the distribution of electric or stress fields occurring in a material. By contrast, as is well known, elastic or transport moduli are related to the second moment of such distributions. We define a quantity related to the moment spectrum that interpolates between low moments (such as moduli) and extreme moments (such as breakdown properties), and show that for most cleavage cracks and for diluted networks away from p_c, a crossover from low moment scaling to high moment scaling occurs at a critical moment value that scales as $m_c \sim \ln V$, where V is the system size. For especially sharp cracks, however, this crossover may occur as low as the third (3-D dielectric) or fourth moment.

2) The multifractal spectrum that occurs in crack propagation problems is induced by narrow necks, and only occurs very close to final failure. Therefore, although the occurrence of this multifractal spectrum is interesting, it is unlikely to be experimentally observable.

CHAPTER V

Statistics of Transport Properties and Breakdown Strengths

We have studied how the average transport properties (conductivity) and breakdown strength of random media depend on disorder and system size. But, due to the presence of random flaws, disordered materials may exhibit a wide scatter from sample to sample variations in their transport and breakdown properties. Therefore, the ensemble averages of these quantities do not tell the whole story especially in quenched strongly disordered systems and that a complete knowledge comes, for example, from the full ensemble probability distribution of each variable of interest. In this chapter, we will discuss their statistical properties and try to answer the following question: what is the conductivity and breakdown strength distributions and how do they fluctuate from sample to sample?

For conventional statistical variables, the central limit theorem guarantees their distribution approaches a Gaussian function. This leads to the result that these statistical variables self-average and have small sample to sample fluctuations (for $L>>\xi$). But, for unconventional non-Gaussian statistical variables, which violate the central limit theorem, the appropriate statistical distribution is often very broad, with large sample to sample fluctuations.

In section 1, we will review various statistics to be used in this chapter, i.e., central limit theorem for random additive process, log-normal distribution for random multiplicative process and the statistics of extreme. Then, in section 2, we will discuss the distributions and fluctuations in the conductivity of percolation networks. By using the central limit theorem, we find that this distribution is Gaussian, and that sample to sample fluctuations are

relatively small [$\propto (L/\xi)^{-d/2}$, where L is the size of system and ξ is the correlation length]. In section 3, we study the probability distribution of resistances in one dimensional quantum electronic systems. We find that the sample resistance is a product of a series of random numbers, which is a typical multiplicative process. Based on this, we argue that the logarithm of the resistance is the right statistical variable and that it has Gaussian distribution (i.e., the distribution of resistances is a log-normal). We also briefly discuss the resistance distribution for higher dimensional quantum systems. In section 4, we apply extreme statistical argument to the distribution of breakdown strengths in percolation networks and find that it is very broad. This results in that the sample to sample fluctuations are O[1/(lnV)]. This chapter concludes in section 5.

V.1 Review of Various Statistics.

a) Random additive process and central limit theorem[127-131].

The central limit theorem tells us that if we have a large number of experiments which measure some stochastic variable, X, then the probability distribution of the average of all the measurements approaches a Gaussian function (provided the tail of the distribution decays faster than $1/x^2$, i.e., the second moment is finite), regardless of the form of the distribution for X itself. It is a very important result and has fundamental implications for numerical studies of stochastic processes governed by random additive process. It guarantees that one can approach the real average by sampling only an infinitesimal fraction of the total number of states of the system with a relative small error ($\sim 1/\sqrt{N}$, where N is the number of measurements). Here, we will give a proof of central limit theorem and derive the Gaussian distribution function.

Given a random variable X with a probability density $f_X(x)$, we wish to find the distribution of the random variable, Y, where the value of Y corresponds to the average of N measurements of X:

$$y_N = \frac{x_1 + x_2 + \cdots + x_N}{N} \tag{5.1}$$

[This is called a <u>random additive process</u>. A typical example of this is the one-dimensional random walk problem. Then, X corresponds to the displacement of a particle after one step and $f_X(x)dx$ corresponds

to the probability that it is displaced a distance x→x+dx in one step.] Let us consider the probability density $f_Y(y_N-\langle X\rangle)$, where $\langle X\rangle$ is the mean:

$$\langle X\rangle = \int dx\, x f_X(x) \tag{5.2}$$

Define the characteristic function:

$$\Phi(k) = \int \exp[ik(y_N-\langle X\rangle)]\, f_Y(y_N-\langle X\rangle)\, dy_N \tag{5.3}$$

Because

$$f_Y(y_N-\langle X\rangle) = \int dx_1 dx_2 \cdots dx_N\, \delta\left[\frac{x_1 + x_2 + \cdots + x_N}{N} - y_N\right] f_X(x_1) f_X(x_2) \cdots f_X(x_N)$$

We can rewrite Eq. (5.3) as

$$\Phi(k) = \int dx_1 dx_2 \cdots dx_N \exp[i(k/N)([x_1-\langle X\rangle]+[x_2-\langle X\rangle]+\cdots+[x_N-\langle X\rangle])]\, f_X(x_1) f_X(x_2) \cdots f_X(x_N)$$

$$= \left\{\int dx_1 \exp[i(k/N)(x_1-\langle X\rangle)]\, f_X(x_1)\right\}^N$$

$$= [\phi(k/N)]^N \tag{5.4}$$

It will be shown later that $k/N \ll 1$, so that we can calculate $\phi(k/N)$ by expanding $\exp[i(k/N)(x-\langle X\rangle)]$ and keeping to the second order term. Therefore, we have,

$$\phi(k/N) = \int dx \exp[i(k/N)(x-\langle X\rangle)] f_X(x)$$

$$= \int dx \left[\sum_{n=0}^{\infty} (ik/N)^n (x-\langle X\rangle)^n/n!\right] f_X(x)$$

$$= \sum_{n=0}^{\infty} (ik/N)^n/n! \int dx\ (x-\langle X\rangle)^n f_X(x) \qquad (5.5)$$

By the definition of the moments $\langle X^n\rangle$,

$$\langle X^n\rangle = \int dx\ x^n f_X(x) \qquad (5.6)$$

we get that

$$\phi(k/N) = \sum_{n=0}^{\infty} (ik/N)^n/n!\ \langle (x-\langle X\rangle)^n\rangle$$

$$= 1 + (ik/N)\langle (x-\langle X\rangle)\rangle - (k/N)^2/2\ \langle (x-\langle X\rangle)^2\rangle + \cdots$$

$$\phi(k/N) = 1 + (ik/N)(\langle X\rangle - \langle X\rangle) - (k/N)^2/2\ [\langle X^2\rangle - \langle X\rangle^2]$$

$$= 1 - (k/N)^2[\langle X^2\rangle - \langle X\rangle^2] \qquad (5.7)$$

Because the standard deviation σ of X is,

$$\sigma^2 = \langle X^2\rangle - \langle X\rangle^2 \qquad (5.8)$$

Then

$$\phi(k/N) = 1 - (k/N)^2/2\ \sigma^2 + \cdots$$

The function $\phi(k/N)$ decreases with increasing k and is less than unity for $K/N<<1$. The function $[\phi(k/N)]^N$ then decreases even more rapidly with increasing k. Then,

$$\Phi(k) = [1 - (k\sigma/N)^2/2 + O(k^3/N^3)]^N \underset{N\to\infty}{\to} \exp[-(k\sigma)^2/(2N)] \qquad (5.9)$$

The probability density $f_Y(y_N - \langle X\rangle)$ then becomes

$$f_Y(y_N-\langle X\rangle) = (1/2\pi)\int_{-\infty}^{+\infty} dk\ \Phi(k)\ \exp[-ik(y_N-\langle X\rangle)$$

$$=(1/2\pi)\int_{-\infty}^{+\infty} dk\ \exp[-ik(y_N-\langle X\rangle)-(k\sigma)^2/(2N)]$$

$$= \sqrt{(N/2\pi)}\ (1/\sigma)\ \exp[-N(y_N-\langle X\rangle)^2/2\sigma^2] \qquad (5.10)$$

In this equation, it is obvious to see that $\Phi(k)$ [and $\phi(k/N)$] contributes to f_Y only for small k, this is due to the oscillatory character of $\exp[-ik(y_N-\langle X\rangle)]$ for large k. For simplicity, we can assume $k<<N$, i.e., $k/N<<1$.

From this distribution function, we can calculate the average value of Y and its standard deviation. And they are as follows

$$\langle Y\rangle = \langle X\rangle, \quad \langle Y^2\rangle - \langle Y\rangle^2 = \sigma^2/N.$$

Thus, regardless of the form of $f_X(x)$, the average of a large number of measurements of X will be a Gaussian function centered at $\langle X \rangle$, with a standard deviation $N^{-1/2}$ times the standard deviation of the probability density of X. The only requirements are that f(x) have finite moments, that the measurements of X be statistically independent, and that N be large. This result is called the central limit theorem and helps explain why the Gaussian distribution describes so many phenomena that occur in nature. From Eq. (5.10), we can get that the sum of N random numbers is also a Gaussian distribution and

$$f_N(Y_N - N\langle X \rangle) = [1/\sqrt{(2\pi N\sigma^2)}]\exp[-(Y_N - N\langle X \rangle)^2/(2N\sigma^2)] \qquad (5.11)$$

where $Y_N = x_1 + x_2 + \cdots + x_N$, and as N increases it approaches

$$\langle Y_N \rangle = N\langle X \rangle \qquad (5.12)$$

its standard deviation is

$$\sigma_Y^2 = N\sigma^2 \qquad (5.13)$$

b) Random multiplicative process and log-normal distribution[132].

There exist many natural phenomena which depend on the statistical properties of a product of random variables, such as the distribution of incomes, body weights, rainfall, fragment sizes in rock crushing processes, multifractal phenomena, etc[133,134].

Recently, the notions of random multiplicative processes have been applied to diffusive transport in random media[135-137]. Here, we will derive the log-normal distribution and discuss the statistical properties of random multiplicative processes.

Consider a sequence of random variables x_1, x_2, $\cdots$, x_N, in which x_i has the probability density $f_X(x_i)$. We are interested in the statistical properties of the product of these N random numbers:

$$P_N = x_1 x_2 \cdots x_N \tag{5.14}$$

i.e., we ask what is the average value of this N-fold product, $\langle P_N \rangle$ and what is the probability density $f_P(P_N)$.

Take the logarithm of Eq. (5.14), we have,

$$\ln P_N = \ln x_1 + \ln x_2 + \cdots + \ln x_N \tag{5.15}$$

Because x_i is a random variable, $\ln x_i$ is also random number. Therefore, this is a random additive process and the central limit theorem applies. From Eq. (5.11), the distribution function of $\ln P_N$ then is Gaussian function

$$f(\ln P_N) = 1/\sqrt{(2\pi N)}\ (1/\sigma)\ \exp[-(\ln P_N - \langle \ln P \rangle)^2/(2N\sigma^2)] \tag{5.16}$$

This is called log-normal distribution, whose name reflects the fact that the logarithm of the product is normally distributed. The parameters $\langle \ln P \rangle$ and σ can be calculated by finding the probability density of $f(z=\ln x)$, which is

$$f(z=\ln x) = \int dx\ \delta(z-\ln x) f_X(x)$$

$$= f_X(e^z) \tag{5.17}$$

Then

$$\langle \ln P \rangle = \int dz\ z\ f(z)$$

$$= \int dz\ z\ f_X(e^z)$$

$$= \int d\ln x\ \ln x\ f_X(e^{\ln x})$$

$$= \int dx\ [\ln x\ f_X(x)]/x \tag{5.18}$$

and

$$\sigma^2 = \langle (\ln P)^2 \rangle - \langle \ln P \rangle^2$$

$$= \int dz\ z^2 f(z) - \langle \ln P \rangle^2$$

$$= \int dx\ [(\ln x)^2 f_X(x)]/x - \langle \ln P \rangle^2 \tag{5.19}$$

It is interesting to note the fact

$$\langle P \rangle = \langle \exp(\ln P) \rangle \neq \exp\langle \ln P \rangle \tag{5.20}$$

which shows that the logarithm of the random product is a right quantity to study statistically, instead of the product itself. But, we

should point out that the log-normal distribution provides a poor approximation for the asymptotic behavior of the average value, and also for the higher moments of the product. This is due to the fact that the extreme events, although exponentially rare in N, are exponentially different from the typical, or most probable value of the product, and they have a dominant contribution to the average value. In the log-normal distribution, information about the tail of the distribution is lost, and these details are crucial in determining the higher moments of the product (for detailed study, see Ref. 133).

c) Statistics of extreme[87,138-141] and three type of asymptotic distributions.

Consider a sequence of random variables, x_1, x_2, $\cdots$, x_N, which are independent and identically distributed with a probability density f(x). We can find the largest value x of this sequence of random variables,

$$x = \max\{x_1, x_2, \cdots, x_N\}, \tag{5.21}$$

We ask the following questions: what is the average value of x? What is the distribution function of x and how does the average value and the distribution function depend on N? The answer to these questions comes from the statistics of extreme. In this section, we will argue that there exist three different types of limiting distribution for maxima and derive these three different types of distribution functions.

Consider n samples, each of size N, taken from the same population. In each sample there is a largest value and the largest value in the nN realizations is the largest of the n largest values taken from samples of size N. The distribution of the largest value in nN realizations will tend to the same asymptotic expression as the distribution of the largest value in samples of size N, provided that such an asymptote exists. Consequently, the asymptote must be such that the largest value of a sample of size N taken from it must have the same asymptotic distribution.

Since a linear transformation does not change the form of the distribution, the probability that the largest value is below x should be equal to the probability of a linear function of x,

$$F^n(x) = F(a_n x + b_n) \tag{5.22}$$

the two parameters a_n and b_n being functions of n. Eq. (5.22) is called the Stability Postulate and it can be generalized as follows:

Stability Postulate: If F is an asymptotic distribution, there exist real functions $a(s)>0$ and $b(s)>0$ defined for $s>0$ such that,

$$F^s[a(s)x + b(s)] = F(x) \tag{5.23}$$

for all real x, $s>0$.

Before we start to find the asymptotic distributions, it will be convenient for us to list some useful results without proof for inverses of monotone functions:

$\psi(x)$ is a nondecreasing continuous function and ψ^{-1} is the inverse function.

(i) If $a>0$, b and c are constants, and $H(x) = \psi(ax + b) - c$, then,

$$H^{-1}(y) = [\psi^{-1}(y + c) - b]/a; \tag{5.24}$$

(ii) If ψ^{-1} is continuous, then,

$$\psi^{-1}[\psi(x)] = x. \tag{5.25}$$

Now, we try to obtain the possible asymptotic distributions for maxima and show there exist only three different types of asymptotic distributions.

If F is a asymptotic distribution, then Eq. (5.23) holds for all $s>0$ and all x. Our task is to solve this equation and find all the possible solutions. From Eq. (5.23), we have,

$$-s \ln\{F[a(s)x + b(s)]\} = - \ln F(x), \tag{5.26}$$

so that,

$$-\ln(-\ln\{F[a(s)x + b(s)]\}) - \ln s = -\ln[-\ln F(x)]. \tag{5.27}$$

Now it is easily seen that the nondecreasing function $\psi(x) = -\ln[-\ln F(x)]$ has an inverse function $U(y)$ defined for all y. Further, Eq. (5.27) implies,

$$\psi[a(s)x + b(s)] - \ln s = \psi(x),$$

so that by Eq. (5.24), we have,

$$U(y) = [U(y + \ln s) - b(s)]/a(s)$$

Substracting this for $y=0$, we have

$$U(y) - U(0) = [U(y + \ln s) - b(s)]/a(s) - [U(\ln s) - b(s)]/a(s)$$

$$= [[U(y + \ln s) - U(\ln s)]/a(s), \qquad (5.28)$$

Now, we write $z = \ln s$, $a'(z) = a(e^z)$ and $U'(y) = U(y) - U(0)$, thus Eq. (5.28) becomes,

$$U'(y) = [U(y + z) - U(0) - U(z) + U(0)]/a'(z)$$

$$= [U'(y + z) - U'(z)]/a'(z)$$

i.e.,

$$U'(y + z) - U'(z) = U'(y)\, a'(z) \qquad (5.29)$$

for all real y, z.

Interchanging y and z and subtracting, we obtain,

$$U'(y)[1 - a'(z)] = U'(z)[1 - a'(y)]. \tag{5.30}$$

In order to satisfy this equation, we can have two possible cases, (1) and (2) as follows:

(1) $a'(z) = 1$ for all z when Eq. (5.29) gives,

$$U'(y + z) = U'(y) + U'(z).$$

The only monotone increasing solution to this equation is well known to be simply,

$$U'(y) = \rho y,$$

for some $\rho > 0$. Then,

$$U'(y) = U(y) - U(0) = \rho y,$$

or

$$\psi^{-1}(y) = U(y) = \rho y + \nu,$$

where $\nu = U(0)$ is a constant. Since this is continuous, Eq. (5.25) gives,

$$x = \psi^{-1}(\psi(x)) = \rho\psi(x) + \nu,$$

or,

$$\psi(x) = -\ln[-\ln F(x)] = (x - \nu)/\rho$$

So, we finally have the first asymptote,

$$F(x) = \exp[-e^{-(x-\nu)/\rho}], \tag{5.31}$$

where ρ, ν are positive parameters independent of N (s). This is also called the Gumbel distribution[87,142]. It is immediately verified that the functional Eq. (5.22) (5.23) are satisfied, provided that

$$a_n = 1, \; b_n = \rho \ln(n) \tag{5.32}$$

(2) $a'(z) \neq 1$ for some z when Eq. (5.30) gives,

$$U'(y)/[1 - a'(y)] = U'(z)/[1 - a'(z)] = c,$$

where c is a non-zero constant [since this would imply that $U'(y)=0$ for all y, hence $U(y) = U(0)$, constant]. Therefore,

$$U'(y) = c[1 - a'(y)] \tag{5.33}$$

From Eq. (5.29), we thus obtain,

$$c[1 - a'(y + z)] - c[1 - a'(z)] = c[1 - a'(y)]a'(z),$$

i.e.,

$$a'(y + z) = a'(y)\, a'(z), \tag{5.34}$$

But a' is monotone, and the only monotone nonconstant solutions of this functional equation have the form

$$a'(y) = e^{\rho y}, \quad \text{for } \rho \neq 0 \tag{5.35}$$

Hence Eq. (5.33) yields,

$$\psi^{-1}(y) = U(y) = U(0) + c[1 - e^{\rho y}]$$

$$= \nu + c(1 - e^{\rho y}) \tag{5.36}$$

where $\nu = U(0)$ is a constant. Since $\psi(x) = -\ln[-\ln F(x)]$ is increasing, so is $U(x)$, so that we must have $c<0$ if $\rho>0$ or $c>0$ if $\rho<0$. By Eq. (5.25),

$$x = \psi^{-1}[\psi(x)] = \nu + c[1 - e^{\rho\psi(x)}]$$

$$= \nu + c(1 - \exp[-\rho\ln[-\ln[-F(x)]]]$$

$$= \nu + c\{1 - [-\ln F(x)]^{-\rho}\} \tag{5.37}$$

giving,

$$F(x) = \exp\{-[1 - (x - \nu)/c]^{-1/\rho}\}$$

or after shifting the origin of x, we have

$$F(x) = \exp\{-[-(x/c)]^{-1/\rho}\} \tag{5.38}$$

If $\rho>0$, $c<0$, we can rewrite Eq. (5.38) as,

$$F(x) = \exp[-(\alpha/x)^{k}], \quad x\geq 0,\ \alpha>0,\ k>0, \tag{5.39}$$

This is the second asymptote, which is also called Frechet distribution[87,138,139]. In this case, we also can find,

$$a_n = n^{-1/k}, \quad \text{and } b_n = 0 \tag{5.40}$$

(for detail, see Ref. 87).

If $\rho<0$, $c>0$, we can get,

$$F(x) = \exp[-(x/\alpha)^{k}], \qquad x\leq 0,\ \alpha<0,\ k>0, \tag{5.41}$$

This is the third asymptote, which is also called the Weibull distribution[143-145]. We also can find that,

$$a_n = n^{1/k} \tag{5.42}$$

So, we have proved that there exist three different types of asymptotic distributions for maxima and they are as follows:

$$\begin{aligned}
&\text{Type I:} && F(x) = \exp[-e^{-\alpha(x-u)}],\ \alpha>0;\\
&\text{Type II} && F(x) = \exp[-(\alpha/x)^{k}],\ x\geq 0,\ \alpha>0,\ k>0;\\
&\text{Type III} && F(x) = \exp[-(x/\alpha)^{k}],\ x\leq 0,\ \alpha<0,\ k>0.
\end{aligned} \tag{5.43}$$

V.2 Conductivity Distribution and Fluctuation in Percolation Networks.

The average conductivity or elastic moduli varies on length $L<\xi$, but saturates on length $L>\xi$, where ξ is the correlation length in percolation models, and a length scale over which the system is disordered in general. Since regions on length $L>\xi$ are uncorrelated, we can assume that the average conductivities at length scale ξ are independent random variables with the same probability distribution. Then, finding the average conductivity of systems of size L^d becomes to find the average value of $(L/\xi)^d$ random variables, which is a random additive process. Therefore, the average value for the moduli measured on samples of size L^d have fluctuations of order $(L/\xi)^{-d/2}$. This qualitative argument is valid for $L>>\xi$, but must be modified for $L\sim\xi$. By similar reasoning, the central limit theorem shows that the full distribution function for such a moduli and $L>>\xi$ is Gaussian, with

$$P(\Sigma_N) \sim \exp[\ -N(\Sigma_N - \Sigma_\infty)^2/c_e(p)] \tag{5.44}$$

where $P(\Sigma_N)$ is the probability that the conductivity of a sample measured on a sample of size $N=L^d$ has value Σ_N. $c_e(p) \sim C_e\xi^d$, and c_e is a constant for the electrical problem. Similar expressions apply to capacitance in dielectric problems and elastic moduli in mechanical systems, and c_e is changed to c_d and c_m respectively. Since the distribution in Eq. (5.44) is very narrow (for large N and away from the

percolation point), sample to sample fluctuations are also small for $L>>\xi$. This is the origin of the statement that, conductivity and elastic moduli self average for large enough system sizes. We have calculated the conductivity for a set of 2000, 50x50 random resistor networks at p=0.90 and the result is plotted in Fig. 5.1. It is readily seen that the distribution is a Gaussian function.

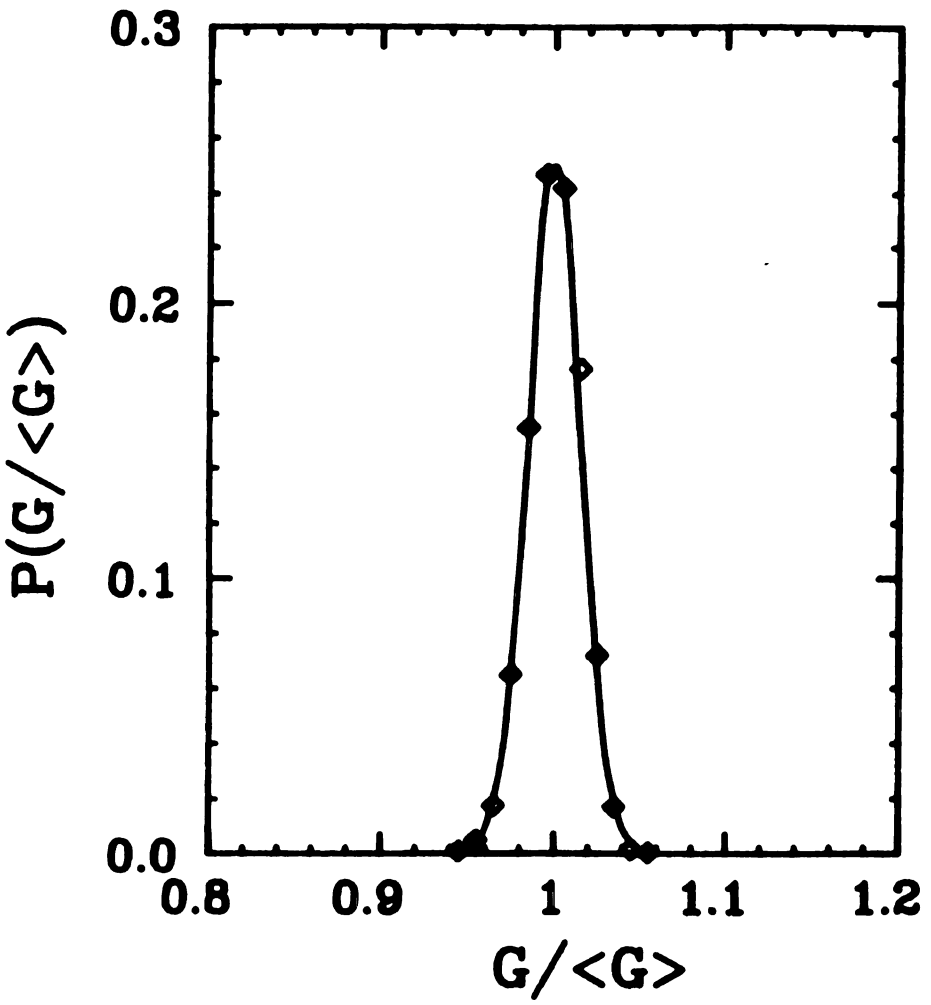

Fig. 5.1 The probability that a 50x50 random resistor network has conductivity G. The distribution was calculated from 2000 realizations of the random resistor networks and <G> is the average of the conductivity. (<>) is the numerical data and the curve is the best fitting to the Gaussian function. It clearly shows that the distribution is a Gaussian.

V.3 The Resistance Distribution in Disordered Quantum Systems.

It is well established that the slightest amount of disorder in a perfect lattice suffices to localize all electronic states in one dimension[146-158]. Therefore, due to the exponential localization of the states, the averaged residual resistance of long finite chains grows exponentially with length L, as was first shown by Landauer[159]. Along with the exponential growth of the average resistance with length, one finds that the relative mean-square fluctuations also grow exponentially at an even faster rate than the average value[160-174], thus violating the central limit theorem. This implies that the residual resistance is a non-additive as well as non-self-averaging quantity (see more detailed discussion in this section). Instead, Anderson et al[161,162] showed that the problem of resistance of a disordered conductor could be reformulated in terms of a new scaling variable $[\ln(1+\rho)]$, such that, the concepts of additivity, self-averaging, and central limit theorem do remain valid in the usual ensemble sense. Here, we will briefly give these arguments and calculate the probability distribution of resistances for one dimensional disordered conductors.

The resistance of a one dimensional conductor with many scatters may be written[159] as follows,

$$\rho = (h/e^2)\,\frac{R}{T} = (h/e^2)\,(1/T - 1) \qquad (5.45)$$

where $h/e^2 \approx 26k\Omega$, T and R=1-T are the transmission and reflection coefficients. Using the model proposed by Anderson et al[161], we can calculate the total resistance by combining two resistances (scatters) by first calculating the total transmission coefficient. The law of composition of two scatters is

$$t = t_1 [1/(1-r_1' r_2)] t_2 \tag{5.46}$$

Here, the reflectivities of each systems r_1' and r_2 are assumed stochastically unrelated to each other. Therefore, the total resistance in unit of (h/e^2) is

$$\rho = (1/T - 1) = (1/|t|^2 - 1)$$

$$= |t_1[1-r_1' r_2)] t_2|^{-2} - 1 \tag{5.47}$$

i.e.,

$$(1 + \rho) = (1 + \rho_1)|1 - r_1' r_2|^{-2}(1 + \rho_2)$$

$$= (1 + \rho_1) [1 - 2r_1 r_2 \cos\theta + r_1^2 r_2^2]^{-1} (1 + \rho_2) \tag{5.48}$$

where θ is a cumulative phase depending on the characteristics of the two scatters. In the random phase model[161], phases of the individual scatters are independent of each other and distributed uniformly between 0 and 2π (this is true if the distance between scatters is larger than the dephasing length). This ensures a uniform distribution for the phase θ in Eq. (5.48). Thus, the resistance ρ_N of a one

dimensional conductor with N scatters can be calculated from the following equation:

$$1 + \rho_N = \prod_{i=1}^{N} (1 + \rho_i) \prod_{i=2}^{N} [1 - 2r_{i-1}r_i\cos\theta_i + r_{i-1}^2 r_i^2]^{-1} \qquad (5.49)$$

It is clearly seen that $(1 + \rho_N)$ is like a product of a series of random numbers. To clarify this perception, we rewrite Eq. (5.49) as follows,

$$\ln(1 + \rho_N) = \sum_{i=1}^{N} \ln(1 + \rho_i) - \sum_{i=2}^{N} \ln[1 - 2r_{i-1}r_i\cos\theta_i + r_{i-1}^2 r_i^2]$$

If the phase θ_i are uniformly distributed and unrelated to ρ_i, we can first do the phase average for this equation (this approximation is valid only in the large ρ_i limit, i.e., the strong disorder limit),

$$\int_0^{2\pi} d\theta_i \ln(1 - 2r_{i-1}r_i\cos\theta_i + r_{i-1}^2 r_i^2)$$

$$= \pi \ln \frac{1}{2} [1 + r_{i-1}^2 r_i^2 + [(1 + r_{i-1}^2 r_i^2)^2 - 4r_{i-1}^2 r_i^2)^{1/2}] = 0$$

so that Eq. (5.49) becomes,

$$\ln(1 + \rho_N) = \sum_{i=1}^{N} \ln(1 + \rho_i) \qquad (5.50)$$

This implies $\ln(1 + \rho_N)$ has a Gaussian distribution for large N. Shapiro et al[166-174] have studied the distribution of ρ_N itself, $P(\rho_N)$, and showed that $P(\rho_N)$ is log-normal in the large ρ limit and

$P(\rho_N)$ is exponential in the small ρ limit. Now, we just briefly review these calculations.

From Eq. (5.47), the total resistance ρ can be represented in terms of ρ_1, ρ_2 and the phase θ,

$$\rho = \rho(\rho_1, \rho_2, \theta) = \rho_1 + \rho_2 + 2\rho_1\rho_2 - 2[\rho_1\rho_2(1 + \rho_1)(1 + \rho_2)]^{1/2} \cos\theta \qquad (5.51)$$

Then, we get the following equation for the distribution function $P(\rho)$ of the total resistance in terms of the distribution functions $P_1(\rho_1)$ and $P_2(\rho_2)$ for the individual resistances:

$$P(\rho) = (1/2\pi)\int_0^{2\pi} d\theta \int_0^{\infty} d\rho_1 \int_0^{\infty} d\rho_2 \{P_1(\rho_1)P_2(\rho_2)\, \delta[\rho - \rho(\rho_1, \rho_2, \theta)]\} \qquad (5.52)$$

After integrating over ρ_2 and rewriting the integral over θ in terms of $y=\cos\theta$, Eq. (5.52) becomes

$$P(\rho) = (1/\pi)\int_{-1}^{1} dy\, (1-y^2)^{-1/2} \int_0^{\infty} d\rho_1 P(\rho_1)P_2(u), \qquad (5.53)$$

where

$$u(\rho, \rho_1, y) = \rho + \rho_1 + 2\rho\rho_1 + 2y[\rho(1 + \rho)\rho_1(1 + \rho_1)]^{1/2} \qquad (5.54)$$

We assume that ρ_2 is the resistance of a chain with N scatters, ρ_1 is the resistance of a single (N+1)th scatter, $P_1(\rho_1)$ is known and it is same for all individual scatters. If we also assume that $P_1(\rho_1)$ is concentrated at very small ρ_1 value, i.e., all scatters are weak. Then, expanding Eq. (5.54), we have the following recursion relation:

$$P_{N+1}(\rho) = P_N(\rho) + \langle\rho_1\rangle \frac{\partial}{\partial\rho} [(\rho^2 + \rho) \frac{\partial}{\partial\rho} P_N] \tag{5.55}$$

where $\langle\rho_1\rangle = \int_0^\infty d\rho_1\ \rho_1 P_1(\rho_1)$ is much smaller than unity. In continuous limit, this equation becomes a differential equation:

$$\frac{\partial}{\partial L} P_L(\rho) = \alpha \frac{\partial}{\partial\rho} [(\rho^2 + \rho) \frac{\partial}{\partial\rho} P_L(\rho)] \tag{5.56}$$

where L is the length of the disordered chain and α is the small-scale resistivity.

In the large ρ limit [for $L>>\xi=\alpha^{-1}$ (localization length)], the ρ-term in Eq. (5.56) can be neglected, and this equation becomes a diffusion equation in terms of $\ln\rho$. In this case, the solution is:

$$P_L(\rho) = (4\pi\alpha L)^{-1/2} \exp[-(\ln\rho - \langle\ln\rho\rangle)^2/(4\alpha L)] \tag{5.57}$$

This is a Gaussian centered at a mean (most probable) value $\langle\ln\rho\rangle$. This shows that $\ln\rho$, rather than ρ itself, is a proper scaling variable of physical significance for large L ($\rho>>1$). By using the transfer matrix technique, we have numerically calculated the resistance distribution for one-dimensional lattice of random delta functions. The physical systems which we studied consists of

uniformly spaced delta-function potentials of random strengths[153]. The numerical simulation result is plotted in Fig. 5.2. It is clearly seen that $P_L(\ln\rho)$ exhibits a Gaussian distribution in agreement with theory. We can calculate the ensemble average $\langle\ln\rho\rangle$ and the standard deviation σ^2. And they are,

$$\langle\ln\rho\rangle = \int d(\ln\rho)\ (\ln\rho)\ P_L(\rho) = \alpha L \tag{5.58}$$

$$\sigma^2 = \langle(\ln\rho)^2\rangle - \langle\ln\rho\rangle^2 = 2\alpha L \tag{5.59}$$

Thus, $\langle\ln\rho\rangle$ scales additively with length and the relative rms deviation is

$$\sigma/\langle\ln\rho\rangle = (2\alpha L)^{1/2}/(\alpha L) = (2/\alpha L)^{1/2} \tag{5.60}$$

which decreases with increasing length L. This implies that $\ln\rho$ has a central limit.

The most probable value (5.58) of $\ln\rho$ yields a typical or scale resistance

$$\rho = \exp(\alpha L),$$

which agrees with the result from the Landauer's formula for chains with $L>>\xi$.

In the small ρ limit (for $L<<\xi$), the ρ^2 term in Eq. (5.56) can be neglected and the equation becomes,

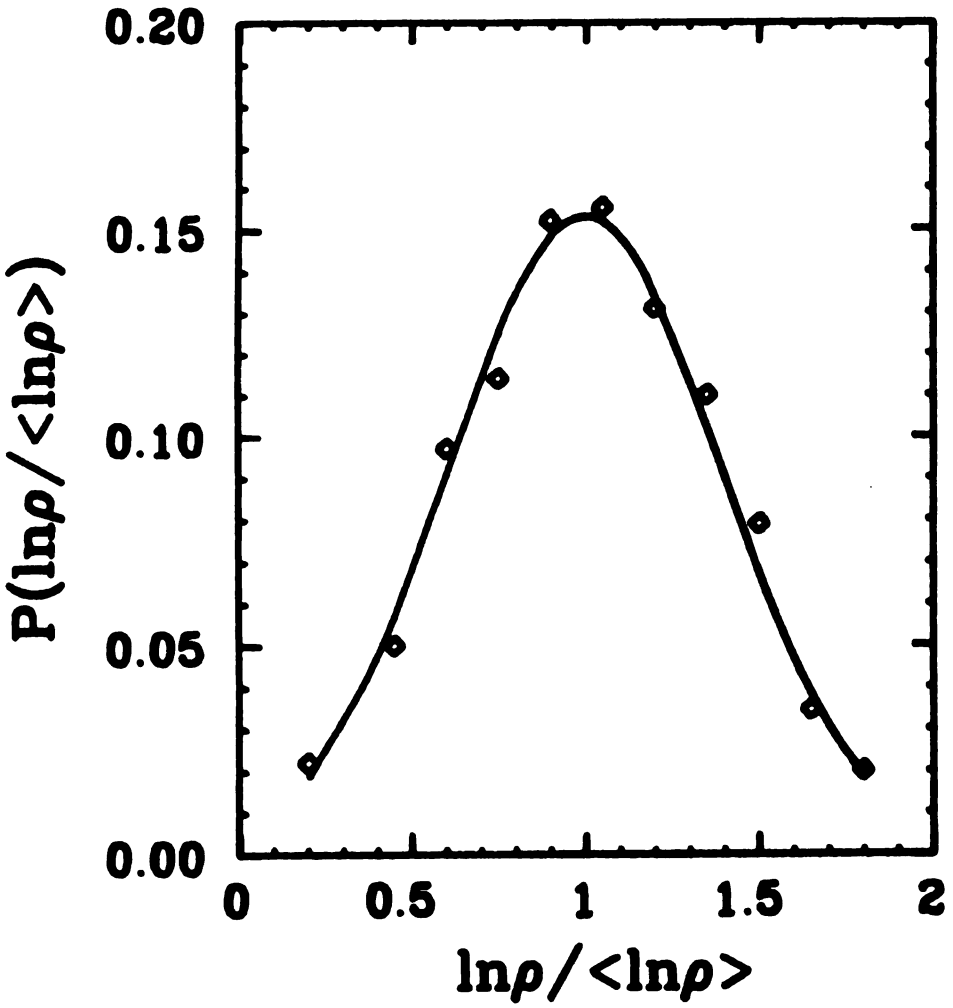

Fig. 5.2 Resistance distribution for one-dimensional chains of 500 scatters. $\langle \ln\rho \rangle$ is the average of $\ln\rho$. $\langle\rangle$ are the numerical data, and the solid curve is the best fitting to the theoretical Gaussian distribution. The distribution was calculated from 2000 realizations.

$$\frac{\partial}{\partial L} P_L(\rho) = \frac{\partial}{\partial \rho} [\rho \frac{\partial}{\partial \rho} P_L(\rho)] \tag{5.61}$$

The solution is

$$P_L(\rho) = 1/(\alpha L) \exp[-\rho/(\alpha L)] \tag{5.62}$$

This is a very broad distribution and has a large fluctuations. In fact,

$$\langle \rho \rangle = \alpha L \tag{5.63}$$

$$\sigma^2 = (\alpha L)^2 \tag{5.64}$$

Eq. (5.63) recovers the classical Ohm's law, but the fluctuations are of order of the mean.

Finally, we briefly discuss the resistance distribution for d-dimensional disordered systems. In this case, the system consists of many parallel chains and each chain is a series of scatters. The resistance can be calculated through the multichannel Landauer's formula[175],

$$\rho = g^{-1} = [2\mathrm{Tr}(tt^+)]^{-1} \tag{5.65}$$

where t is the transmission matrix for the plane-wave amplitudes. It is clearly seen that, due to the transverse fluctuations (this fluctuation arises from the addition of L^{d-1} channels and is called

"classical fluctuation"), the resistance is not multiplicative. And the transverse fluctuations will produce substantial changes in the distributions[167,170,173]. Instead giving the detail discussion, we just point out that, in the strong disorder limit (isolating regime), one recovers the one-dimensional result, and the resistance distribution is a log-normal distribution. In this case, the "classical" transverse fluctuations have relatively small contributions compared to the very large fluctuations inside the one-dimensional channels. Therefore, we can neglect the transverse fluctuations and assume all L^{d-1} parallel chains have the same resistance. Indeed, this becomes a one-dimensional problem.

V.4 Strength Distribution and Fluctuation in Percolation Models of Breakdown.

Because breakdown properties are dominated by extreme events, the breakdown strength follows one of the extreme value distributions given in section 1 of this chapter. In particular, for a fixed amount of disorder, sample to sample fluctuations in strength are far larger than those for conductivity or elastic moduli. This is clearly seen by comparing the probability distribution for the largest currents in Fig. 5.3 to the conductivity distribution displayed in Fig. 5.1. In Fig. 5.3, we plot the largest currents in the bonds of the network (for brittle systems this is proportional to the inverse of the electrical breakdown strength) for a set of 2000 50x50 random resistor networks at p=0.90. It is readily seen that the maximum current (or extreme moment) distribution is far broader than the

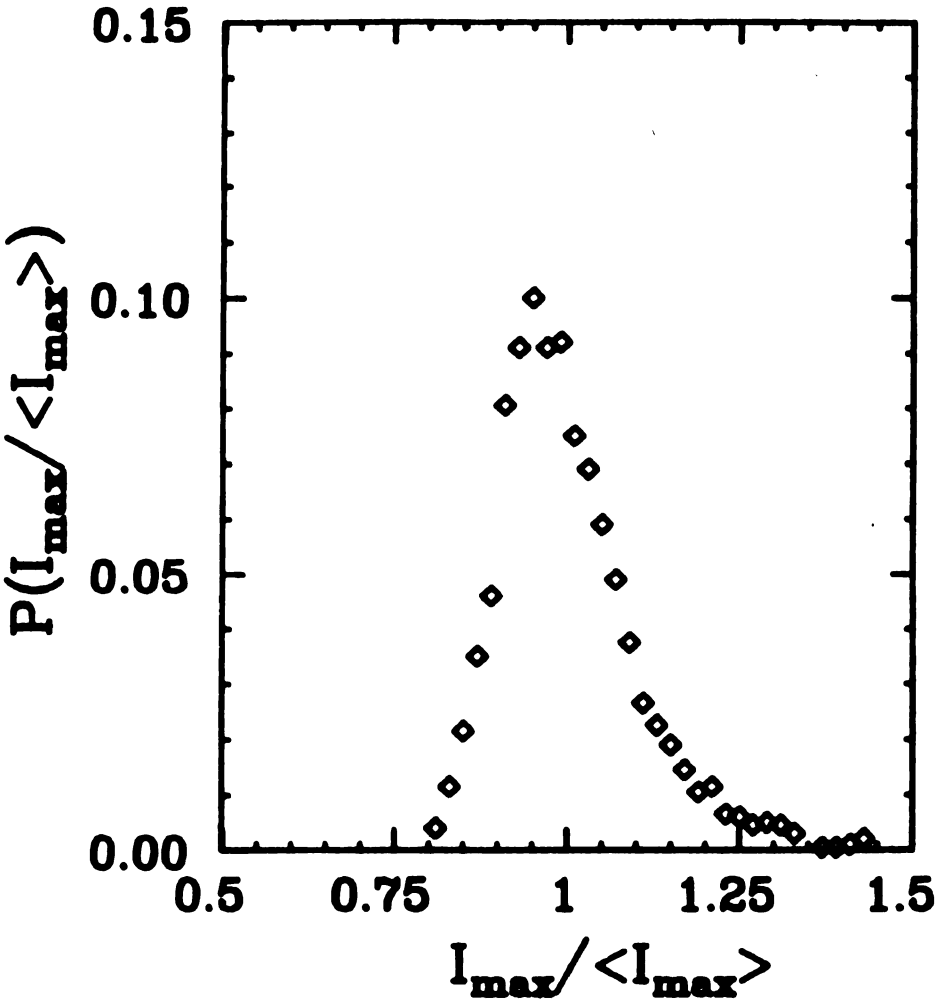

Fig. 5.3 The probability that a 50x50 random resistor network contains a maximum current I_{max} in any bond. This distribution was calculated from 2000 realizations of the random resistor networks, and $\langle I_{max} \rangle$ is average of the maximum currents.

conductivity (or low moment) distribution. It is possible to derive the form to be expected for the distribution given in Fig.5.3 in several ways depending on the amount of mathematical rigor you wish to pursue. The most direct is to use the fact that we know that the distribution of bond currents is exponential for large currents for $p>p_c$ (see Chapter III and Ref. 43),

$$P(I) \sim b \exp(-bI) \tag{5.66}$$

where b is a constant. Then the cumulative probability, $C_1(I<I_{max})$, that a bond current is less than a maximum value, I_{max}, is given by,

$$C_1(I<I_{max}) \sim \int_0^{I_{max}} b \exp(-bI')dI'$$

$$= 1 - \exp(-bI_{max}) \tag{5.67}$$

If we consider the bond currents to be uncorrelated, then the probability that no current in the $N = L^d$ bonds in the network is greater than I_{max} is given by:

$$C_N(I<I_{max}) \sim [1 - \exp(-bI_{max})]^N \tag{5.68}$$

Since I_{max} is large, the exponential term is small, and the Eq. (5.68) is approximated by

$$C_N(I<I_{max}) \sim \exp[-N \exp(-bI_{max})] \tag{5.69}$$

The probability that a system of size N has maximum current I_{max} is, then given by

$$P(I_{max}) \sim N[b \exp(-bI_{max})] \{\exp[-(N-1) \exp(-bI_{max})]\} \quad (5.70)$$

$$\sim N\, b \exp(-bI_{max}) \exp[-N\exp(-bI_{max})] \quad (5.71)$$

where $b\exp(-bI_{max})$ term is the probability that one bond inside the network carries current I_{max}, $\exp[-(N-1) \exp(-bI_{max})]$ is the probability that the rest N-1 bonds in the network carrying currents less than I_{max}, and the factor N is due to the reason that there are N possible bonds at which the maximum current I_{max} occurs. This form is clearly skew. The typical (or average) strength, $\langle I_{max} \rangle$, is found from,

$$N \exp(-b\langle I_{max} \rangle) \sim 1 \quad (5.72)$$

which implies,

$$\langle I_{max} \rangle \sim \ln L \quad (5.73)$$

which has the correct size dependence as discussed in chapter III. Because of $I_b \sim 1/I_{max}$, Eq. (5.69) implies that the cumulative distribution of breakdown current is

$$C(I_b) = 1 - \exp[-N\exp(-b'/I_b)] \quad (5.74)$$

This is a Gumbel distribution. Indeed, in extreme statistics, it has been proved that for the exponential parent distribution given in Eq. (5.66), the asymptotic strength distribution must be a Gumbel distribution[138,139]. A more complete analysis that includes the dependence on dilution p was given by Duxbury et al[42,176]. The method relies on 1) the estimation of the probability of finding the largest defect cluster in a finite percolation network and 2) the calculation of the corresponding current enhancement at the tip of this most critical defect. A typical form of these cumulative distributions is shown in Fig. 5.4 for the electrical breakdown problem.

Having the distribution of breakdown strength, we can calculate the sample to sample fluctuation in strengths[5]. The expected sample to sample variations in strength are found by comparing the location of the 25% and 75% percentiles in these curves with the 50% percentile -- the average value (these "percentiles" are more general concepts than the standard deviation and the mean, which besides being most suitable for symmetric distributions, are especially bad indicators of observables when the local load distribution is very broad). Taking the electrical cases, Eq. (5.74), as an illustrative example, we then find that the typical breakdown current value at the pth percentile is defined by:

$$c = p/100 = C(I_b^c)$$

$$= 1 - \exp[-N\exp(-b'/I_b^c)] \qquad (5.75)$$

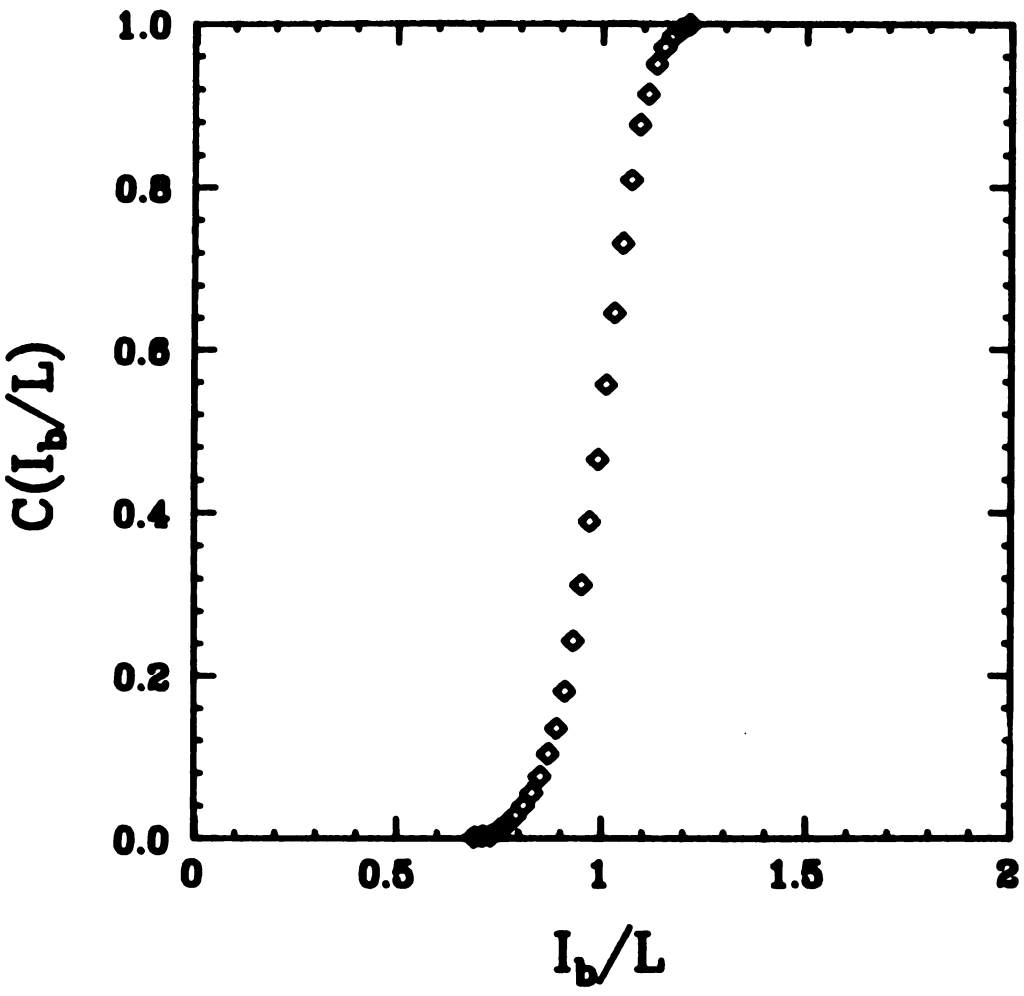

Fig. 5.4 The probability that a network will fail when an external current of size I_b is applied. The distribution was calculated from 2000 realizations of 50x50 random resistor network at p=0.90. <> is numerical data and the solid line is a fit to the data using Eq. (5.74).

Isolating I_b^c from this equation, we find that,

$$I_b^c = -b'/\ln[-\ln(1 - c)/N] = -b'/\{\ln[-\ln(1 - c)] - \ln N\} \qquad (5.76)$$

and,

$$\Delta I_b^c = I_b^c(c=75\%) - I_b^c(c=25\%)$$

$$= -b'[\{\ln[-\ln(1 - 75\%)] - \ln N\}^{-1} - \{\ln[-\ln(1 - 25\%)] - \ln N\}^{-1}]$$

$$= -b'[(0.33 - \ln N)^{-1} - (-1.25 - \ln N)^{-1}]$$

$$= -b'(-1.25 - \ln N - 0.33 + \ln N)/[(0.33 - \ln N)(-1.25 - \ln N)]$$

$$= 1.58b'/[(\ln N)^2 + 0.92\ln N - 0.41]$$

$$\sim 1.58b'/(\ln N)^2 \qquad (5.77)$$

The main point of this equation is that sample to sample variations in a system of size N are logarithmic. Therefore,

$$\Delta I_b^c/I_b^c(c=50\%) = [1.58b'/(\ln N)^2]/(-b'/\ln[-\ln(1 - 50\%)/N])$$

$$= [1.58/(\ln N)^2]\ (0.37 + \ln N)$$

$$\sim (\ln N)^{-1} \qquad (5.78)$$

This is in contrast to conductivity or elastic moduli which have sample to sample variations $O(1/\sqrt{N})$. A similar analysis may be carried out for the dielectric and mechanical cases and the strength fluctuations are again logarithmic. For p approaching the pure limit, the strength fluctuations become smaller, so that exactly at the pure limit, they are zero. A practical consequence of the large sample to sample fluctuations occurring in measured strength values, in combination with the destructive character of typical experiments, make experimental studies of breakdown phenomena more demanding than corresponding experiments of transport or elastic moduli.

V.5 CONCLUSION AND DISCUSSION.

We have discussed the use of unconventional statistics in the study of disordered systems. Our specific results can be summarized as follows:

(1) For $p \neq p_c$, the distribution of the moduli of percolation networks is a Gaussian and the sample to sample fluctuations in moduli are small [$O(1/V^{1/2})$];

(2) Resistance of a disordered one dimensional quantum electronic chain is a product of a series of random numbers, which exhibits a large sample to sample fluctuations. Instead, the logarithm of resistance is a right statistical variable and it has a Gaussian distribution;

(3) We calculated the distribution of breakdown strengths in percolation networks and found it is a Gumbel distribution. In contrast to moduli, the sample to sample fluctuations in strengths are $O[1/(\ln V)]$. This can be explained by the fact that strengths depend on extreme fluctuations, while moduli depend on an average over all fluctuations.

In chapter IV, we have shown that transport properties are related to the low moments of local load distribution and strengths are related to the very high moments of local load distribution. The moment spectrum thus links the two very different classes of scaling behaviors, i.e., the moduli scaling and breakdown scaling, and quantifies their crossover. Generally, we would like to ask the following

general statistical question: for any given distribution, what is the critical moment m_c and how does this depend on the system size N? As discussed in last chapter, this can be studied by calculating the full distribution function of m-th moment for a set of N random numbers. Unfortunately, we have not succeeded in calculating the various moment distribution functions. But, people in mathematics have extensively studied a similar problem, what is the influence of the maximum term in the addition of independent random variables and when the maximum term will dominate the sum and thus violate the central limit theorem. There the asymptotic distribution is the major interest. They have found that, under the condition that the moments of the initial distribution diverge, the maximum term has a non-negligible contribution to the sum and the sum follows an extreme form[177-179]. Following this result, we can give an intuitive argument which leads to the calculation of m_c for a given distribution. The idea is as fellows. For a set of random numbers with a given distribution , we can calculate the expectation value of the m-th moment and its standard deviation. We can expect that the crossover occurs when the standard deviation is of order of expectation value. This is due to the fact that for a Gaussian distribution the deviation is much smaller than the expectation. To illustrate this idea, we now calculate m_c for an exponential distribution discussed in last chapter.

$$P(x) = b \exp(-bx) \tag{5.79}$$

where b is a positive constant. We first calculate the expectation value and standard deviation for the m-th moment, which is given by following equation:

$$Y_N = \sum_{i=1}^{N} X^m \tag{5.80}$$

We know that,

$$\langle X^m \rangle = \int_0^{+\infty} dx\ x^m\ P(x)$$

$$= b \int_0^{+\infty} dx\ x^m \exp(-bx) \quad = m!/b^m \tag{5.81}$$

and

$$\sigma^2 = \langle X^{2m} \rangle - \langle X^m \rangle^2$$

$$= (2m)!/b^{2m} - (m!/b^m)^2$$

$$= [(2m)! - (m!)^2]/b^{2m} \tag{5.82}$$

Assume that the central limit theorem works here, then we have the following result for Y_N:

$$\langle Y_N \rangle = N \langle X^m \rangle = N[m!/b^m] \tag{5.83}$$

and

$$\sigma_N^2 = N\ \sigma^2 = N[(2m)! - (m!)^2]/b^{2m} \tag{5.84}$$

Then, m_c can be determined by the following equation:

$$\langle Y_N \rangle^2 = \sigma_N^2,$$

or

$$N^2 [m_c!/b^{m_c}]^2 = N [(2m_c)! - (m_c!)^2]/b^{2m_c}$$

or

$$(N + 1) (m_c!)^2 = (2m_c)! \tag{5.85}$$

For large m, we can use the Stirling's formula,

$$\ln(m!) \approx m\ln m - m,$$

then Eq. (5.85) can be rewritten as,

$$\ln(N + 1) + 2[m \ln m - m] = (2m) \ln(2m) - (2m)$$

Thus we find that,

$$m_c = [\ln(N + 1)]/[2\ln 2] \sim \ln N \tag{5.86}$$

This agrees with the result we found in last chapter. Generally, we believe this idea will give a reasonable estimate for m_c for any distribution function. Research in calculating the full distribution function of Y_N and studying the detailed crossover behavior is going on now.

CHAPTER VI

Overview and Future Perspective

I have argued that breakdown strengths are related to the extreme fluctuations or the very high moments of the local load distribution, but the transport properties are related to the average over all fluctuations or the low moments of the local load distributions. One consequence is that the breakdown strengths of percolation networks exhibit a "dilute limit catastrophe" in which any finite fraction of disorder drastically reduces the network strength. This is in contrast to transport or elastic moduli which are linear in dilution with slope O(1) near the pure limit. A logarithmic size effect also occurs in this limit. Another implication of the dependence of breakdown properties on the tail (or high moments) of the local load distribution is that sample to sample variations in strength conform to extreme statistics distribution, rather than the central limit form appropriate to the conductivity or elastic moduli.

I can list many other statistical properties, such as specific heat and magnetic susceptibility, which are quantities related to an average over all fluctuations and conform to the central limit theorem. These conventional Gaussian type statistical variables have been intensively studied in statistical mechanics. But, it is important to note there exist many other physical problems in which the conventional central limit type microscopic averaging does not apply. Instead, the novel idea and scaling theories used to study extreme processes may eventually impact on these problems. Examples include relaxation processes in disordered systems, transport in quantum systems and nucleation and growth processes.

I put this thesis in a broader perspective by discussing some of the problems which are not in the category of breakdown phenomena, but

in which I believe the extreme fluctuations or unconventional statistics may play a key role.

VI.1 Relaxation Processes in Disordered Systems.

Due to disorder, the various parts of a random system relax at different rates and often a rare statistical fluctuations will dominate the asymptotic relaxation behavior of the system. One particular example is the relaxation process[180-190] of random magnetic systems in the "Griffiths phase", which refers to the temperature regime between the transition temperature T_c for magnetic long-range order in the random system and the Griffiths temperature T_G. The Griffiths temperature is the highest possible transition temperature allowed in principle by a rare statistical fluctuation of the disorder over the whole system[191]. For a ferromagnet with site or bond dilution, T_G is the critical temperature of the undiluted system; for a ferromagnet with a bounded distribution of exchange interactions, T_G is the critical temperature obtained when all bonds take the maximum value. For a ferromagnet with an unbounded distribution of exchange interactions, the Griffiths phase extends to infinite temperature.

The free energy of systems in the Griffiths phase exhibits singularities, which are called the Griffiths singularities. Griffiths singularities have important consequences for the dynamics of the system. In particular, relaxation is nonexponential for $T_c < T < T_G$,

$$C(t) \sim \begin{cases} \exp[-A(\ln t)^{d/(d-1)}] & \text{Ising systems} \quad (6.1a) \\ \exp(-Bt^{1/2}) & \text{Heisenberg systems} \quad (6.1b) \end{cases}$$

where d is the spatial dimension, amplitudes A and B are constants and depend on the system parameters (temperature, concentration of missing sites or bonds, etc.). The physics behind Eq. (6.1) concerns the dominance, as $t \to \infty$, of large regions in which, due to rare statistical fluctuations in the disorder, the exchange interactions have values characteristic of an ordered phase at the given temperature. Because these regions are finite they do relax, but only slowly due to their large size. This is a similar effect as in the breakdown problems, in which the rare statistical events, largest defect clusters, have a dominant contribution to the breakdown strengths. Therefore, I believe that the statistics of extreme will apply in this problem. Actually, following this direction, I can find the lower and upper bounds for C(t) of the form in Eq. (6.1a) for the dilute Ising ferromagnets below the percolation threshold[186-190], where the systems are sufficiently dilute they consist of finite clusters only. The idea is as follows. The lower bound is derived by considering only compact clusters. These are fewer in number than typical clusters, but relax more slowly. The upper bound is obtained by including all clusters, but replacing their lifetimes by those of compact clusters of the same size. And the result is,

$$C(t) \sim \exp[-A(\ln t)^{d/(d-1)}] \quad (6.2)$$

and

$$A_{min} \leq A \leq A_{max} \tag{6.3}$$

A_{min} and A_{max} have the form of $(T/\sigma)^{d/(d-1)}f(p)$, where T is the temperature, σ is the surface tension and f(p) is a function of p.

There are many other problems in disordered systems where the same rare statistical fluctuations or large cluster regions are dominant in the long time relaxation processes. One example is the asymptotic behavior of the survival probability P(t) for a diffusive particle in a background with randomly distributed traps[192-195], where the distribution of the large regimes without traps is crucial to the asymptotic behavior of P(t). Another example is nucleation and growth processes[196-198], in which the nucleation and growth of the largest droplet will dominate the growth rate. This is due to the fact that the largest droplet will reach the critical size first and then start to grow. Other examples include dynamic processes in spin glass[199-200].

VI.2 Transport in Quantum Systems.

As discussed in last chapter, one dimensional quantum transport process in disordered systems are another class of problems in which non-Gaussian type statistics apply. Here, I briefly discuss two other non-Gaussian quantum transport problems which have attracted considerable attention. One is Lifshitz tails in the density of states of disordered systems and the other on is universal conductance fluctuations in mesoscopic systems.

a) Lifshitz Tail in Disordered Systems.

Lifshitz[201] argued that in random systems the van Hove band-edge singularities in the density of states disappear and are replaced by exponential singularities. In the language of harmonic chains with two types of masses the underlying mechanism is that having a mode with a frequency close to the maximal frequency one needs a large region containing light masses only[202-205]. The probability of occurrence of such a region is exponentially small and so is the probability to find such an eigenfrequency, i.e., the density of states. It is clear to see that the Lifshitz tails in disordered systems in related to the rare statistical fluctuations.

b) Universal Conductance Fluctuations.

An interesting concept which is clearly emerging in recent theoretical and experimental studies of quantum transport is that of non-self-averaging of the conductance of samples in the mesoscopic size range. This is the regime intermediate between microscopic and macroscopic where the sample's dimensions are less than a phase coherence length L_ϕ, which is the distance across which the electrons lose phase memory. In these systems, the conductances exhibit large sample to sample fluctuations, and the so-called universal conductance fluctuations are found[206-210], i.e.,

$$\langle G^2 \rangle - \langle G \rangle^2 = \text{constant} \cdot (e^2/h) \qquad (6.4)$$

where the angular brackets signify ensemble averaging and the constant is a number of order unity, universal in the sense that it is independent of both disorder and sample size. This result is very different from the typical inverse square-of-the-size [O(1/√N)] dependence of the relative fluctuations in conventional statistics. The physical reason is that the electrons are phase coherent and the quantum mechanical coherence of the electron waves dominates the physics under these circumstances[211-215]. In particular, in two-dimensional films the motion of even a single impurity atom leads to a change of order (e^2/h) in conductance, no matter what the sample size L. This effect is very similar to the "dilute limit catastrophe" in breakdown problems.

At present the above mentioned problems are treated by seemingly different analysis methods. It is probable that a new unified class of theoretical techniques for all these problems, based on the study of rare statistical fluctuations instead of the average over all fluctuation, can be developed.

APPENDIX A

COMPUTER CODE TO CALCULATE THE BREAKDOWN CURRENT AND VOLTAGE IN A RANDOM RESISTOR NETWORK

```
      Program Fuse
C
C     Purpose and method: to calculate the breakdown current and
C                voltage in a Lx(L+1) random resistor network with
C                percolation probability p by using the conjugate-
C                gradient method.
C
C     Inputs:    System Size = L; Percolation Probability = Prob;
C                Number of the Average Configurations = Nsys;
C                The Seed to Generate the Random Number = Iseed.
C
C     Outputs:   Conductivity = Cond; Total Current = Curr;
C                Breakdown Current = Cb; Breakdown Voltage = Vb.
C
C     IMPLICIT DOUBLE PRECISION(A-H, O-Z)
C
C--------------------------------------
      COMMON  GX(12000),GY(12000),V(12000),V1(12000),V2(12000),
     1        R(12000),P(12000),Z(12000)
      LOGICAL LX,LY
      COMMON  /SPAN/ L,MAX,LEVEL(500),NN(12000),LX(12000),
     1        LY(12000),PROB
C--------------------------------------
C
      INTERMX=5000
      EPS=1.0D-9
      MAX=12000
C
C   TO READ THE INPUT DATA
C
   10 READ(5,*) L,PROB,NSYS,ISEED
      IF(L.LT.0) GO TO 999
C
      N=L*(L+1)
      N2=N+N
```

```
      L1=L+1
      L2=L+2
      LL1=L+L+1
      NL=N-L
      NLL=N-L-L
C
C   LOOP 800 IS TO AVERAGE OVER NSYS CONFIGURATIONS
C
      DO 800 ISYS = 1, NSYS
C
C   SET UP INITIAL VOLTAGES AT EACH SITE: V(I)
C
      DO 30 I = 1, N
          X=DBLE((I-1)/L)/DBLE(L)
          V(I)=(1.0D0-X)
   30 CONTINUE
   40 CONTINUE
C
C   SET UP THE RANDOM RESISTOR NETWORK
C
      DO 50 I = 1, N
          GX(I0=0.0D0
          LX(I)=.FALSE.
          GY(I)=0.0D0
          LY(I)=.FALSE.
C     CALL THE RANDOM NUMBER GENERATOR: RAN()
          RAND1=RAN(ISEED)
          RAND2=RAN(ISEED)
          IF ( RAND1.LE.PROB) THEN
                GX(I)=1.0D0
                LX(I)=.TRUE.
          ENDIF
          IF (RAND2.LE.PROB) THEN
                GY(I)=1.0D0
                LY(I)=.TRUE.
          ENDIF
   50 CONTINUE
C
C   FREE BOUNDARY CONDITION IN TRANVERSE DIRECTION
C
      DO 60 I = L, N, L
          GY(I)=0.0D0
          LY(I)=.FALSE.
   60 CONTINUE
C
C   TO CHECK IF THE CONNECTION OF THE NETWORK
C
      DO 70 I = 1, L
          LEVEL(I)=1
   70 CONTINUE
      ITEST = ISPAN(0)
C-----  IF NETWORK NOT CONNECTED, REGENERATE IT
      IF ( ITEST.LT.0 ) GO TO 40
C
```

```
C-----------------------------------------
C
      CURR=0.0D0
      VB=0.0D0
      CB=0.0D0
      ITER=0
      DIFF=0.0D0
C
C   CONJUGATE GRADIENT TECHNIQUE
C
C   STARTING PROCEDURE
C
      DO 90 I = 1, N
          P(I)=0.0D0
          V1(I)=0.0D0
          R(I)=0.0D0
   90 CONTINUE
      DO 100 I = L1, NL
          V1(I)=(V(I-L)-V(I))*GX(I-L)+V1(I)
          V1(I)=(V(I+L)-V(I))*GX(I)+V1(I)
          V1(I)=(V(I-1)-V(I))*GY(I-1)+V1(I)
          V1(I)=(V(I+1)-V(I))*GY(I)+V1(I)
          R(I)=V1(I)
          P(I)=-R(I)
          V1(I)=R(I)*R(I)
  100 CONTINUE
      RR=0.0D0
      DO 110 I = L1, NL
          RR=RR+V1(I)
  110 CONTINUE
C
C   RELAXATION PROCEDURE
C
      DO 120 ITER = 1, ITERMX
          IF ( ITER.GE.2 ) THEN
                RRLAST=RR
                RR=0.0D0
                DO 130 I = L1, NL
                   V1(I)=R(I)*R(I)
                   RR=RR+V1(I)
  130           CONTINUE
                RR1=DSQRT(RR)
                IF ( RR1.LT.EPS ) GO TO 180
                E=RR/RRLAST
                DO 140 I = L1, NL
                   P(I)=E*P(I)-R(I)
  140           CONTINUE
          ENDIF
          DO 150 I = L1, NL
                V1(I)=0.0D0
  150     CONTINUE
          ZP=0.0D0
          DO 160 I = L1, NL
                V1(I)=(P(I-L)-P(I))*GX(I-L)+V1(I)
```

```
                V1(I)=(P(I+L)-P(I))*GX(I)+V1(I)
                V1(I)=(P(I-1)-P(I))*GY(I-1)+V1(I)
                V1(I)=(P(I+1)-P(I))*GY(I)+V1(I)
                Z(I)=V1(I)
                V1(I)=Z(I)*P(I)
                ZP=ZP+V1(I)
  160       CONTINUE
            Q=RR/ZP
            DO 170 I = L1, NL
                V(I)=V(I)+Q*P(I)
                R(I)=R(I)+Q*Z(I)
  170       CONTINUE
  120 CONTINUE
C
C    END OF RELAXATION PROCEDURE
C
  180 CONTINUE
      WRITE(6,111) ITER
  111 FORMAT(1X,'ITER',I5)
C
C    CALCULATE VB, CB, COND, CURR
C
      POWER=0.0D0
      POWMAXX=0.0D0
      DO 200 I = 1, NL
          V1(I)=0.0D0
          V1(I)=(V(I+L)-V(I))*(V(I+L)-V(I))*GX(I)
          IF ( GX(I).EQ.1.0D0.AND.POWMAXX.LE.V1(I) ) THEN
                POWMAXX=VA(I)
                IMAXX=I
          ENDIF
          POWER=POWER+V1(I)
  200  CONTINUE
      POWMAXY=0.0D0
      DO 220 I = L1, NL
          V2(I)=0.0D0
          V2(I)=(V(I+1)-V(I))*(V(I+1)-V(I))*GY(I)
          IF ( GY(I).EQ.1.0D0.AND.POWMAXY.LE.V2(I) ) THEN
                POWMAXY=V2(I)
                IMAXY=I
          ENDIF
          POWER=POWER+V2(I)
  220 CONTINUE
      POWMAX=DMAX1(POWMAXX,POWMAXY)
      CURR=POWER
      COND=CURR
      VB=1.0D0/DSQRT(POWMAX)
      CB=CURR*VB
      WRITE(6,1000) L,PROB,CURR,COND,VB,CB,ITER,RR
 1000 FORMAT(1X,I4,5F12.6,I7,F14.10)
C--------------------------------------
  800 CONTINUE
      GO TO 10
  999 STOP
```

```
      END
C
C   THE FOLLOWING TWO SUBROUTINES ARE TO CHECK THE
C             CONNECTION OF THE BETWORK
C


      INTEGER FUNCTION LASS(M)
C-------------------------------------------------------
      IMPLICIT DOUBLE PRECISION (A-H,O-Z)
      LOGICAL LX,LY
      COMMON /SPAN/ L,MAX,LEVEL(500),N(12000),LX(12000),
     1     LY(12000),PROB
C-------------------------------------------------------
      IF ( M.NE.MAX ) GO TO 1
      LASS=MAX
      RETURE
    1 MO=M
      M=N(M)
      IF ( MO.NE.M ) GO TO 1
      LASS=M
  999 RETURE
      END


      INTEGER FUNCTION ISPAN(IDUM)
C-------------------------------------------------------
      IMPLICIT DOUBLE PRECISION (A-H,O-Z)
      LOGICAL LX,LY
      COMMON /SPAN/ L,MAX,LEVEL(500),N(12000),LX(12000),
     1     LY(12000),PROB
C-------------------------------------------------------
      LP1=L+1
      INDEX=1
      DO 1000 I = 1, 12000
 1000 N(I)=0
      N(1)=1
      DO 2 K = 2, LP1
          ICONN=0
          DO 3 I = 1, L
                J=L*(K-1)+I
                IF ( LX(J-L) ) THEN
                      MOLD=LASS(LEVEL(I-1))
                ELSE
                      MOLD=MAX
                ENDIF
                IF ( LY(J-1) ) THEN
                      M1=LEVEL(I-1)
                ELSE
                      M1=MAX
                ENDIF
                MTR=MINO(MOLD,M1)
                IF ( MTR.EQ.MAX ) GO TO 5
                IF ( MTR.EQ.1 ) ICONN=1
```

```
            IF ( MOLD.LT.MAX ) N(MOLD)=MTR
            IF ( M1.LT.MAX) N(M1)=MTR
            GO TO 8
5           INDEX=INDEX+1
            MTR=INDEX
8           LEVEL(I)=MTR
            N(MTR)=MTR
            GO TO 4
7           LEVEL(I)=MAX
4           CONTINUE
3       CONTINUE
        IF ( ICONN.EQ.0) GO TO 6
2 CONTINUE
  ISPAN=1
  RETURN
6 ISPAN=-1
  RETURE
  END
```

APPENDIX B

ANALYTIC SOLUTIONS FOR DEFECT PROBLEMS

In this appendix, we outline the derivations of the analytic results for defect problems used before, i.e., scaling forms for a cracklike elliptical (or ellipsoidal) void in electrical and mechanical problems and for a long, thin metallic inclusion in a dielectric. In all cases we consider an external electric field or tensile stress applied along the z direction. We also restrict our attention to the most severe flaws, namely ellipses and oblate ellipsoid voids with their long axis perpendicular to the direction of applied load in the electrical and elastic cases, and ellipse and prolate ellipsoid perfect conductors with their long axis parallel to the direction of applied electric field in the case of dielectric problems. These ellipses and ellipsoids are characterized by one or two long axes, a, and one or two short axes, b, and we consider a/b large to simulate the most severe flaws.

B. 1 Electric problems.

a. Two-dimensional insulating void in a conducting background.

Consider an elliptical defect in an infinite two-dimensional system. The equation for an ellipse centered at the origin is

$$x^2/a^2 + z^2/b^2 = 1, \tag{B1}$$

which is depicted in Fig. 3.1(b). To find the current density at any point outside the boundary of the elliptical defect (ξ_0) solve the Laplace's equation with the boundary condition

$$\frac{\partial \Psi}{\partial \xi} = 0, \qquad \text{for } \xi=\xi_0 \tag{B2}$$

which ensures that no current flows into the insulating defect. Laplace's equation is invariant under a transformation to elliptical coordinates[a1], and in that frame, the appropriate form of the solution is,

$$\Psi(\xi,\eta) = Az + Be^{-\xi}\sin(\eta+\epsilon) + Ce^{\xi}\sin(\xi+\eta), \tag{B3}$$

where

$$x = c\cosh(\xi)\cos(\eta); \quad z = c\sinh(\xi)\sin(\eta), \tag{B4}$$

$$a = c\cosh(\xi_0), \tag{B5}$$

$$b = c\sinh(\xi_0), \tag{B6}$$

$$c = (a^2 - b^2)^{1/2}. \tag{B7}$$

where A, B, C, and ε are constants. Choose $\varepsilon = C = 0$ and $A = -E_0$ to produce the externally applied electric field. Then,

$$\begin{aligned}\Psi(\xi,\eta) &= -E_0 z + Be^{-\xi}\sin(\eta) \\ &= -E_0 c\sinh(\xi)\sin(\eta) + Be^{-\xi}\sin(\eta)\end{aligned} \tag{B8}$$

and the boundary condition (B2) implies

$$B = -E_0 c e^{\xi_0}\cosh(\xi_0). \tag{B9}$$

The electric field in the z direction is then

$$E_z = \frac{\partial\Psi}{\partial z} = -[\cosh(\xi)\sin(\eta)\ (\frac{\partial\Psi}{\partial\xi}) +$$

$$\sinh(\xi)\cos(\eta)\ (\frac{\partial\Psi}{\partial\eta})]/[c(\cosh^2\xi - \cos^2\eta)] \tag{B10}$$

$$= E_0 - Be^{-\xi}[\cosh(\xi)\sin^2(\eta) -$$

$$\sinh(\xi)\cos^2(\eta)]/c[\cosh^2\xi - \cos^2\eta] \tag{B11}$$

the current density in the z direction is $j_z = \sigma E_z$, where σ is the conductivity. Setting η=0, yields for the electric field and current

density in the z direction as a function of distance from the ellipse tip (on the z=0 line):

$$E_z(\xi) = E_0[1 + \cosh\xi_0 \exp(\xi_0-\xi)/\sinh\xi], \tag{B12}$$

and

$$J_z(\xi) = J_0\,[1 + \cosh\xi_0 \exp(\xi_0-\xi)/\sinh\xi] \tag{B13}$$

This is the Eq. (3.4) used in Chapter III.

The electric field at the defect tip is then

$$E_{tip} = E_0\,(1 + a/b) = E_0\,[1 + 2^{1/2}(a/2\kappa)^{1/2}] \tag{B14}$$

where κ is the curvature at the defect tip and $\kappa=b^2/a$. Eq. (B12) can be written in terms of r, the distance from the defect tip,

$$E_z(r) = E_0\left(1 + \frac{a(a+b)[(a+r)-(2ar+r^2+b^2)^{1/2}]}{c^2(r^2+2ar+b^2)^{1/2}}\right) \tag{B15}$$

A plot of this equation is given in Fig. 4.2(a). When r is large, $E_z(r)$ asymptotes to a dipole form,

$$E_z(r) = E_0(1 + \alpha_{2e}/r^2) \tag{B16}$$

with the electric dipole moment

$$a_{2e} = a(a+b)/2. \tag{B17}$$

Since the inclusion is sharp, the electric field becomes large near the defect tip [as seen in Eq. (B14)], the nature of this divergence is found from a small r expansion of Eq. (B15) which shows

$$E_z(r) \sim E_{tip}, \qquad \text{when } r \ll \kappa \tag{B18}$$

and

$$E_z(r) \sim E_0[1 + a(a+b)/c^2(a/2r)^{1/2}], \quad \text{when } a>r>\kappa \tag{B19}$$

$$= E_0[c_{1e} + c_{2e}(a/2r)^{1/2}] \tag{B20}$$

with

$$c_{1e} = 1 \quad \text{and} \quad c_{2e} = a/(a-b) \tag{B21}$$

Note that c_{1e} and c_{2e} are O(1) as $a \to \infty$ and $\kappa \to \infty$. Therefore, we get the scaling form of electric field,

$$E_z(r)/E_0 \sim \begin{cases} 1 + a_{2e}/r^2 & \text{for } r \gg a, \\ c_{1e} + c_{2e}(a/2r)^{1/2} & \text{for } \kappa < r < a, \\ k_{1e} + k_{2e}(a/2\kappa)^{1/2} & \text{for } r < \kappa. \end{cases} \tag{B22}$$

which is the Eq. (4.15) used in Chapter IV.

b. Three-dimensional insulating void in a conducting background.

The single inclusion shape and orientation that is most effective in enhancing electric fields for this case is penny shaped and oriented perpendicular to the electric field direction. To simulate this we use an oblate ellipsoidal void inclusion, and the electric fields are found by solving the Laplace's equation in ellipsoidal coordinates. The geometry is like that of Fig. 3.1(b), with the ellipsoid found by making a solid of revolution about the z axis. The relationships between Cartesian and oblate ellipsoidal coordinates is given by[83]

$$\begin{aligned} x &= c\cosh\xi\cos\eta\cos\phi, \\ y &= c\cosh\xi\cos\eta\sin\phi, \\ z &= c\sinh\xi\sin\eta. \end{aligned} \tag{B23}$$

The electric potential for a uniform conducting background containing this "penny-shaped" void, with a constant electric field E_0 at infinity in the z direction, is then found by solving Laplace's equation in oblate ellipsoidal coordinates to find

$$\Psi = -cE_0\sinh\xi\sin\eta[1 - (\cot^{-1}\sinh\xi - 1/\sinh\xi)/A] \tag{B24}$$

where

$$\begin{aligned} A &= \cot^{-1}\sinh\xi_0 - \tanh\xi_0/\cosh\xi_0 \\ &= \cot^{-1}(b/c) - bc/a^2 \end{aligned} \tag{B25}$$

The z-direction electric field as a function of distance, r, from the ellipse tip in x=y=0 plane is then given by

$$E_z(\xi) = -\frac{\partial \Psi}{\partial z}\Big|_{x=y=0}$$

$$= E_0[1 - (\cot^{-1}\sinh\xi - 1/\sinh\xi)/A] \qquad \text{(B26)}$$

The electric field at the tip of the defect is found by evaluating Eq. (B26) at $\xi=\xi_0$ and gives

$$E_{tip} = E_0(1 - [\cot^{-1}(b/c) - (c/b)]/A) \qquad \text{(B27)}$$

which for large a and small b reduces to

$$E_{tip} \sim E_0[2/\pi + 4a(\pi b)]$$

$$= E_0[k_{1e} + k_{2e}(a/2\kappa)^{1/2}] \qquad \text{(B28)}$$

with

$$k_{1e} = 2/\pi \quad \text{and} \quad k_{2e} = 4(2^{1/2})/\pi \qquad \text{(B29)}$$

for large a. Rewriting Eq. (B26) in terms of the distance from the defect tip yields

$$E_z(r,z=0) = E_0 - E_0(\cot^{-1}[(a+r)^2/c^2 - 1]^{1/2} -$$

$$[(a+r)^2/c^2 - 1]^{-1/2})/A \qquad \text{(B30)}$$

and expanding for large r then shows that the "far-field solution" is of a dipole form

$$E_z(r) \sim E_0(1 + \alpha_{3e}/r^3) \quad \text{for } r>>a \tag{B31}$$

where the dipole moment

$$\alpha_{3e} = \text{dipole moment} = c^3/3A \tag{B32}$$

A small-r expansion of Eq. (B30) shows the near-field solution yields

$$E_z(r) \sim E_0[c_{1e} + c_{2e}(a/2r)^{1/2}] \quad \text{for } \kappa<r<a \tag{B33}$$

with

$$c_{1e} = 2b/\pi c \quad \text{and} \quad c_{2e} = 1/A. \tag{B34}$$

When $r<\kappa$, Eq. (B30) reduces to $E_z(r) \sim E_{tip}$.

c. Use of the complex mapping method for solving the tip enhancement in 2D two defect problem.

In this section, we will use the complex mapping method to calculate the tip current enhancement for 2D two slit-like defect problem. In the complex mapping method, we can find the required electric potential solution to Laplace's equation in two dimension from the complex potential function ω defined by,

$$\omega = u + iv \tag{B35}$$

The electric field is also cast into a complex form as

$$E = E_x + iE_z = -\frac{\partial u}{\partial x} - i\frac{\partial u}{\partial z}$$

by the Cauchy's relation, this becomes

$$E = E_x + iE_z = -\frac{\partial u}{\partial x} + i\frac{\partial v}{\partial x} \tag{B36}$$

and so the complex electric field is found from the complex potential from the equation

$$E = \frac{d\bar{\omega}}{d\zeta} \tag{B37}$$

where $\zeta = x + iz$. It is straightforward to then find the physical electric fields E_x and E_z from the complex electric field E. Now if we assume that $\omega(\zeta)$ is analytic, u and v in Eq. (B35) obey Laplace's equation. Under a conformal transformation, the transformed u and v again obey Laplace's equation, and we look for conformal transformations that simplify the geometry of the original problem.

We first illustrate the process with a single crack of infinitesimal thickness as depicted in Fig. B1(a). In this figure, the electric potential at infinity is linearly increasing with vertical direction, and has no dependence on the horizontal direction. It is very easy to solve this one crack problem by the mapping method. We can use the following mapping

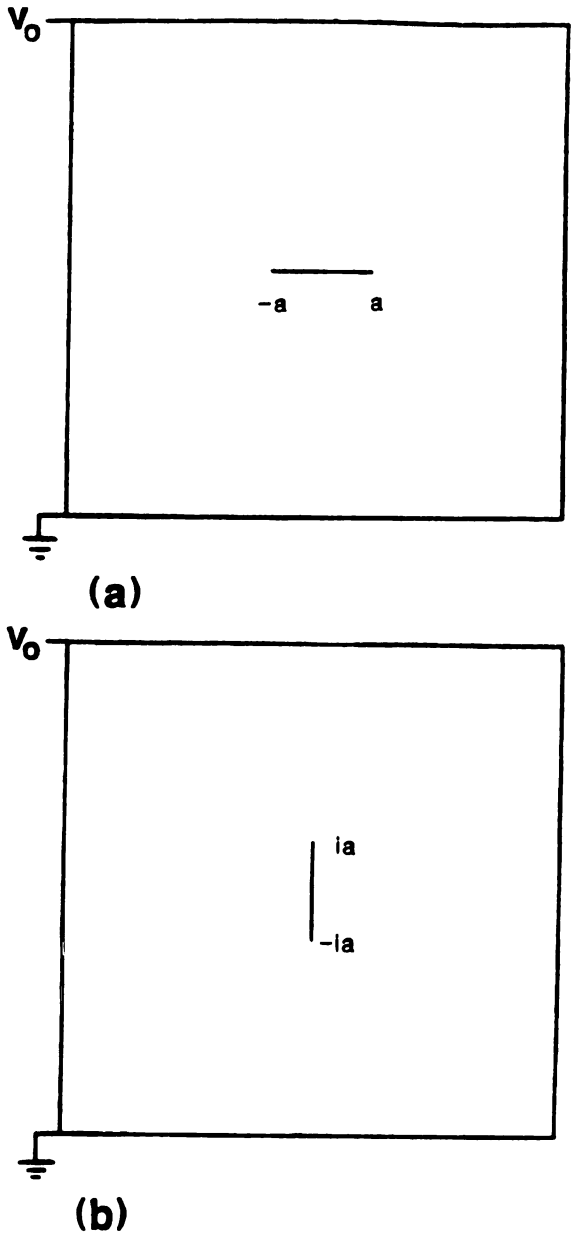

Fig. B1 The single slit representation of the elliptic defect. (a) is the original geometry; (b) is the geometry after conformal transformation. In this geometry, the solution is trivial provided the slit has infinitesimal thickness.

$$\xi = (\zeta^2 - a^2)^{1/2} \tag{B38}$$

to transform the ζ plane to the ξ plane as shown in Fig. B1(b) where the slit is transformed to an orientation parallel to the external field. The boundary conditions at infinity are unaltered in the transformation, and so the solution in the presence of the transformed slit is trivial provided the slit is of infinitesimal thickness. We then see that in the ξ plane, the complex potential is

$$\omega(\xi) = -iE_0\xi \tag{B39}$$

which using Eq. (B37) gives the correct solution in the transformed space. This solution in the ξ space is then transformed back to the ζ space to find the required solution

$$u + iv = -iE_0[(\zeta^2 - a^2)^{1/2}] \tag{B40}$$

and so from Eq. (B37) we find

$$\begin{aligned} E_x - iE_z &= iE_0\zeta/(\zeta^2 - a^2)^{1/2} \\ &= iE_0(x+iz)/(x^2-z^2-a^2+2ixz)^{1/2} \end{aligned} \tag{B41}$$

On x axis, z=0, the complex electric field becomes

$$E_x - iE_z = iE_0x/(x^2 - a^2)^{1/2} \tag{B42}$$

As a function of distance (in the x-direction along the z=0 line) from the defect tip, the electric field is

$$E_z = \pm E_0 x/(x^2 - a^2)^{1/2} \tag{B43}$$

It is interesting to note that E_z and hence the current density in the z direction is singular at the defect tip, in contrast to the ellipse result where the current density is finite at the ellipse tip (x=a). However, the two types of continuum defects give the same result in the lattice limit for large system sizes, as may be seen by integrating the result (B43) over the lattice spacing d:

$$I_{slit} = j_\infty (2ad + d^2)^{1/2} \tag{B44}$$

and taking the large a/d limit, this gives,

$$I_{slit} \sim I_\infty (2a/d)^{1/2} \tag{B45}$$

Which is the same in the large a/d limit as the ellipse result Eq. (3.7) quoted in Chapter III.

We know illustrate how to use this method to solve the two slit problem depicted in Fig. 3.2(b). First, make a transformation

$$\zeta = \frac{x + iz}{a + b} \tag{B46}$$

where a and b are defined in Fig. 3.2(b) and define

$$k = a/(a+b) \tag{B47}$$

Now, make the mapping[84,85]

$$\xi = i\int_0^{\zeta} (\zeta^2 - \lambda^2)/[(\zeta^2 - 1)(\zeta^2 - k^2)]^{1/2}d\zeta \tag{B48}$$

This mapping transforms the two collinear cracks problem of Fig. 3.2(b) to the biplane configuration of Fig. 3.2(c). The boundary conditions are unaltered in this transformation except for a rotation by ninety degrees, and in the new geometry, the potential in the transformed space is again trivial for infinitesimally thin cracks. We find the positions of the biplanes from the mapping Eq. (B48).

$$c = \int_k^{\lambda} (\lambda^2 - \zeta^2)/[(1 - \zeta^2)(\zeta^2 - k^2)]d\zeta \tag{B49}$$

and

$$h = \int_0^{k} (\lambda^2 - \zeta^2)/[(1 - \zeta^2)(k^2 - \zeta^2)]d\zeta \tag{B50}$$

where c and h are as defined as in Fig. 3.2(c). λ is fixed by the requirement that the mapping (B48) should be independent of path, i.e.,

$$I = \int_C (\zeta^2 - \lambda^2)/[(1 - \zeta^2)(\zeta^2 - k^2)]^{1/2}d\zeta = 0 \tag{B51}$$

where the integral path C includes each of the cracks. Thus

$$I = 2\int_k^1 (\zeta^2 - \lambda^2)/[(1 - \zeta^2)(\zeta^2 - k^2)]^{1/2}d\zeta = 0 \tag{B52}$$

i.e.,

$$\int_k^1 \zeta^2/[(1-\zeta^2)(\zeta^2-k^2)]^{1/2}d\zeta = \lambda^2\int_k^1 [(1-\zeta^2)(\zeta^2-k^2)]^{-1/2}d\zeta \qquad (B53)$$

Let $\zeta = [1 - (1 - k^2)u^2]^{1/2}$ and $k'^2 = 1 - k^2$, then,

$$\lambda^2 = \int_k^1 \zeta^2/[(1-\zeta^2)(\zeta^2-k^2)]^{1/2}d\zeta/\int_k^1 [(1-\zeta^2)(\zeta^2-k^2)]^{-1/2}d\zeta$$

$$= \int_0^1 [(1 - k'^2u^2)/(1-u^2)]^{1/2}du/\int_0^1[(1-u^2)(1-k'^2u^2)]^{-1/2}du$$

$$= E(k')/K(k') \qquad (B54)$$

where K(k') and E(k') are elliptic integrals of the first and second kind respectively. In the ξ plane, we know the complex potential function is simply

$$\omega(\xi) = -E_0\xi \qquad (B55)$$

so, in the ζ plane, the potential is

$$\omega(\zeta) = -iE_0\int_0^\zeta (\zeta^2-\lambda^2)/[(\zeta^2-1)(\zeta^2-k^2)]^{1/2}d\zeta \qquad (B56)$$

And from Eq. (B37), we get

$$E_x - iE_z = iE_0(\zeta^2-\lambda^2)/[(\zeta^2-1)(\zeta^2-k^2)]^{1/2} \qquad (B57)$$

On x axis, we then have:

$$E_x - iE_y = iE_0[x^2-\lambda^2(a+b)^2]/([x^2-(a+b)^2][x^2-a^2])^{1/2} \qquad (B58)$$

and hence the behavior of the physical electric fields is,

for $-a<x<a$:

$$E_x = 0, \quad E_z = \pm E_0[x^2-\lambda^2(a+b)^2]/([x^2-(a+b)^2][x^2-a^2])^{1/2} \qquad (B59)$$

for $|x|>a+b$:

$$E_x = 0, \quad E_z = \pm E_0[x^2-\lambda^2(a+b)^2]/([x^2-(a+b)^2][x^2-a^2])^{1/2} \qquad (B60)$$

for $a<|x|<a+b$:

$$E_x = \pm E_0[x^2-\lambda^2(a+b)^2]/([(a+b)^2-x^2][x^2-a^2])^{1/2}, \quad E_z = 0 \qquad (B61)$$

To find the current between the two cracks, we integrate Eq. (B59),

$$I_{slits} = \pm 2\sigma E_0 \int_0^a dx[x^2-\lambda^2(a+b)^2]/([x^2-(a+b)^2][x^2-a^2])^{1/2}$$

$$= 2\sigma E_0(a+b)[E(k) - K(k) + E(k')K(k)/K(k')] \qquad (B62)$$

where σ is the conductivity of the system. We are interested in the limit $a<<b$, which implies $k\to 0$. In this case,

$$I_{slits} \to 2\sigma E_0(a+b)E(k')K(k)/K(k') \qquad (B63)$$

As $k \to 0$, $k' \to 0$, $E(k') \sim K(k)$ and both are finite, and $K(k')$ is singular. Because $K(k')$ is singular as $\ln(1-k'^2)$, we find

$$I_{slits} \sim \sigma E_0 (a+b) E(k') K(k) / \ln[a/(a+b)] \qquad \text{(B64)}$$

which is the result quoted in Eq. (3.14) in Chapter III.

To make contact with the result for one slit when the distance between the two slits is zero, take the limit $a \to 0$, then $\lambda^2 = E(k')/K(k') \to 0$, and Eq. (B60) becomes

$$E_z = -E_0 x/(x^2 - b^2)^{1/2} \quad \text{for } |x| > b \qquad \text{(B65)}$$

which is the one crack result reported in Eq. (B43).

B.2 Dielectric problems.

a. 2D problem of a conducting ellipse in an insulating background.

The most effective-field enhancing inclusion is a thin ellipse with its long axis parallel to the direction of the electric field (z axis). The electric field outside the inclusion can be found by solving the Laplace's equation in elliptical coordinates:

$$x = c\sinh\xi\sin\eta, \quad z = c\cosh\xi\cos\eta \qquad \text{(B66)}$$

and

$$a = c\cosh\xi_0, \quad b = c\sinh\xi_0$$

The calculation is analogous to that described in Appendix B.1 a for the 2D electrical problem. The only change is that the boundary condition on the ellipse is now

$$\Psi(\xi_0) = 0 \tag{B67}$$

The solution in this case is

$$\Psi(\xi,\eta) = A\cosh\xi\cos\eta + Be^{-\xi}\cos\eta$$

where

$$A = -cE_0$$

Boundary condition (B67) determines that

$$B = -A\cosh\xi_0\exp(\xi_0)$$

$$= cE_0\cosh\xi_0\exp(\xi_0) \tag{B68}$$

Thus,

$$\Psi(\xi,\eta) = -cE_0\cosh\xi\cos\eta + cE_0\cosh\xi_0\exp(\xi_0-\xi)\cos\eta \tag{B69}$$

The electric field in the z direction and on the z axis is then

$$E_z(\xi,\eta)|_{x=0} = -\frac{\partial\Psi}{\partial z}\Big|_{x=0}$$

$$= -[\sinh\xi\cos\eta(\frac{\partial\Psi}{\partial\xi}) -$$

$$\cosh\xi\sin\eta(\frac{\partial\Psi}{\partial\eta})]/[c(\cosh^2\xi - \cos^2\eta)] \mid_{x=0}$$

$$= E_0[1 + \cosh\xi_0\exp(\xi_0-\xi)/\sinh\xi] \qquad \text{(B70)}$$

Therefore, the solution is mathematically identical to that given above for the 2D electrical case (although geometrically the conducting ellipse has its long axis parallel to the applied field), and expression for the electric field at the crack tip, in the near field and in the far field are identical to those given in Eqs. (B16) - (B21) for the electrical case.

b. 3D problem of a conducting ellipsoid in a dielectric background.

The most efficient-field enhancing defect is formed by making a solid of revolution about the z axis of an ellipse with its long axis in the z direction. This "finger-like" inclusion is the most important single inclusion for this case of dielectric problem. Solving Laplace's equation in the probate ellipsoidal coordinates

$$\begin{aligned} x &= c\sinh\xi\sin\eta\cos\phi \\ y &= c\sinh\xi\sin\eta\sin\phi \\ z &= c\cosh\xi\cos\eta \end{aligned} \qquad \text{(B71)}$$

leads to the electric potentials

$$\Psi_{in} = 0 \tag{B72}$$

$$\Psi_{out} = -cE_0\cosh\xi\cos\eta(1 - [\ln(\tanh\tfrac{\xi}{2}) + 1/\cosh\xi]/B) \tag{B73}$$

where

$$B = \ln[\tanh(\xi_0/2)] + 1/\cosh\xi_0 \tag{B74}$$

The electric field in the z direction and at the z axis, as a function of distance from defect tip is then

$$E_z(\xi) = E_0 + E_0(\ln[\tanh(\xi/2)] + \cosh\xi/\sinh^2\xi)/B \tag{B75}$$

From this expression we find the electric field at the defect tip to be

$$E_{tip} = E_0(1 + a^2/[b^2\ln(2a/b)]) \tag{B76}$$

The far-field (large r) solution again has a dipole form

$$E_z(r) - E_0 \sim \alpha_{3d}/r^3 \tag{B77}$$

where the 3D electric dipole moment

$$\alpha_{3d} = 2c^3/3B \tag{B78}$$

For $\kappa<r<a$, the electric field reduces to

$$E_z(r) - E_0 \sim E_0[\ln(r/2a) + a/2r]/B \tag{B79}$$

and for $r<\kappa$,

$$E_z(r) \sim E_{tip} \tag{B80}$$

B.3 Elastic problems.

a. 2D void in an elastic background.

We consider the geometry of Fig. 4.1 with the external electric field replaced by a tensile stress. The calculation of the stress field due to this inclusion is a standard calculation, and the vertical stress along the horizontal direction is given by [taken from Ref. 216, Eq. (130)]

$$\sigma_z(\xi,\eta=0) = \sigma_0(1 + (A[3\exp(-\xi)-\exp(-3\xi)] + B\cosh\xi)/\sinh^3\xi) \tag{B81}$$

where

$$A = \cosh\xi_0[\exp(3\xi_0) - 3\exp(\xi_0)], \quad B=\cosh^2\xi_0 \tag{B82}$$

The stress at the defect tip is then given by

$$\sigma_{tip} = \sigma_0(1 + 2a/b) \tag{B83}$$

Expression (B81) in terms of r the radial distance from the crack tip, and doing the large-r expansion, we find

$$\sigma_z(r) - \sigma_0 \sim \alpha_{2m}/r^2 \qquad \text{for } r>>a \tag{B84}$$

with the 2D elastic dipole moment

$$\alpha_{2m} = a^2/2 \tag{B85}$$

A small-r expansion of (B81) yields

$$\sigma_z(r) - \sigma_0 \sim \sigma_0(a/2r)^{1/2} \qquad \text{for } \kappa<r<a \tag{B86}$$

b. 3D void in an elastic background.

The most important single defect is a penny-shaped inclusion with its long axis oriented perpendicular to the direction of the applied tensile stress. To study this, we form a solid of revolution about the z axis of the ellipse inclusion of Fig. 4.1. The exterior stress and strain fields are most easily found using the equivalent inclusion method, and the z-direction stress as a function of distance from the defect tip is given by [this is found after simplifying Eq. (126) of Ref. 216],

$$\sigma_z(\xi) = \sigma_0[1 + a^4 b(K_1 \cot^{-1}\sinh\xi - K_1/\sinh\xi + K_2/\sinh^3\xi)/(N_1 c^5)] \tag{B87}$$

where

$$K_1 = (12-10/\nu)g + 2a^4/c^4 - (25 - 22/\nu)a^2c^2 \quad \text{(B88)}$$

$$K_2 = 12a^4/c^4 - 6(g + 2)a^2/c^2 + 6g \quad \text{(B89)}$$

$$N_1 = 6[4a^4b^2/c^6 - 2(1 - 1/\nu)g^2 - (2a^4 - 8a^2b^2)g/c^4] \quad \text{(B90)}$$

and

$$g = [a^4bcot^{-1}(b/c) - a^2b^2c]/c^5 \quad \text{(B91)}$$

where ν is Poisson's ratio. The stress intensity at the defect tip is found to be

$$\sigma_{tip} = \sigma_0a^2([2a^4/b^4 - (1.5 - 1/\nu)a^2/b^2 + 1 - 1/\nu] +$$

$$a^2A[1/\nu - (1.5 + 1/\nu)a^2/b^2])/[(a^2/b^2 + 1 - 1/\nu)/bc$$
$$+ a^2A(a^2/b^2 - 2 - 2/\nu) - a^4A^2(1 + 1/\nu)/bc] \quad \text{(B92)}$$

where

$$A = \tan^{-1}(c/b) \quad \text{(B93)}$$

For large a/b and $1/\nu << a/b$, we find

$$\sigma_{tip} \sim -\pi(3\nu + 2)/4 + 2a/b = k_{1m} + k_{2m}(a/2\kappa)^{1/2} \quad \text{(B94)}$$

with

$$k_{1m} = -\pi(3\nu + 2)/4, \quad k_{2m} = 8^{1/2} \tag{B95}$$

A large-r expansion, yields the expected dipole behavior

$$\sigma_z(r) - \sigma_0 \sim \alpha_{3m}/r^3 \qquad \text{for } r>>a \tag{B96}$$

where

$$\alpha_{3m} = (K_2 - K_1/3)a^4 b\sigma_0/(c^2 N_1) \tag{B97}$$

is the dipole moment. A small-r expansion yields

$$\sigma_z(r) - \sigma_0 \sim 1/r^{1/2} \qquad \text{for } \kappa<r<a \tag{B98}$$

and

$$\sigma_z(r) \sim \sigma_{tip} \qquad \text{for } r<<\kappa \tag{B99}$$

REFERENCES

[1] N.F. Mott and H. Jones, 1936, The Theory of the Properties of Metals and Alloys, Oxford, reprinted by Dover Publications, New York; C. Kittel, 1971, Introduction to Solid State Physics, Wiley.

[2] R. Zallen, 1983, The Physics of Amorphous Solids, Wiley.

[3] N.F. Mott and E.A. Davis, 1971, Electronic Processes in Non-crystalline Materials, Oxford University Press.

[4] For general introduction about the percolation theory see: D. Stauffer, 1985, Introduction to Percolation Theory, Taylor & Francis Ltd; S. Kirkpatrick, Rev. Mod. Phys., 574 (1973); H.L. Frisch and J.M. Hammersley, J. Soc. Indust. Appl. Math. 11, 894 (1963).

[5] P.M. Duxbury and Y.S. Li, Proceeding of the SIAM Workshop on Random Media and Composites, Leesburg, Virginia, 1988.

[6] R. Landauer in AIP Conference Proceedings, No. 40, 1978, eds. by J. Garland and Tanner.

[7] P.G. de Gennes, J. Phys. (Paris) 37, L-1 (1976).

[8] S. Alexander, J. Phys. (Paris) 45, 1939 (1984).

[9] P.-z Wong, Phys. Today, 41, No. 12, 24 (1988); J.R. Banavar, J. Koplik, K.W. Winkler, eds., Physics and Chemistry of Porous Media II, AIP Conference Proceedings 154, AIP, New York (1987).

[10] For a review, see Ref 2 and 4; D. Stauffer, Phys. Rep. 54, 1 (1979); V.K.S. Shante and S. Kirkpatrick, Adv. Phys. 20, 325 (1971); D.J. Thouless, in Ill-Condensed Matter, eds. by R. Balian, R. Maynard and G. Thoulouse (North-Holland, Amsterdam, 1979).

[11] D.A.G. Bruggeman, Ann Phys. (Leipz.) 24, 636 (1935).

[12] R. Landauer, J. Appl. Phys. 23, 779 (1952).

[13] W.F. Brown, Handb. Phys. 17, 104 (1956).

[14] E.H. Kerner, Proc. Phys. Soc. Lond. B69, 802 (1956).

[15] E.H. Kerner, Proc. Phys. Soc. Lond. B69, 808 (1956).

[16] W.T. Elam, A.R. Kerstein and J.J. Rehr, Phys. Rev. Lett. 52, 1516 (1984).

[17] J.N. Roberts and L.M. Schwartz, Phys. Rev. B31, 5990 (1985).

[18] B.I. Halperin, S. Feng and P.N. Sen, Phys. Rev. Lett. 54, 2391 (1985).

[19] S. Feng, B.I. Halperin and P.N. Sen, Phys. Rev. B35, 197 (1987).

[20] see reference 6; G. Deutscher, A. Kapitulnik and M. Rappaport, Ann. Israel Phys. Soc. 5, 207 (1983); P.N. Sen, C. Scala and M.H. Cohen, Geophys. 46, 781 (1981).

[21] R.I. Cukier, J. Phys. Chem. 89, 246 (1985).

[22] J. Berryman, J. Acoust. Soc. Am. 68, 1820 (1980), and reference therein.

[23] M.F. Thorpe and P.N. Sen, J. Acoust. Soc. Am. 77, 1674 (1985).

[24] R. Hill, J. Mech. Phys. Solid., 13, 213 (1965); B. Budiansky, ibid., 13, 223 (1965); T.T. Wu, Int. J. Solid. Struct., 3, 1 (1966).

[25] W. Xia and M.F. Thorpe, Phys. Rev. A38, 2650 (1988).

[26] L.M. Schwartz and J.R. Banavar, Phys. Rev. B39, 11965 (1989).

[27] C.J. Lobb and M.G. Forrester, Phys. Rev. B35, 1899 (1987).

[28] E.N. Martinez, private communication.

[29] B.R. Lawn and T. Wilshaw, Fracture of Brittle Solids (Cambridge Univ. Press, 1975).

[30] R. Thomson, in Solid State Phys., ed. by H. Ehrenreich and D. Turnbull, 39, 1 (Academic Press, N. Y., 1986).

[31] D.R. Clarke and K.J. Faber, J. Phys. Chem. Solids, 48, 1151 (1987).

[32] J.E. Gordon, The New Science of Strong Materials, Princeton Univ. Press, Princeton (1987).

[33] A. Kelly and N.H. Macmillan, Strong Solids, Clarendon Press, Oxford (1986).

[34] See, e.g., the collection of articles in Fracture, ed. by H. Liebowitz (Academic Press, New York, 1984), Vols. I-VII.

[35] S.M. Weiderhorn, Annu. Rev. Mater. Sci., 14, 373 (1984).

[36] F. McClintock, in Fracture Mechanics of Ceramics, ed. by R.C. Brandt, D.D.H. Hasselman and F.F. Lange (Plenum, New York, 1974).

[37] R.W. Davidge, Mechanical Behavior of Ceramics, Cambridge Solid State Science Series (Cambridge Univ. Press, Cambridge, 1979).

[38] H. Takayasu, Phys. Rev. Lett. 54, 1099 (1985).

[39] L. de Arcangelis, S. Redner and H.J. Herrmann, J. Physique Lett. 46, L585 (1985).

[40] M. Sahimi and J.D. Goddard, Phys. Rev. B33, 7848 (1986).

[41] P.M. Duxbury, P.D. Beale and P.L. Leath, Phys. Rev. Lett. 57, 1052 (1986).

[42] P.M. Duxbury, P.L. Leath and P.D. Beale, Phys. Rev. B36, 367 (1987).

[43] Y.S. Li and P.M. Duxbury, Phys. Rev. B36, 5411 (1987).

[44] P.D. Beale and P.M. Duxbury, Phys. Rev. B37, 2785 (1988).

[45] P.D. Beale and D.J. Srolovitz, Phys. Rev. B37, 5500 (1988).

[46] D.J. Srolovitz and P.D. Beale, Am. Ceram. Soc., 71, 362 (1988).

[47] P.L Leath and W. Tang, Phys. Rev. B39, 6485 (1989); W. Xia and P.L. Leath, Phys. Rev. Lett. 63, 1428 (1989).

[48] For example see,H.L. Ewalds and R.J.H. Wanhill, Fracture Mechanics (Edward Arnold, 1984).

[49] Y.S. Li and P.M. Duxbury, Phys. Rev. B40, 4889 (1989).

[50] A.A. Griffith, Phil. Trans. R. Soc. London, 221, 163 (1920).

[51] E.J. Garboczi, Phys. Rev. B38, 9005 (1988).

[52] J. Tobochnik, preprint; J. Tobochnik, M.A. Dubson, M.L. Wilson and M.F. Thorpe, Phys. Rev. A, in press.

[53] M.F. Thorpe, M. DeVries and J. Tobochnik, unpublished.

[54] P.G. de Gennes, Recherche, 7, 919 (1976).

[55] S. Alexander and R. Orbach, J. Physique Lett. 43, L625 (1982).

[56] Y. Gefen, A. Aharony and S. Alexander, Phys. Rev. Lett. 50, 77 (1983).

[57] D. Ben-Avraham and S. Havlin, J. Phys. A15, L691 (1982).

[58] R.B. Laibowitz and Y. Gefen, Phys. Rev. Lett. 53, 380 (1984).

[59] G. Deutscher, A. Kapitulnik and M. Rappaport, Ann. Isral. Phys. Soc. 5, 207 (1983).

[60] H.E. Stanley and A. Coniglio, Phys. Rev. B29, 522 (1984).

[61] R.B. Pandey, D. Stauffer, A. Margolina and J.G. Zabolitzky, J. Stat. Phys. 34, 427 (1984).

[62] C. Mitescu and J. Roussenq, Ann. Israel Phys. Soc. 5, 81 (1983).

[63] H. Scher and M. Lax, Phys. Rev. B10, 4491 (1973).

[64] K.W. Kehr, J. Stat. Phys. 30, 509 (1983).

[65] R. Kutner and K.W. Kehr, Phil. Mag. A48, 199 (1983).

[66] P.G. de Gennes, J. Physique Colloq. 41, C3 (1980).

[67] A. Coniglio and H.E. Stanley, Phys. Rev. Lett. 52, 1068 (1984).

[68] H.J. Herrmann, D. Derrida and J. Vannimenus, Phys. Rev. B30, 4080 (1984).

[69] A. Bunde, A. Coniglio, D.C. Hong and H.E. Stanley, J. Phys. A18, L137 (1985).

[70] D.C. Hong, H.E. Stanley and A. Coniglio, Phys. Rev. B33, 4564 (1986).

[71] R.C. McPhedran, Proc. R. Soc. Lond. A408, 31 (1986).

[72] L. Poladian and R.C. McPhedran, Proc. R. Soc. Lond. A408, 45 (1986).

[73] R.C. McPhedran and D.R. McKenzie, Proc. R. Soc. Lond. A359, 45 (1978).

[74] G.K. Batchelor, F.R.S. and R.W. O'brien, Proc. R. Soc. Lond. A355, 313 (1977).

[75] W.T. Perrins, R.C. McPhedran and D. McKenzie, Thin Solid Films, 57, 321 (1979).

[76] L. Rayleigh, Phil. Mag. 34, 481 (1892).

[77] I. Runge, Z. Tech. Phys. 6, 61 (1925).

[78] H.B. Keller and D. Sachs, J. Appl. Phys. 35, 537 (1964).

[79] W.T. Perrins, D.R. McKenzie and R.C. McPhedran, Proc. R. Soc. Lond. A369, 207 (1979).

[80] J.B. Keller, J. Appl. Phys. 34, 991 (1963).

[81] S. Roux, J. Stat. Phys., 48, 201 (1987).

[82] J. Machta and R.A. Guyer, Phys. Rev. B36, 2142 (1987).

[83] G. Arfken, Mathematical Methods for Physicists, 2nd ed. (Academic, New York, 1970).

[84] G.C. Sih, Method of Analysis and Solution of Crack Problems, (Noordhoff, Amsterdam, 1973); O.L. Bowie, ibid., and references therein.

[85] Th. von Karman and J.M. Burgers, in Aerodynamic Theory, Vol.II, Div. E, 83, ed. W.F. Durand, 1943.

[86] H. Tada, P. Paris and G. Irwin, The Stress Analysis of Cracks Handbook (Doll Research, St. Louis, 1973).

[87] E.J. Gumbel, Statistics of Extremes, (Columbia University Press, New York, 1958).

[88] L. de Arcangelis, S. Redner and A. Coniglio, Phys. Rev. B31, 4725 (1985).

[89] L. de Arcangelis, S. Redner and A. Coniglio, Phys. Rev. B34, 4656 (1986).

[90] G.G. Batrouni, A. Hansen and Nelkin, J. Physique, 48, 771 (1987).

[91] R. Blumenfeld, Y. Meir, A.B. Harris and A. Aharony, J. Phys. A19, L791 (1986).

[92] B. Kahng, G.G. Batrouni and S. Redner, J. Phys. A20, L827 (1987).

[93] S.K. Chan, J. Machta and R.A. Guyer, Phys. Rev. B39, 9236 (1989).

[94] J. Helsing, J. Axell and G. Grimvall, Phys. Rev. B39, 9231 (1989).

[95] For introduction about multifractal, see G. Paladin and A. Vulpiani, Phys. Rep. 156, 147 (1987).

[96] Y. Kantor and I. Webman, Phys. Rev. Lett. 52, 1891 (1984).

[97] A.R. Day, R.R. Tremblay and A.M.S. Tremblay, Phys. Rev. Lett. 56, 2501 (1986).

[98] S. Feng, M.F. Thorpe and E. Garboczi, Phys. Rev. B31, 276 (1985).

[99] M. Soderberg, Phys. Rev. B35, 352 (1987).

[100] B. Kahng, G.G. Bartrouni, S. Redner, L. de Arcangelis and H.J. Herrmann, Phys. Rev. B37, 7625 (1988).

[101] H.J. Herrmann, A. Hansen and S. Roux, Phys. Rev. B39, 637 (1989).

[102] R. Rammal, C. Tannous ans A.M.S. Tremblay, Phys. Rev. A31, 2662 (1985).

[103] B. Fourcade and A.M.S. Tremblay, Phys. Rev. B34, 7802 (1986).

[104] D.J. Bergman, Phys. Rev. B39, 4598 (1989).

[105] M.A. Dubson, Y.C. Hui, M.B. Weissmann and J.C. Garland, Phys. Rev. B39, 6807 (1989).

[106] L. de Arcangelis and H.J. Herrmann, Phys. Rev. B39, 2678 (1989).

[107] H.J. Herrmann, A. Hansen and S. Roux, Phys. Rev. B39, 637 (1989).

[108] L. Niemeyer, L. Pietronero and H.J. Wiesmann, Phys. Rev. Lett. 52, 1033 (1984); L. Pietronero and H.J. Wiesmann, J. Stat. Phys. 36, 909 (1984).

[109] M. Murat, Phys. Rev. B32, 8420 (1985).

[110] H.J. Wiesmann and H.R. Zeller, J. Appl. Phys. 60, 1770 (1986).

[111] R.B. Blodgett, R.M. Wade and W.D. Wilkins, IEEE Trans. Elec. Insul. Vol. EI-16, 564 (1981).

[112] A.C. Ashcraft, Proc. World Electrochem. Congress (Moscow: Union Carbide Kabelitems, 1976), p152; L.A. Dissado, J. Fothergill and S. Wolfe, CEIDP Conf. Proc. p264, 1981.

[113] Y.S. Li and P.M. Duxbury, submitted to Phys. Rev. Lett.

[114] T.A. Witten and L.M. Sander, Phys. Rev. Lett. 47, 1400 (1981).

[115] T.A. Witten and L.M. Sander, Phys. Rev. B27, 5686 (1983).

[116] H.E. Stanley, F. Family and H. Gould, Phys. Rev. Lett. 50, 686 (1983).

[117] Y. Termonia and P. Meakin, Nature, 320, 429 (1986).

[118] E. Louis and F. Guinea, Europhys. Lett. 3, 871 (1987).

[119] L. Fernandez, F. Guinea and E. Louis, J. Phys. A21, L301 (1988).

[120] L. Pietronero, A. Erzan and C. Evertsz, Physica, A151, 207 (1988).

[101] H.J. Herrmann, A. Hansen and S. Roux, Phys. Rev. B39, 637 (1989).

[102] R. Rammal, C. Tannous ans A.M.S. Tremblay, Phys. Rev. A31, 2662 (1985).

[103] B. Fourcade and A.M.S. Tremblay, Phys. Rev. B34, 7802 (1986).

[104] D.J. Bergman, Phys. Rev. B39, 4598 (1989).

[105] M.A. Dubson, Y.C. Hui, M.B. Weissmann and J.C. Garland, Phys. Rev. B39, 6807 (1989).

[106] L. de Arcangelis and H.J. Herrmann, Phys. Rev. B39, 2678 (1989).

[107] H.J. Herrmann, A. Hansen and S. Roux, Phys. Rev. B39, 637 (1989).

[108] L. Niemeyer, L. Pietronero and H.J. Wiesmann, Phys. Rev. Lett. 52, 1033 (1984); L. Pietronero and H.J. Wiesmann, J. Stat. Phys. 36, 909 (1984).

[109] M. Murat, Phys. Rev. B32, 8420 (1985).

[110] H.J. Wiesmann and H.R. Zeller, J. Appl. Phys. 60, 1770 (1986).

[111] R.B. Blodgett, R.M. Wade and W.D. Wilkins, IEEE Trans. Elec. Insul. Vol. EI-16, 564 (1981).

[112] A.C. Ashcraft, Proc. World Electrochem. Congress (Moscow: Union Carbide Kabelitems, 1976), p152; L.A. Dissado, J. Fothergill and S. Wolfe, CEIDP Conf. Proc. p264, 1981.

[113] Y.S. Li and P.M. Duxbury, submitted to Phys. Rev. Lett.

[114] T.A. Witten and L.M. Sander, Phys. Rev. Lett. 47, 1400 (1981).

[115] T.A. Witten and L.M. Sander, Phys. Rev. B27, 5686 (1983).

[116] H.E. Stanley, F. Family and H. Gould, Phys. Rev. Lett. 50, 686 (1983).

[117] Y. Termonia and P. Meakin, Nature, 320, 429 (1986).

[118] E. Louis and F. Guinea, Europhys. Lett. 3, 871 (1987).

[119] L. Fernandez, F. Guinea and E. Louis, J. Phys. A21, L301 (1988).

[120] L. Pietronero, A. Erzan and C. Evertsz, Physica, A151, 207 (1988).

[121] H.E. Stanley and N. Ostrowsky eds., Random Fluctuations and Pattern Growth - Experiments and Growth, Kluwer Academic (1988).

[122] A.T. Skjeltorp and P. Meakin, Nature, 335, 424 (1988).

[123] P. Meakin, Crystal Properties & Preparation, Vols. 17 & 18, 1 (1988).

[124] P. Meakin, G. Li, L.M. Sander, E. Louis and F. Guinea, J. Phys. A22, 1393 (1989).

[125] E.L. Hinrichsen, A. Hansen and S. Roux, Europhys. Lett. 8, 1 (1989).

[126] H.J. Herrmann, J. Kertesz and L. de Arcangelis, preprint.

[127] B.V. Gnedenko and A. N. Komogorov, Limit Distributions for Sums of Independent Random Variables (Addison-Wesley, Cambridge, MA, 1954).

[128] L.E. Reichl, A Modern Course in Statistical Physics, (University of Texas Press, Austin, 1980).

[129] W. Feller, Introduction to Probability Theory and Its Applications, (John Wiley & Sons, Inc., 1966).

[130] F. Reif, Fundamentals of Statistical and Thermal Physics (McGraw-Hill, New York, 1965).

[131] J.L. Doob, Stochastic Processes (Wiley, New York, 1953).

[132] J. Aitcheson and J.A.C. Brown, The Lognormal Distribution (Cambridge University Press, London, England, 1957).

[133] S. Redner, preprint (1989).

[134] S. Redner, Random Multiplicative Processes and Multifractals, in Universality in Condensed-Matter Physics Preceedings of the Les Houches Winter Conference, March 1988 (Springer-Verlag).

[135] S. Havlin, R.L. Blumberg, M. Schwartz, H.E. Stanley and A. Bunde, Phys. Rev. Lett. 61, 1428 (1988).

[136] S. Havlin and D. ben-Avraham, Adv. Phys. 36, 695 (19877).

[137] J.W. Haus and K.W. Kehr, Phys. Rep. 150, 263 (1987).

[138] J. Galambos, The Asymptotic Theory of Extreme Order Statistics (J. Wiley, New York, 1978).

[139] E. Castillo, Extreme Value Theory in Engineering, (Academic Press, Inc., 1988).

[121] H.E. Stanley and N. Ostrowsky eds., Random Fluctuations and Pattern Growth - Experiments and Growth, Kluwer Academic (1988).

[122] A.T. Skjeltorp and P. Meakin, Nature, 335, 424 (1988).

[123] P. Meakin, Crystal Properties & Preparation, Vols. 17 & 18, 1 (1988).

[124] P. Meakin, G. Li, L.M. Sander, E. Louis and F. Guinea, J. Phys. A22, 1393 (1989).

[125] E.L. Hinrichsen, A. Hansen and S. Roux, Europhys. Lett. 8, 1 (1989).

[126] H.J. Herrmann, J. Kertesz and L. de Arcangelis, preprint.

[127] B.V. Gnedenko and A. N. Komogorov, Limit Distributions for Sums of Independent Random Variables (Addison-Wesley, Cambridge, MA, 1954).

[128] L.E. Reichl, A Modern Course in Statistical Physics, (University of Texas Press, Austin, 1980).

[129] W. Feller, Introduction to Probability Theory and Its Applications, (John Wiley & Sons, Inc., 1966).

[130] F. Reif, Fundamentals of Statistical and Thermal Physics (McGraw-Hill, New York, 1965).

[131] J.L. Doob, Stochastic Processes (Wiley, New York, 1953).

[132] J. Aitcheson and J.A.C. Brown, The Lognormal Distribution (Cambridge University Press, London, England, 1957).

[133] S. Redner, preprint (1989).

[134] S. Redner, Random Multiplicative Processes and Multifractals, in Universality in Condensed-Matter Physics Preceedings of the Les Houches Winter Conference, March 1988 (Springer-Verlag).

[135] S. Havlin, R.L. Blumberg, M. Schwartz, H.E. Stanley and A. Bunde, Phys. Rev. Lett. 61, 1428 (1988).

[136] S. Havlin and D. ben-Avraham, Adv. Phys. 36, 695 (19877).

[137] J.W. Haus and K.W. Kehr, Phys. Rep. 150, 263 (1987).

[138] J. Galambos, The Asymptotic Theory of Extreme Order Statistics (J. Wiley, New York, 1978).

[139] E. Castillo, Extreme Value Theory in Engineering, (Academic Press, Inc., 1988).

[140] A.E. Sarhan and B.G. Greenberg, Contributions to Order Statistics, (John Wiley & Sons, Inc., 1962).

[141] S.D. Volkov, Statisticl Strength Theory, (Gordon and Breach Science Publishers, New York, 1962).

[142] E.J. Gumbel, Ann. Math. Statist. 25, 76 (1954).

[143] W. Weibull, J. Appl. Mech. 18, 293 (1951).

[144] W. Weibull, J. Appl. Mech. 19, 109 (1952).

[145] W. Weibull, Appl. Mech. Rev. 5, 449 (1952).

[146] K. Ishii, Sup. Prog. Theor. Phys. 53, 77 (1973).

[147] D.J. Thouless, Phys. Rev. Lett. 39, 1167 (1977).

[148] E. Abrahams, P.W. Anderson, D.C. Licciardello and T.V. Ramakrishnan, Phys. Rev. Lett. 42, 673 (1979).

[149] P.A. Lee, Phys. Rev. Lett. 42, 1492 (1979).

[150] N.F. Mott and W.D. Twose, Adv. Phys. 10, 107 (1961).

[151] R.E. Borland, Proc. Phys. Soc. London, 78, 926 (1961).

[152] B.S. Andereck and E. Abrahams, J. Phys. C13, L383 (1980).

[153] P. Erdos and R.C. Herndon, Adv. Phys. 31, 63 (1982).

[154] G. Bergmann, Phys. Rep. 107, 1 (1984).

[155] M. Pepper, Contemp. Phys. 26, 257 (1985).

[156] P.A. Lee and T.V. Ramakrishnan, Rev. Mod. Phys. 57, 287 (1985).

[157] N.F. Mott and M. Kaveh, Adv. Phys. 34, 329 (1985).

[158] A.A. Abrikosov and I.A. Ryzhkin, Adv. Phys. 27, 147 (1978).

[159] R. Landauer, Philos. Mag. 21, 863 (1970).

[160] A.A. Abrikosov and I.A. Ryzhkin, Adv. Phys. 27, 147 (1978).

[161] P.W. Anderson, D.J. Thoules, E. Abrahams, and D.S. Fisher, Phys. Rev. B22, 3519 (1980).

[162] P.W. Anderson, Phys. Rev. B23, 4828 (1981).

[163] A.A. Abrikosov, Solid State Commun. 37 997 (1981).

[164] V.I. Mel'nikov, Zh. Eksp. Teor. Fix. Pis'ma. 32, 244 (1980) [JETP Lett. 32, 225 (1980)].

[165] A. Peres, M. Revzen, and A. Ron, Phys. Rev. B24, 7463 (1981).

[166] P.A. Mello, J. Math. Phys. 27, 2876 (1986).

[167] B. Shapiro, Phys. Rev. B34, 4394 (1986).

[168] J. Flores, P.A. Mello, and G. Monsivais, Phys. Rev. B35, 2144 (1987).

[169] P.A. Mello, Phys. Rev. B35, 1082 (1987).

[170] B. Shapiro, Philos. Mag. B56, 1031 (1987).

[171] P.A. Mello, P. Pereyra, and N. Kumar, Ann. Phys. 181, 290 (1988).

[172] P.A. Mello and B. Shapiro, Phys. Rev. B37, 5860 (1988).

[173] A. Cohen, Y. Roth and B. Shapiro, Phys. Rev. B38, 12125 (1988).

[174] I. Edrei, M. Kaveh, and B. Shapiro, Phys. Rev. Lett. 62, 2120 (1989).

[175] P.A. Lee and D.S. Fisher, Phys. Rev. Lett., 47, 1546 (1981).

[176] P.M. Duxbury and P.L. Leath, J. Phys. A20, L411 (1987).

[177] D.A. Darling, Trans. Amer. Math. Soc. 73, 95 (1952).

[178] D.Z. Arov and A.A. Bobrov, Theor. Prob. Appl. 5, 377 (1960).

[179] A.V. Nagaev, Theor. Prob. Appl. 16, 126 (1971), and references therein.

[180] D. Dhar, in Stochastic Processes: Formulasim and Applications, ed. by S. Agarwal and S. Dattagupta, (Berlin: Springer, 1983), p 300.

[181] M. Randeria, J.P. Sethna and R.G. Palmer, Phys. Rev. Lett. 54, 1321 (1985).

[182] A.J. Bray and M.A. Moore, J. Phys. C15, L765 (1982).

[183] J.A. Hertz, L. Fleishman and P.W. Anderson, Phys. Rev. Lett. 43, 942 (1979).

[184] A.J. Bray, Phys. Rev. Lett. 59, 586 (1987).

[185] A.J. Bray, Phys. Rev. Lett. 60, 720 (1988).

[186] D. Dhar, M. Randeria and J.P. Sethna, Europhys. Lett. 5, 485 (1988).

[187] A.J. Bray and G.J. Rodgers, J. Phys. C21 L243 (1988).

[188] A.J. Bray and G.J. Rodgers, Phys. Rev. B38, 9252 (1988).

[189] A.J. Bray and H. Deng, Phys. Rev. B40, 6980 (1989).

[190] A.J. Bray, J. Phys. A22, L81 (1989).

[191] R.B. Griffiths, Phys. Rev. Lett. 23, 17 (1969).

[192] R.F. Kayser and J.B. Hubbard, Phys. Rev. Lett. 51, 79 (1983).

[193] U. Seiferheld, H. Bassler and B. Movagher, Phys. Rev. Lett. 51, 813 (1983).

[194] S. Redner and K. Kang, Phys. Rev. Lett. 51, 1729 (1983).

[195] J.K. Anlauf, Phys. Rev. Lett. 52, 1845 (1984).

[196] J.S. Langer, Ann. Phys. 54, 258 (1969).

[197] J.S. Langer and A.J. Schwartz, Phys. Rev. A21, 948 (1980).

[198] J.D. Gunton, M.S. Miguel and P.S. Sahni, in Phase Transition and Critical Phenomena, Vol. 8 (C. Domb and M.S. Green, eds. Academic Press London, 1983).

[199] K. Binder and A.P. Young, Rev. Mod. Phys. 58, 801 (1986).

[200] D.S. Fisher and D.A. Huse, preprint.

[201] I.M. Lifshitz, Adv. Phys. 13, 483 (1964).

[202] T.M. Nieuwenhuizen, J.M. Luck, J. Canisius, J.L. Hemmen and W.J. Ventevogel, J. Stat. Phys. 45, 395 (1986).

[203] T.M. Nieuwenhuizen and J.M. luck, Physica A145, 161 (1987).

[204] T.M. Nieuwenhuizen and J.M. Luck, J. Stat. Phys. 48, 393 (1987).

[205] J.M. Luck and T.M. Nieuwenhuizen, J. Stat. Phys. 52, 1 (1988).

[206] R.A. Webb, S. Washburn, C.P. Umbach and R.B. Laibowitz, Phys. Rev. Lett. 54, 2696 (1985).

[207] V. Chanderasekhar, M.J. Rooks, S. Wind and D.E. Prober, Phys. Rev. Lett. 55, 1610 (1985).

[208] S. Datta, M.R. Melloch, S. Brandyopadyay, R. Noren, M. Varizi, M. Miller and R. Reifenberger, Phys. Rev. Lett. 55, 2344 (1985).

[209] S.B. Kaplan and A. Hartstein, Phys. Rev. Lett. 56, 2403 (1986).

[210] S. Washburn and R.A. Webb, Adv. Phys. 35, 375 (1986).

[211] A.D. Stone, Phys. Rev. Lett. 54, 2692 (1985).

[212] B.L. Al'tshuler, JETP Lett. 41, 648 (1985).

[213] P.A. Stone and A.D. Stone, Phys. Rev. Lett. 55, 1622 (185).

[214] S. Feng, P.A. Lee and A.D. Stone, Phys. Rev. Lett. 56, 1960 (1986).

[215] P.A. Lee, A.D. Stone and H. Fukuyama, Phys. Rev. B35, 1039 (1987).

[216] H. Neuber, Theory of Notch Stresses (Edwards Brothers, Ann Arbor, Michigan, 1946).